Organoids as a Test System for Cell-Stress and -Death in the Intestinal Epithelium

Dissertation zur Erlangung des

akademischen Grades des

Doktors der Naturwissenschaften

vorgelegt von

Bode, Konstantin

an der

Mathematisch-Naturwissenschaftliche Sektion

Fachbereich Biologie

Konstanz, 2019

Tag der mündlichen Prüfung : 18.07.2019

1. Referent: Prof. Dr. Thomas Brunner
2. Referent: Prof. Dr. Christof Hauck

Danksagung

Zuallererst möchte ich Herrn Prof. Dr. Thomas Brunner für die Möglichkeit danken, die Doktorarbeit an seinem Lehrstuhl zu verfassen. Durch sein kollegiales, professionelles und verständnisvolles Auftreten habe ich fachlich aber auch persönlich etliches gelernt und mich stets sehr gut betreut gefühlt.

Weiterhin möchte ich mich bei Herrn Prof. Dr. Christof Hauck für die Übernahme des Zweitgutachtens bedanken.

Frau Eugenia Salzmann, Herr Dieter Stoll und Herr Markus Templin danke ich für die interessante Kooperation bezüglich der Verbindung von Organoiden und Digi-West.

Mein Dank gilt außerdem der gesamten AG Biochemische Pharmakologie. Ihr Alle habt mich in wechselnder Besetzung die letzten Jahre durch alle Hochs und Tiefs begleitet und dabei immer eine Atmosphäre geschaffen, in welcher ich mich wohl gefühlt habe – macht weiter so, bessere Kollegen kann ich mir nicht vorstellen.

Speziell danke ich in diesem Zusammenhang Truong San Phan, der als Freund und Kollege unzählige gute Ratschläge, beste Laune und immer ein offenes Ohr für alles von der ersten bis zur letzten Minute hatte.

Danken möchte ich auch all meinen anderen Freunden außerhalb des Labors, welche mir immer wieder durch andere Blickwinkel neue Motivation und den nötigen Abstand gegeben haben.

Besonders danken möchte ich meinen Eltern und Schwiegereltern, welche mich in vielen Entscheidungen unterstützt und in unzähligen Situationen geholfen haben – ohne euch hätte das alles so nicht funktioniert.

Mein größter Dank gilt Anna und Theo.

Table of Contents

1. Zusammenfassung

Organoide werden in einer Vielzahl von Forschungsgebieten eingesetzt, um Teile von Organen *ex vivo/in vitro* zu modellieren. Organoide bestehen aus mehreren Zelltypen, einschließlich Stammzellen. Somit bilden Sie die Physiologie / Pathophysiologie bestimmter Organe deutlich besser ab als klassische Zellkulturen. Deswegen werden Organoide, sowohl in der Grundlagenforschung, wie der Entwicklungsbiologie, aber auch in der angewandten Forschung, wie der Toxikologie verwendet, um zelluläre Prozesse in einer dreidimensionalen Umgebung zu untersuchen. In der Biomedizin haben Organoide zukünftig, besonders in der Transplantationsmedizin und bei personalisierten Medikationsplanungen ein vielversprechendes Potenzial für die klinische Anwendung.

Da Darmkrebs eine der häufigsten Formen von Krebs ist, die in der westlichen Welt bekannt sind und Biopsie-Material leicht verfügbar ist, ist die individualisierte Chemotherapie, die auf Erkenntnissen basiert, die von Patienten abgeleiteten Organoiden gewonnen wurden, ein vielversprechendes Beispiel. Darüber hinaus können bereits generierte Biobanken dazu beitragen, einen spezifischen Behandlungsplan zu entwickeln, der auf bestimmten Treibermutationen basiert. Weiterhin haben Organoide das Potenzial, in der pharmazeutischen Wirkstoffentwicklung verwendet zu werden. Bis heute sind jedoch nur wenige Methoden zur Analyse von Zelltod in Organoiden bekannt. Daher sind robuste Assays, die hochskalierbar sind, erforderlich, um zelluläre und molekulare Veränderungen in dreidimensionaler Zellkultur quantitativ zu untersuchen.

Die hier beschriebene flurorometrische Methode ermöglicht es, Zelltod in intestinalen Organoiden quantitativ zu messen. Durch die Verwendung von zwei verschiedenen DNS-Farbstoffen können tote Zellen auf die Gesamtzellzahl normiert werden – ein Weg um die stark variierende Zelldichte von Organoiden zu berücksichtigen. Darüber hinaus ermöglicht das einfache, schnell durchführbare Protokoll Anwendungen im großen Maßstab, was durch die Verwendung von Standard-Laborgeräten und Verbrauchsmaterialien weiterhin erleichtert wird. Weiterhin wurden die oben genannten Farbstoffe bereits bei der Quantifizierung des Zelltods von Organoiden etabliert, jedoch in einem anderen Messsystem. Dennoch schlagen wir vor, diese Methode in Kombination mit bereits etablierten Methoden einzusetzen, um zusätzlich z.B. Veränderungen der mitochondriellen Respiration zu

analysieren. Die Kombination dieser Ansätze wird die Analyse von Zellstress und -tod in intestinalen und anderen Organoiden deutlich verbessern.

2. Abstract

Organoid technology is used in a broad variety of research areas to model parts of organs *ex vivo/in vitro*. Comprised of several cell types, including stem cells, organoids resemble the physiology/pathophysiology of certain organs much closer than classical cell culture. Therefore, basic research as developmental biology but also more applied fields, like toxicology use this state of the art technology to study cellular processes in a three-dimensional environment. In Biomedicine, with respect to transplantation and personalized medication, organoid culture has promising potential for future clinical application.

Since colon cancer is one of the most prevalent forms of cancer known in the western world and biopsy material is easily available, individualized chemotherapy, based on knowledge gained from patient-derived organoids, is one auspicious example. Moreover, biobanks, which have already been generated, may help to develop specific treatment-plans, based on certain driver mutations. Furthermore, organoids can be used in drug development using human tissue samples rather than animal-derived material. However, until today few methods are reported to analyze cell death in organoids. Thus, robust assays which can be scaled up are needed to quantitatively monitor cellular and molecular changes in three-dimensional cell culture.

Here, a fluorometric method is described, which allows to quantitatively measure treatment specific intestinal organoid cell death. By using two different nuclear dyes, it is possible to normalize dead cells to total cell number. With this, the acute problem of seeding density of organoids can be circumvented. Moreover, providing a simple and fast protocol, large scale applications are more likely. Additionally, usage of standard laboratory equipment and consumables will ease the acceptance to use this methodology as an everyday standard. Furthermore, the abovementioned dyes have already been established in quantifying organoid cell death, although in a different system.

However, this method should be used in combination with already established methods, analyzing changes in mitochondrial respiratory potential. Combining these two approaches, analysis of cell stress and death in intestinal and other tissue derived organoids will be greatly improved.

3. Introduction

3.1 Intestine

The human gastrointestinal tract is comprised of the stomach and the intestine which is separated into the small and the large intestine. The small intestine (also small bowel) can be further divided into the Duodenum, adjacent to the stomach, the jejunum and the distal ileum. The large intestine (or large bowel) contains the proximal caecum, the colon, and the distal rectum. As absorption of nutrients is the most important task of the small intestine it has a huge surface separating the body from the external environment. The large intestine is mainly involved in the resorption of water from the ingested food. In both cases, this large surface is lined by a single cell-layer epithelium, which is in constant contact with the ingested nourishment, as well as with a huge amount of commensal and potential pathogenic microorganisms (Makki, Deehan et al. 2018). The intestinal epithelium is the most rapidly renewing tissue in mammalian biology with a "complete" turnover within 4-5 days (Eastwood 1977, Bullen, Forrest et al. 2006, Ritsma, Ellenbroek et al. 2014). This is beneficial in a sense that nutriment shear stress and the consistent microbiaological burden is combatted by constant epithelial shedding and renewal (Loktionov 2007, Park, Kotani et al. 2016). The abovementioned large surface of the small intestine is achieved by microstructures protruding in the intestinal lumen, called villi and by smaller invaginations, termed crypts (Yen and Wright 2006).

3.1.1 The intestinal crypt and villus

The intestinal crypt is comprised of several cell types. The Leucine-rich repeat-containing G-protein-coupled receptor 5 ($Lgr5^+$) stem cells reside at the very bottom of the crypts (Barker, van Es et al. 2007, Barker and Clevers 2010, Koo and Clevers 2014). They are responsible for epithelial homeostasis and overall tissue integrity (Barker 2014, Beumer and Clevers 2016). In order to maintain an intestinal stem cell population, Wingless-type (Wnt)-signaling is essential (Clevers, Loh et al. 2014). Wnt is produced by subepithelial telocytes (Shoshkes-Carmel, Wang et al. 2018) as well as by Paneth cells in the small intestine (Sato, van Es et al. 2011). Paneth cells, adjacent to stem cells, also provide further factors/components, such as the Notch ligand DII4, epidermal growth factor (EGF) and transforming growth factor-α (TGF-α), which are additionally required for stem cell maintenance (Sato, van Es et al. 2011).

Moreover, stem cells need further growth factors to retain functional in their micro-architectural niche, mainly R-Spondin, a Wnt-agonist and Noggin, a bone morphogenetic protein (BMP) inhibitor (de Lau, Peng et al. 2014, Thorne, Chen et al. 2018). On top of that, Liver receptor homologue 1 (LRH-1, NR5A2) is known to push Wnt/β-catenin-signaling and thereby contributes to intestinal epithelial proliferation (Botrugno, Fayard et al. 2004, Yumoto, Nguyen et al. 2012). Thus LRH-1^{IEC-KO} have reduced levels of stem cell markers Lgr5 and Olfactomedin4 (Liu, Li et al. 2016, Bayrer, Wang et al. 2018). Furthermore, LRH-1 directly affects Notch expression, as LRH-1^{IEC-KO} show diminished levels of Notch and consequently increased numbers of secretory cells as goblet cells or Paneth cells (Bayrer, Wang et al. 2018). Apart from contributing to the stem cell niche, Paneth cells have an important role in innate immune defense, by expressing α-defensins as well as lysozyme (Peeters and Vantrappen 1975, Ayabe, Satchell et al. 2002). Above the crypt base, there is a transit-amplifying (TA) compartment, which are still not yet fully differentiated, and continue to proliferate (Ritsma, Ellenbroek et al. 2014). Further up the villus in the small intestine and further up the crypt in the large intestine, cells differentiate into either the secretory or the absorptive pathway. The secretory pathway leads to mucus producing goblet cells (Moe 1953), enteroendocrine cells as well as tuft cells, being involved in innate immunity (von Moltke, Ji et al. 2016). Moreover, "reserve stem cells" are preserved and termed, due to their position within the crypt base, as +4 cells (Figure 1) (Sei, Feng et al. 2018), The majority of intestinal cells however are absorptive enterocytes. They are responsive for nutrient uptake within the small intestine and harbor yet another surface enlargement – the apical, actin-rich microvilli brush border (Danielsen and Hansen 2008, D'Aquila, Hung et al. 2016).

In 2010, it was shown that small intestinal crypts and villi are clonal. With *R26R-Confetti* knock in mice, Snippert et al. could show, that "crypt homeostasis resulted from neutral competition between symmetrically dividing Lgr5 stem cells", meaning that intestinal homeostasis is most likely driven by a stochastic and not the long-time favored hierarchical model (Snippert, van der Flier et al. 2010).

Cellular composition varies between the different parts of the intestine. Whereas there are mostly enterocytes in the small intestine, the large intestine is home to much more goblet cells, as the ingested food is getting more and more viscous. Figure 1 shows scanning electron microscopy of small intestinal and colonic crypts as well as schematic drawings of cellular distributions in the different parts of the crypt or villus part (Figure 1, middle panel).

Moreover, the lineage differentiation, starting from single Lgr5^{+} stem cells, to absorptive and secretory pathways are depicted in the right panel.

However, there is another epithelial cell type which is in close contact to adjacent intestinal lymph nodes peyer's patches (PP), the microfold (M) cells (Pickard and Chervonsky 2010). Although important for antigen sampling between the intestinal lumen and PPs, M cell function is still not completely understood (Mabbott, Donaldson et al. 2013).

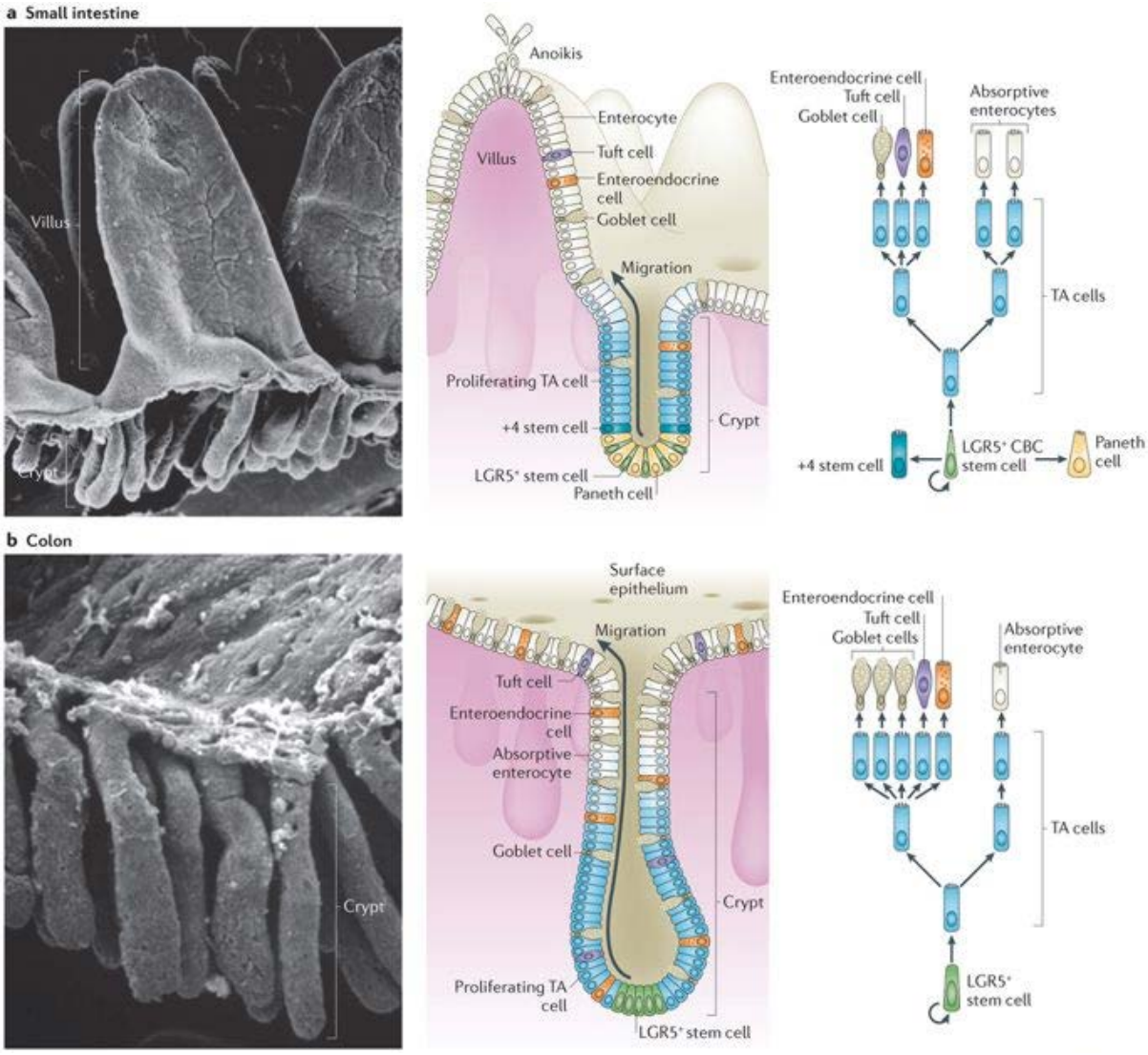

Figure 1: Intestinal crypts and their cellular compositions

Crypts and villi of small (a) and large intestine (b) are shown from electron microscopy. Crypts contain a multitude of cells, ranging from stem cells to Paneth cells, goblet cells, tuft cells, enteroendocrine cells and enterocytes. All originate from Lgr5^{+} stem cells. Figure adapted from (Barker 2014).

3.1.2 Intestinal microbiome, intestinal immune system and their interplay

The intestine is home for the largest number of microbes in the human body. In a healthy individual, there are more bacteria in the intestine than total eukaryotic cells in the body (Delgado, Grabinger et al. 2016). Thus, a strict balance has to be maintained in order to keep inflammation in check (Sekirov, Russell et al. 2010) and at the same time benefit from bacterial metabolic products. This is of major importance as the intestinal microbiome shows not only direct effects on the human metabolism (Canfora, Jocken et al. 2015), the cellular turnover in the intestine (Park, Kotani et al. 2016), but also very likely on the human brain (Mayer, Tillisch et al. 2015). Therefore, the single layer epithelium is equipped with a multitude of innate and adaptive lines of defense to fight off potential pathogens from the intestinal lumen. Starting from physical barriers, as the mucus layer as well as the continuous flow through the intestine, to shedding of epithelial cells as a way to get rid of infected cells – a strategy some bacteria have managed to circumvent (Muenzner, Bachmann et al. 2010). Moreover, especially in the small intestine with its deep invaginations an oxygen gradient determines microbial composition of small and large intestine (Figure 2). Distribution and numbers of antimicrobial peptides as well as pH further influence bacterial distribution (Hall, Tolonen et al. 2017).

The small intestinal epithelium is home of Paneth cells, which fight off pathogens non-specifically with defensins and lysozyme (Peeters and Vantrappen 1975, Ayabe, Satchell et al. 2002). Moreover, highly abundant IgA complexes bacteria at the mucosal barrier (Moor, Diard et al. 2017). Importantly, the intestinal epithelium is not purely made up of epithelial cells – some leucocytes reside there as well. These intraepithelial lymphocytes are a highly specific first line defense of the adaptive immune system (Brunner, Arnold et al. 2001). As abovementioned, M cells serve as antigen transmitters from the intestinal lumen, to adjacent peyer's patches. There, a broad variety of lymphocytes is residing in order to fight off infiltrating pathogens (Gebert, Rothkotter et al. 1996, Reboldi and Cyster 2016). However, dysregulation of immune response due to e.g. chronic inflammation can lead to a multitude of immunopathologies including inflammatory bowel disease (IBD), such as Crohn's disease and ulcerative colitis, or even cancer (Brunner 2009, Francescone, Hou et al. 2015). Again, the composition of the intestinal microbiome has a big influence on IBD development. However, cause and consequence are hard to distinguish conclusively (Kostic, Xavier et al. 2014). Still,

there is evidence that certain genetic alterations can lead to an imbalanced immune response in the intestine, eventually leading to e.g. Crohn's disease.

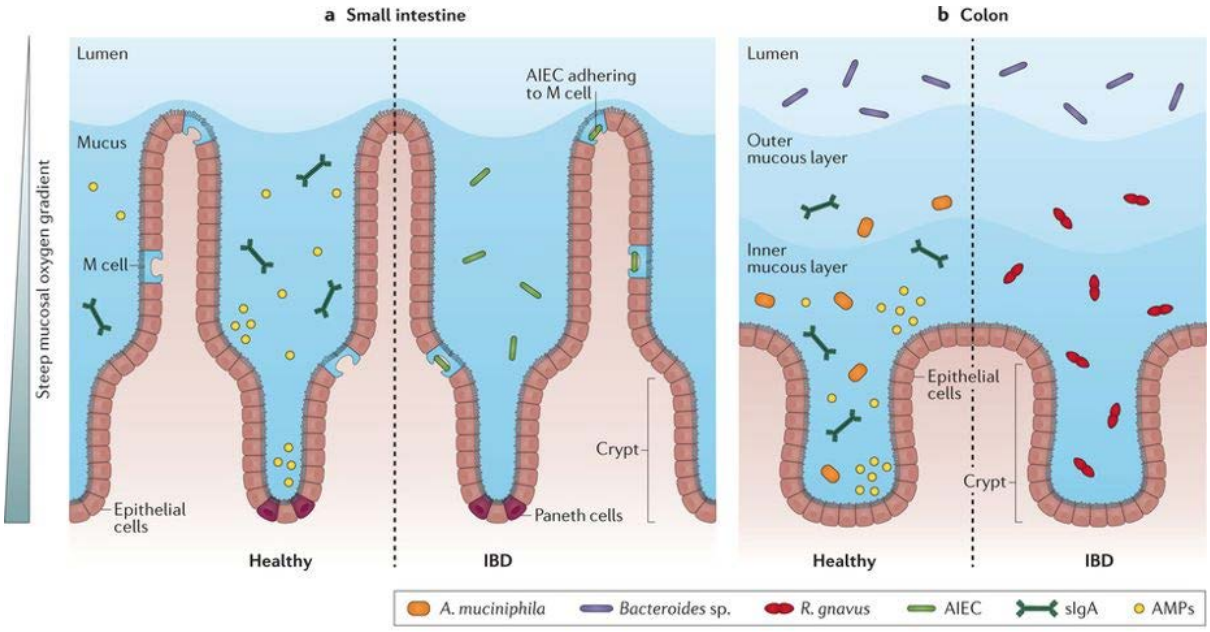

Figure 2: Microbial distribution in small and large intestine

The intestine has a nonhomogeneous bacterial composition. A) In the small intestine, villi and crypts comprise the microscopic surface architecture of the epithelium. This micro-architecture results in different oxygen and pH gradients than in B) the large intestine, where only crypts are found. Contrarily, the large intestine has a much more sophisticated mucous layering then the small intestine, therefore being home to yet different bacterial strains. Lastly, distribution and abundance of antimicrobial peptides and IgA vary, thereby contributing to microbial differences. Figure adapted from (Hall, Tolonen et al. 2017).

A mutated form of Nucleotide binding oligomerization domain-containing protein 2 (NOD2), for example, which senses parts of bacterial cell walls within the epithelium will lead to reduced nuclear factor kappa-light-chain-enhancer of activated B cells (NFκB) activation and thus to a reduced T_H17-cell mediated "protective inflammatory response" (Figure 3Aa). Reduced mucin and defensin production as well as impaired epithelial barrier integrity are the consequence leading to invasion of bacteria and a strong T_H1-cell mediated inflammatory immune response (Figure 3Ab).

Another example is Fucosyltransferase 2 (FUT2), an enzyme adding fucose to extracellular glycosylation patterns. Some bacterial species feed of this sugar, others are being decorated and subsequently hindered in growth (Figure 3Ba).

In sum, lack of this enzyme leads to altered microbial composition in the intestine, which can again, can also lead to an inflammatory response, ultimately resulting in IBD (Figure 3Bb) (Hall, Tolonen et al. 2017).

Thus, in order to control local inflammation and prevent overshooting immune responses resulting in e.g. IBD, the intestinal epithelium produces glucocorticoids (GC) locally (Cima, Corazza et al. 2004). Intestinal GC synthesis is regulated by the nuclear receptor liver receptor homolog-1 (LRH-1) (Mueller, Cima et al. 2006). LRH-1, an orphan nuclear receptor, which is in the intestine mostly expressed at the crypt base, can prevent IBD via induction of local GC production and by controlling cell death in intestinal epithelial cells (Coste, Dubuquoy et al. 2007, Kostadinova, Schwaderer et al. 2014, Bayrer, Wang et al. 2018). Interestingly, colonic tumor cells, may use their capacity to locally produce glucocorticoids as a highly sophisticated immune escape mechanism (Sidler, Renzulli et al. 2011). Nevertheless, immunosuppressive therapy with glucocorticoids is widely used in IBD patients (Dubois-Camacho, Ottum et al. 2017). However, in this scenario, like in leukemic therapy, glucocorticoid resistance has been observed (De Iudicibus, Franca et al. 2011, Jones, Gearheart et al. 2015).

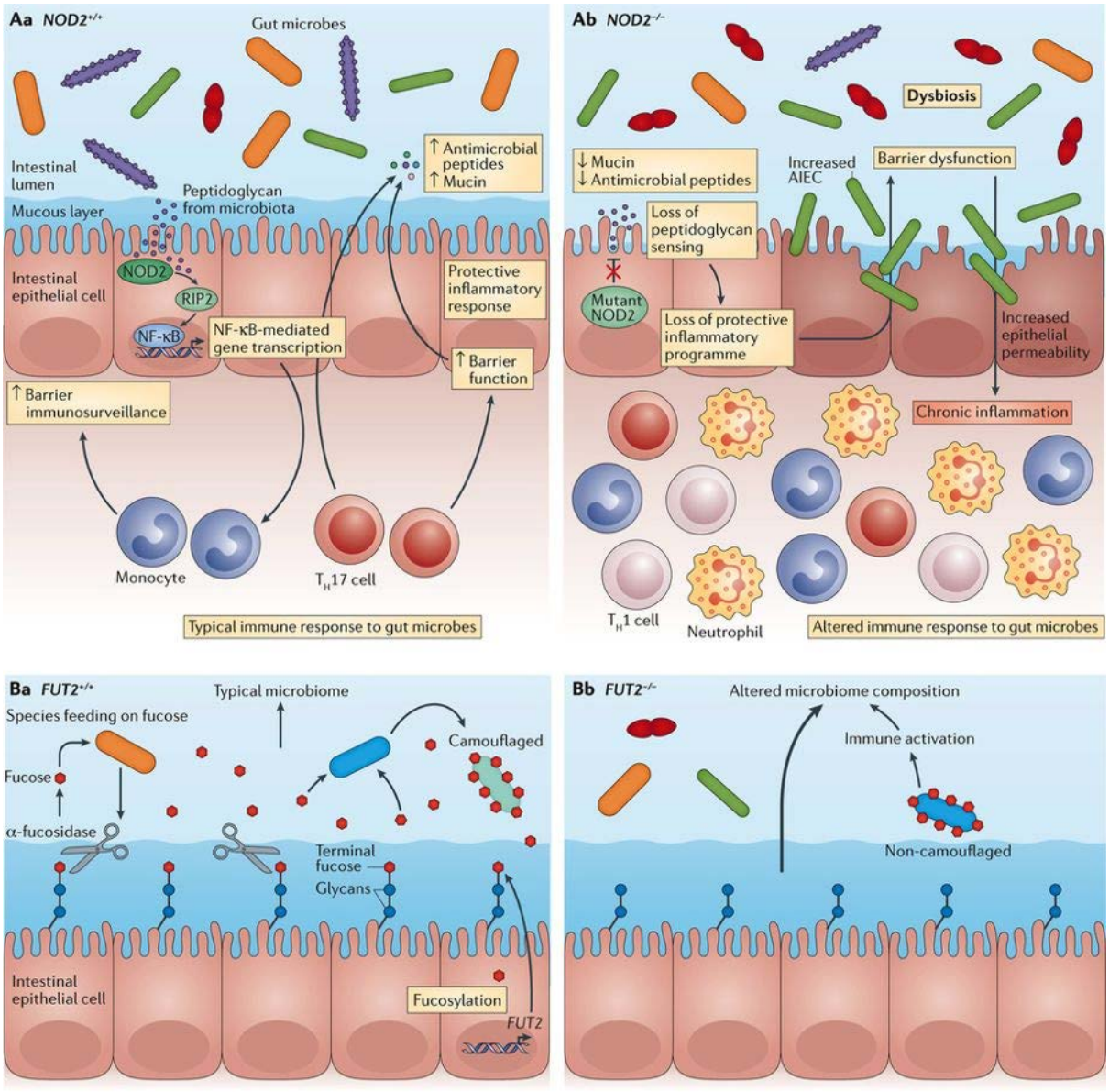

Figure 3: Genetic alterations influencing IBD development

Aa) NOD2 leads via NFκB activation to a "protective inflammatory response". Ab) Mutated NOD2 leads to reduced mucin and defensin production as well as impaired epithelial barrier integrity consequently leading to invasion of bacteria and a strong inflammatory immune response. Ba) FUT2 adds fucose to the extracellular glycosylation pattern of epithelial cells. Bacteria can be either hindered or pushed in growth by this. Bb) Lack of FUT2 enzyme leads to altered microbial composition in the intestine, which can again, lead to an inflammatory response, ultimately resulting in IBD (Figure adapted from (Hall, Tolonen et al. 2017))

3.1.3 Maintenance and renewal of the intestinal epithelium

As mentioned before, the intestinal epithelial Lgr5^{+} stem cells reside at the bottom of the crypt in a specialized stem cell zone comprised of the stem cells themselves and adjacent Paneth cells (see 3.1.1 and Figure 1). These Paneth cells and surrounding mesenchyme produce the exquisite cocktail of growth factors and cytokines being necessary for stem cell maintenance and growth as well as epithelial differentiation. Mainly Notch ligands, Eph/ephrins, EGF, the bone morphogentic protein-4 (BMP-4) Inhibitor Noggin, Wnts, and their agonists (RSpondins) are crucial for intestinal stem cell preservation and eventually indispensable for an intact intestinal epithelium (Crosnier, Stamataki et al. 2006, Kosinski, Li et al. 2007, Van der Flier, Sabates-Bellver et al. 2007, Suzuki, Sekiya et al. 2010, Miguel, Maxwell et al. 2017, Spit, Koo et al. 2018). In the following, the most relevant growth factors for organoid culture are described in more detail.

EGF-signaling

By binding to its receptor, EGF triggers cellular proliferation via the well-described MAPK/ERK-pathway (Zhang and Liu 2002). In the intestine, EGF contributes both to cellular proliferation as well as to apoptosis prevention and is thereby involved in intestinal homeostasis as well as repair after injury (Alison and Sarraf 1994, Podolsky 1997, Suzuki, Sekiya et al. 2010).

Wingless-type (Wnt)-signaling

Binding of Wnt to its receptor Frizzled leads to phosphorylation of adjacent LRP5/6 and thus release of β-catenin which can in turn translocate to the nucleus, bind to members of the TCF/LEF (Transcription Factor/ Lymphoid enhancer-binding factor) group and thus initiate the transcription of Wnt-target genes, such as c-myc, cyclin D1, but also R-Spondin and Rnf43/Znrf3 (Figure 4) (Morgan, Mortensson et al. 2018). Wnt/β-catenin signaling in the small intestinal crypts was found to be regulated by poly (ADP-ribose) polymerases known as tankyrases (Ye, Chiang et al. 2018). Furthermore, olfactomedin 4 regulates Wnt-signaling by binding competition with Frizzled receptor ligands as well as by interfering with Akt-GSK3 (Glycogen Synthase Kinase-3) signaling (Liu, Li et al. 2016). Being a Wnt target gene, olfactomedin is involved in a negative feedback loop, preventing overshooting Wnt-signaling (Liu, Li et al. 2016).

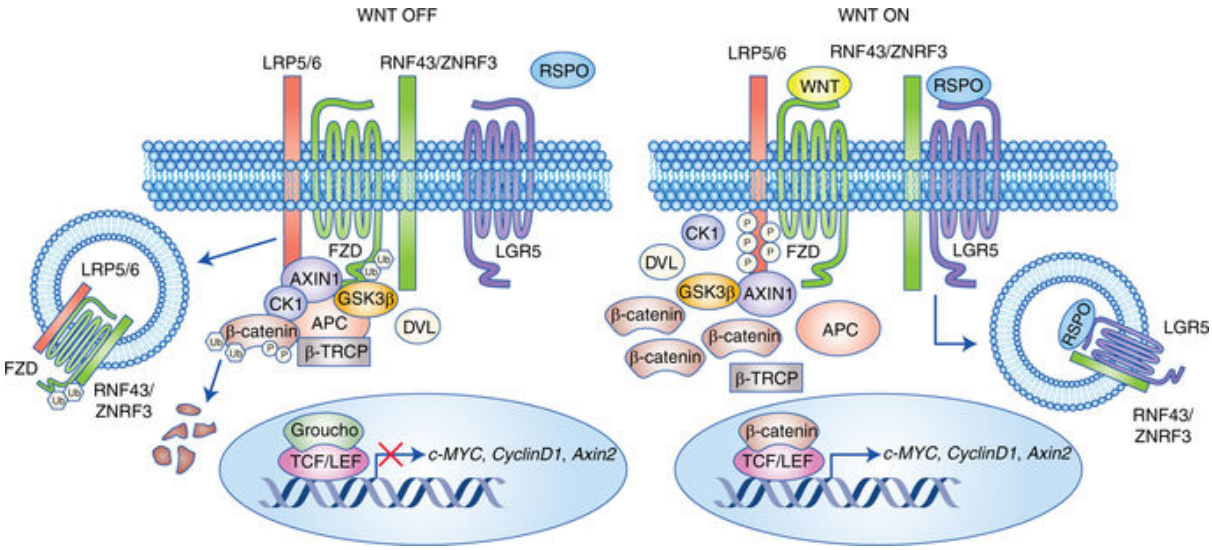

Figure 4: Wnt-signaling in the small intestine

Upon Wnt binding to its receptor Frizzled (FZD), β-catenin gets released from the receptor complex and translocates to the nucleus. Binding of R-Spondin to its receptor Lgr5 stabilizes this signal by internalizing the E3-Ligases RNF43/ZNRF3. Figure adapted from (Morgan, Mortensson et al. 2018)

R-Spondin and its receptor Lgr5

R-Spondin is a Wnt-Agonist and a Wnt target gene at the same time. By binding its receptor Leucine-rich repeat-containing G-protein coupled receptor **(**Lgr5), R-Spondin neutralizes two E3 ligases (RNF43/ZNRF3) that would otherwise ubiquitinate Wnt-receptors, such as Frizzled. This would lead to proteasomal degradation of the latter and thereby overall removal of Wnt-receptors from the plasma membrane (Figure 4) (de Lau, Peng et al. 2014). There are four variants of R-Spondin known, one of which is needed to grow the "small guts" known as organoids (Sato, Vries et al. 2009). R-Spondin inherits two FURIN domains. FURIN1 is necessary for the interaction with the E3-ligases RING finger protein 43 (Rnf43) and zinc/RING finger protein 3(Znrf3), whereas FURIN2 binds Lgr4-6 (Figure 5). Lgr are comprised of Leucine rich repeats (LRR), a flexible hinge region, and the GPCR-known c-terminal heptahelical transmembrane part (Figure 5). The Thrombospondin type-1 (TSR1) repeat domain within R-Spondin binds to cell surface receptors of the syndecan-type (de Lau, Peng et al. 2014). Injected into mice, human R-Spondin 1 leads to dramatically increased proliferation of intestinal crypts, substantiating its role as a mitogen (Kim, Kakitani et al. 2005). Taking this

into consideration, R-Spondin 1 is a crucial component of organoid culturing medium (Huch, Dorrell et al. 2013).

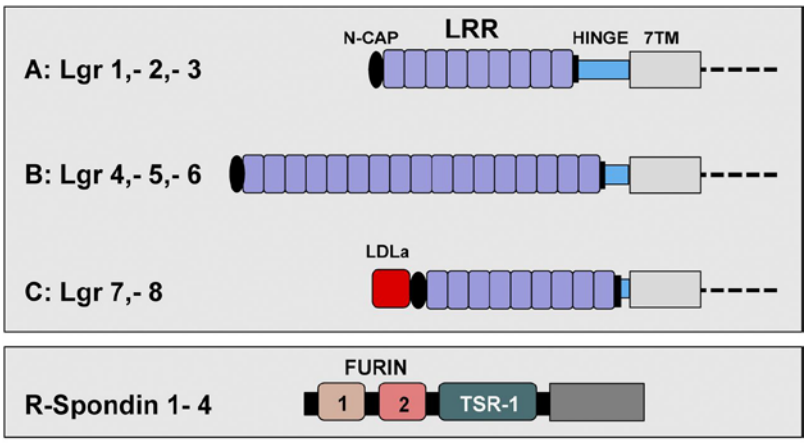

Figure 5: Schematic overview of Lgr-receptors, and R-Spondin variants

Lgr receptors contain Leucine-rich-repeats (LRR) and a 7-transmembrane (7-TM)-region. R-Spondin inherits two FURIN domains and a TSR-1 domain. Figure adapted from (de Lau, Peng et al. 2014).

3.2 Organoids

3.2.1 General

Organoids were first characterized in 2009 (Sato, Vries et al. 2009). Sato et al. described a method how to isolate and cultivate primary intestinal crypt cells over prolonged periods of time. Since then, organoids have gained more and more interest each year.

Organoids are defined as organ-like structures which self-organize in three dimensions. They are comprised of several organ-specific cell types, including stem cells and are capable to fulfill at least some organ-specific functions, e.g. excretion or secretion (Lancaster and Knoblich 2014). As such, organoids enabled for the first time the long-term culture and preservation of primary cells - without genotypic changes. Thus, this was the first method described, to „re-establish" and investigate the intestinal crypt niche ex vivo (Sato, Stange et al. 2011, Date and Sato 2015).

As the parental tissue, small intestinal organoids form crypt-like (buds) and villus like regions (Figure 6)(Kretzschmar and Clevers 2016). They are comprised of $Lgr5^{+}$ stem cells (Koo and Clevers 2014), adjacent paneth cells (Clevers and Bevins 2013) a transit-amplifying-region, as well as members of the secretory and the absorptive pathways, such as enterocytes, enteroendocrine cells, goblet cells and tuft cells (Date and Sato 2015). Above that, intestinal organoids show all coherence factors, found in the parental tissue. From Zonula occludens-1 (ZO-1), indicating tight junctions, to proliferative zones at the bottom of the crypts (Ki-67), to epithelial polarity (phalloidin staining actin-rich brush boarder*)* and β-catenin as well as E-

Cadherin showing desmosomes and adherens junctions (Figure 6) (Fatehullah, Appleton et al. 2013). Thus, organoids derived from the small intestine can serve as a close to *in vivo* model to understand general stem cell biology and tissue organization during organ development (Lander, Kimble et al. 2012, Clevers 2013).

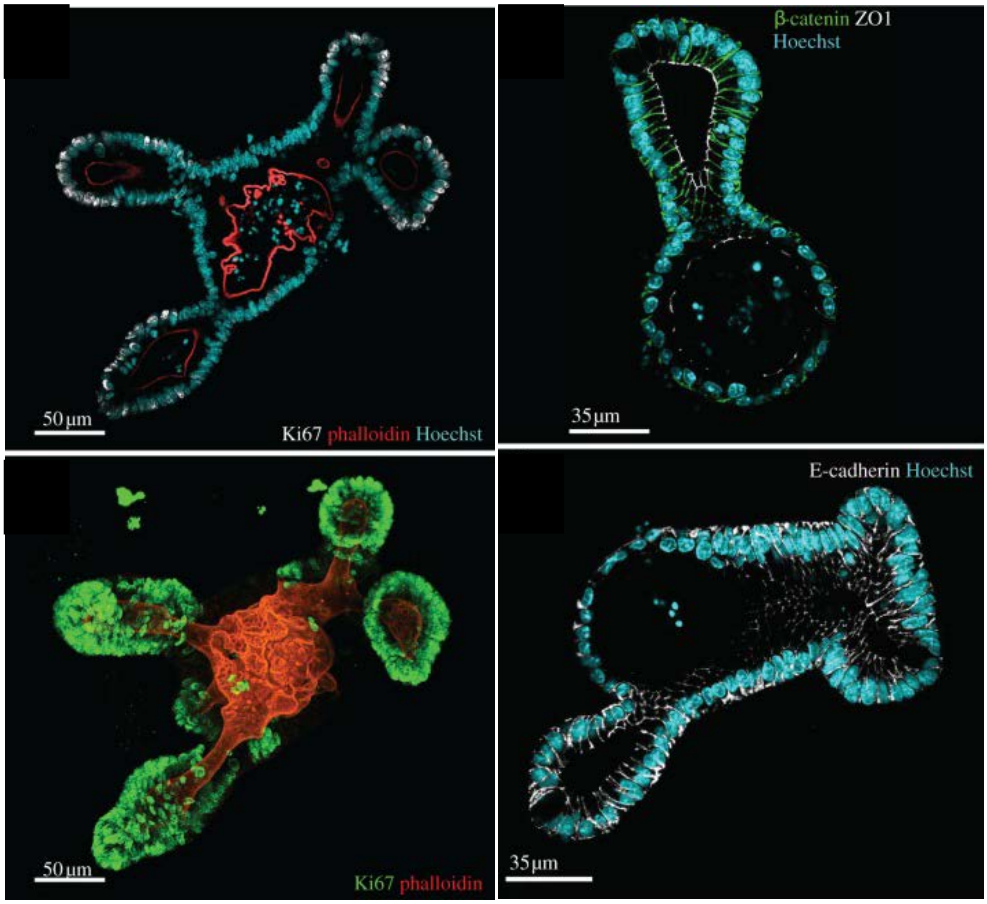

Figure 6:Intestinal organoids harbor all epithelial cell types and show tissue specific polarity

Intestinal organoids show all epithelial cell types. Upper left panel shows proliferating cells (Ki-67) at the end of newly formed "crypt-like regions". Phalloidin (actin staining) staining shows organoid polarity. Hoechst staining: nuclei. Upper right panel: tight junctions (ZO1) and β-catenin: adherens junctions. Lower left panel shows again Ki-67 (proliferation) and phalloidin, showing tissue-like polarity. Lower right panel shows E-Cadherin (Desmosomes and adherens junctions) as well as Hoechst. Figure adapted from (Fatehullah, Appleton et al. 2013)

Furthermore, over the last years, organoids have been generated not only from the small intestine, but from all three germ layers including a multitude of tissues, ranging from liver to pancreas, kidney, brain, esophagus and many more (Figure 7) (Marx 2015, Clevers 2016, Meneses, Schneeberger et al. 2016). By now, organoids are not only generated from tissue

biopsies, but also from single tissue-specific stem cells, most of which can be determined by the surface receptor Lgr5 (Bartfeld and Clevers 2017).

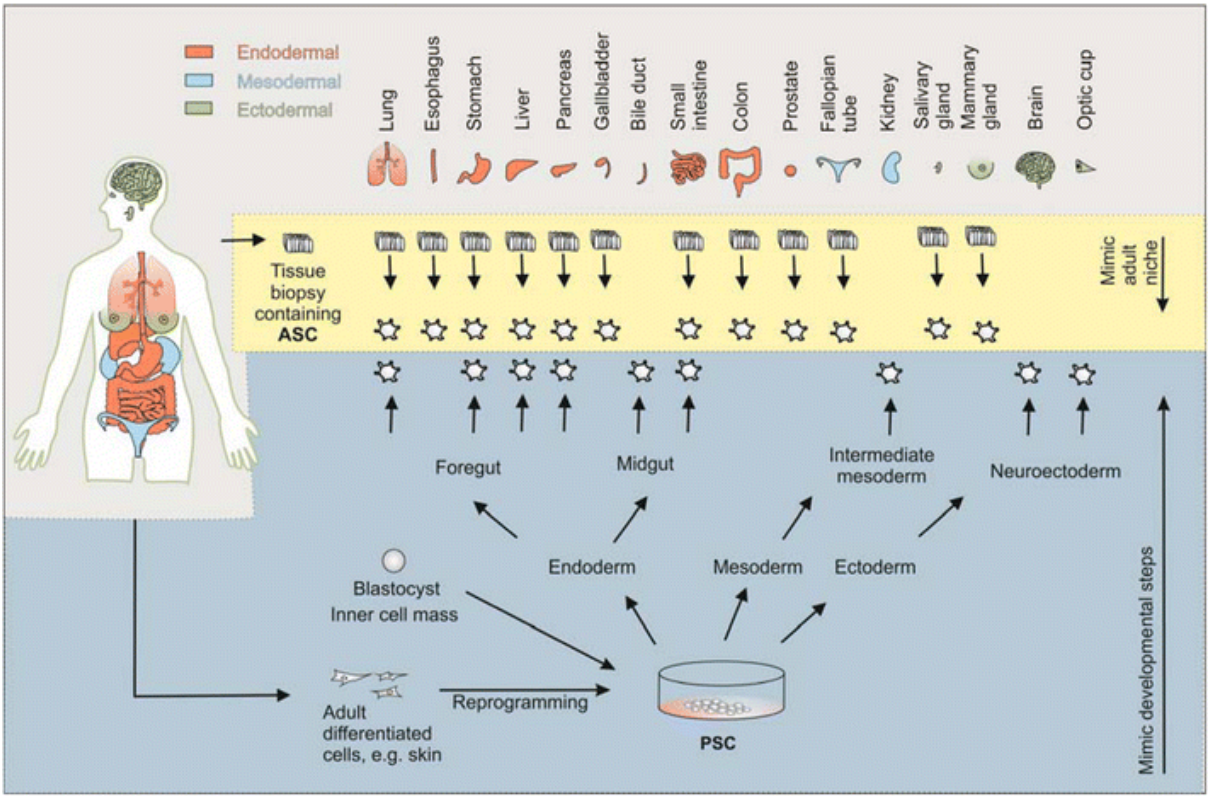

Figure 7: Organoids can be generated from all three germ layers

Organoids can be generated from all three germ layers, endoderm, mesoderm and ectoderm. More specifically, organoids have been generated from tissue biopsies from the lung, intestine, pancreas, prostate and many more. However, organoids have also been generated from iPSCs being guided to develop into specific tissue progenitors. Figure adapted from (Bartfeld and Clevers 2017)

3.2.2 Self-organization and growth factors

In order that organoids develop from stem cells in the first place, two fundamental processes of self-organization have been identified. One being „sorting-out“, a process of spatial organization due to different adhesive proteins in different cell types and the other being subsequent spatially restricted lineage commitment (Lancaster and Knoblich 2014) (Figure 8). $Lgr5^{+}$ stem cells therefore require a delicate niche environment to develop this striking microarchitecture (Huch, Dorrell et al. 2013). In the most well-known situation in the small intestine, crypt base stem cells, require R-Spondin, a Wnt-agonist (de Lau, Peng et al. 2014), Noggin, a bone morphogenetic protein (BMP)-Inhibitor, preventing epithelial differentation

and epidermal growth factor (EGF) as a general growth booster (Sato, Stange et al. 2011). Moreover, Wnt and ROCK-Inhibitor (inhibiting RhoA/ROCK signaling) are needed to provide the chemical basis to reconstitute the crypt base niche, as well as to prevent anoikis (Zhang, Valdez et al. 2011, Sato and Clevers 2013).

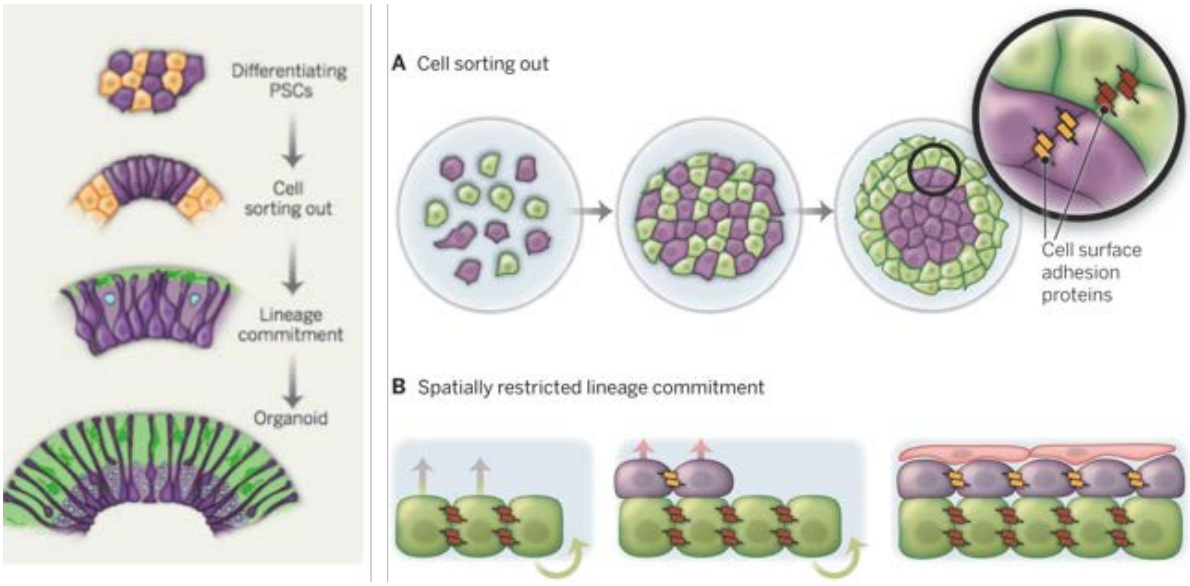

Figure 8: Self-organization of organoids

Left panel shows the development from stem cells to organoids. Critical in this development together with lineage commitment, hence differentiation, is the process of „cell sorting-out". This process of spatial organization is driven by different adhesive molecules in different cells (A). This is a prerequisite for spatially restricted lineage commitment (B). Taken together, these two processes enable the growth of three-dimensional organoids *in vitro*. (Figure adapted from (Lancaster and Knoblich 2014))

In murine small intestinal organoids, Paneth cells produce enough Wnt to sustain a proliferating stem cell pool (Sato, van Es et al. 2011). Before mentioned media components only hold true for murine intestinal cells. For human intestinal crypts/stem cells, additional factors are needed. Here, Wnt3a, as a recombinant protein or conditioned medium has to be added to the medium (Mahe, Sundaram et al. 2015). CHIR99021, a selective glycogen synthase kinase-3 (GSK-3)-Inhibitor is also commonly used as a Wnt-activator. Moreover, A-83-01, a transforming growth factor (TGF) β inhibitor, as well was SB202190 a p38 mitogen-activated protein kinase (MAPK) inhibitor are used to sustain pluripotent stem cell pools (Wang, Scoville et al. 2013, Koo and Clevers 2014). Furthermore, nicotinamide, being a precursor of the redox equivalent of nicotinamide adenine dinucleotide (NADH) has been

described to enable prolonged intestinal organoid culture (Sato, Stange et al. 2011, Mahe, Sundaram et al. 2015). As the role and way of function of stem cells and their ability to prosper and differentiate in a particular tissue-specific niche is until today not completely understood, it is still under extensive investigation (Thalheim, Quaas et al. 2017). Organoids derived from other tissues require each a specific cocktail of growth factors and small molecule inhibitors in order to mimic the individual stem cell niche as close as possible (Lancaster and Knoblich 2014, Rossi, Manfrin et al. 2018).

3.2.3 Extracellular matrix substitutes

In order to grow organoids, not only a chemical, but also a physical basis is needed. Thus, some form of extracellular matrix (ECM) has to be provided in order to enable adhesive points for the epithelial cells (Tibbitt and Anseth 2009). Mostly, Matrigel is used for this purpose. However, Matrigel is generated from murine Engelbreth-Holm-Swarm (EHS)-sarcoma cells (Danielson, Martinez-Hernandez et al. 1992, Hughes, Postovit et al. 2010).

Matrigel or substitutes, mainly consist of Laminin-111, Collagen IV, Nidogen-1 (Entactin), and Heparan sulfate proteoglycan. Moreover, growth factors like fibroblast growth factor (FGF), EGF, transforming growth factor beta (TGF beta), insulin-like growth factors (IGF), and platelet-derived growth factor (PDGF) have been found in Matrigel or substitutes (Benton, Arnaoutova et al. 2014). This further non-defined extracellular-matrix is one current bottleneck for clinical application of organoids, as high batch to batch variability hinders reproducibility of experiments (Serban and Prestwich 2008). Moreover, being an animal-derived product, and thereby inherently containing immunogens, Matrigel and its substitutes represent a major step stone to be eliminated before organoid technology can enter the clinics on a broad scale (Tong, Martyn et al. 2017).

Thus, research in the past years has focused on determining the necessary components found in the abovementioned extracellular matrix substitutes, to generate synthetic matrices (Lutolf and Hubbell 2005, Gjorevski, Sachs et al. 2016). Laminin, fibronectin (or more specifically its Integrin-binding RGD-motif) and a certain physical stiffness of around 190 Pa, mostly achieved by variants of polyethylene glycol (PEG), are the essential ingredients of an extracellular building block for organoids. Materials as such ensure pore-sizes suitable for organoid expansion (Gjorevski, Sachs et al. 2016, Cruz-Acuna, Quiros et al. 2017). In this regard, work

from Lutolf, MP is pioneering, as he and collaborators found, that intestinal stem cells (ISCs) require distinct physical properties as well as different chemical signals in comparison to differentiated intestinal epithelial cells. ISCs require a rather stiff matrix (Figure 9, a), whereas a softer and even degradable matrix is crucial for differentiation and expansion (Figure 9, b) (Gjorevski and Lutolf 2017).

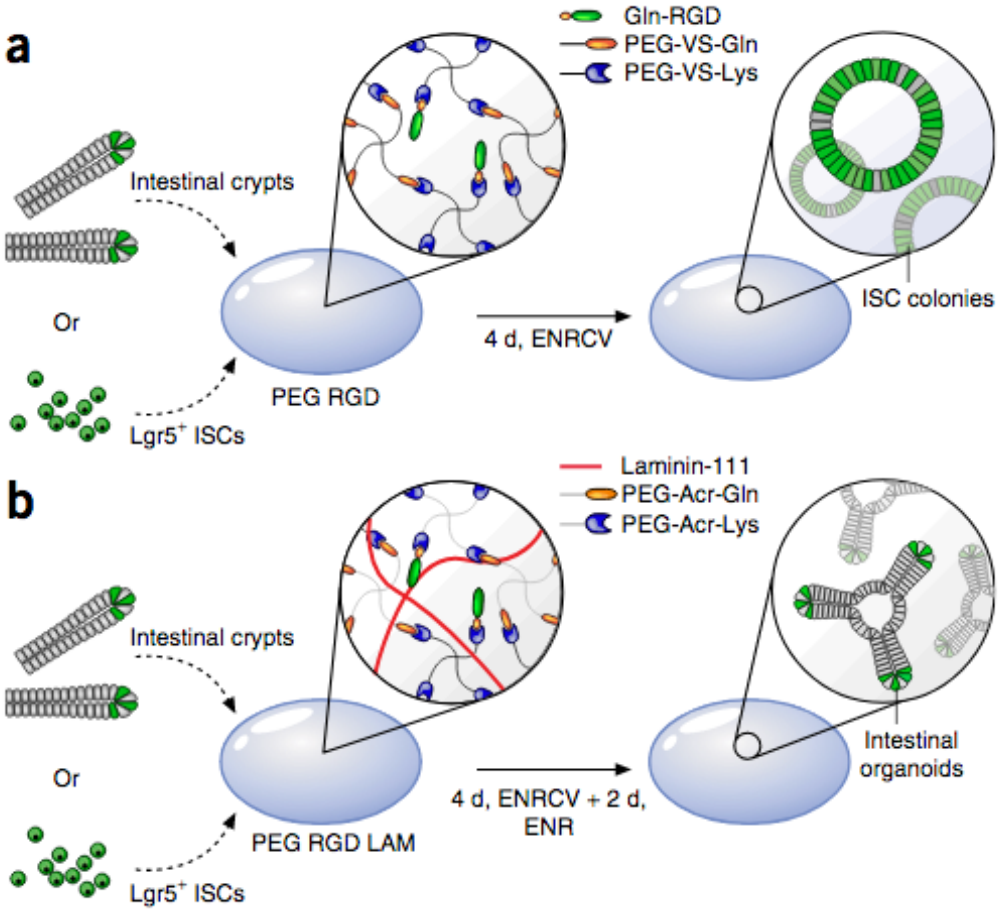

Figure 9: Synthetic extracellular matrices to grow and differentiate ISCs

In their respective growth media, (a) rigid, non-degradable PEG-linkers lead to formation of ISC colonies, whereas (b) soft, degradable matrices, lead to formation of intestinal organoids. Figure adapted from (Gjorevski and Lutolf 2017)

However, with progress being made in material science and 3D-printing, precise structures might be computer-designed and subsequently printed (Hashmi, Zarzar et al. 2014, Tong, Martyn et al. 2017, Swaminathan, Hamid et al. 2019).

Furthermore, organoids initially grown in Matrigel have been transferred to floating collagen rings, where they form a tubular-structure, more closely resembling the *in vivo* condition (Sachs, Tsukamoto et al. 2017). Other groups follow the approach to provide the natural extracellular environment for the cells (Schweinlin, Wilhelm et al. 2016). Therefore, organs

are being de-cellularized and isolated cells subsequently re-seeded (Crapo, Gilbert et al. 2011). This method is by far the closest one in resembling the *in vivo* situation/condition, especially as this type of culture was performed in a bioreactor, enabling laminar flow, creating shear stress – an important physical factor in the physiological intestine (Kim, Ehrman et al. 2017). However, impaired reproducibility and the lack of sufficient primary material still represent significant disadvantages (Rashtbar, Hadjati et al. 2017).

Another very recent approach successfully demonstrated the usage of alginate as an extracellular matrix substitute. Here, human intestinal organoids (HIOs), grown in alginate, showed similar morphology and expression patterns, as well as engrafting at a similar level as conventionally cultivated HIOs (Capeling, Czerwinski et al. 2018). This holds great potential, as algae can be cultivated easily on an industrial scale, and are by their nature, animal-residue-free (Endres, Roth et al. 2018).

Overall, this knowledge will facilitate the progress of organoid technology further to the clinics, as residues from animals will no longer be present in these hydrogels. Moreover, synthetically generated hydrogels enable tissue-specific fine-tuning as organoids from the brain require a different physical as well as chemical environment than organoids from the pancreas (Tibbitt and Anseth 2009, DiMarco, Dewi et al. 2015, Marx 2015, Willemse, Lieshout et al. 2017).

3.2.4 Applications of organoid culture systems

Being used for developmental studies in the beginning (Sato, van Es et al. 2011), organoids have nowadays acquired a broad applicative field, ranging from proof of principle studies (Yui, Nakamura et al. 2012) to pre-clinics (Fujii, Shimokawa et al. 2016) and clinics (Dekkers, Wiegerinck et al. 2013) but also to assay development (Bas and Augenlicht 2014, Gonneaud, Jones et al. 2016, Walsh, Cook et al. 2016). Moreover, research in the past years massively improved organoid culturing techniques, with respect to medium composition and usage of extracellular matrix mimicking substances (Miyoshi and Stappenbeck 2013, Gjorevski, Sachs et al. 2016, Nozaki, Mochizuki et al. 2016, Schweinlin, Wilhelm et al. 2016).

The field of organoid technology started with cells of murine origin. Today, organoids are grown from a wide range of species interesting for veterinary sciences but also from human tissues (Finkbeiner and Spence 2013, Stewart, Freund et al. 2018, van der Hee, Loonen et al. 2018). Figure 7 provides an overview from which organs/tissues organoids can and have been

generated and the two general ways which can be used to generate organoids. One using tissue biopsies as starting material and the other starting from induced pluripotent stem cells (iPSCs).

Traditionally, organoids have been generated mainly from the intestine (Sato, Vries et al. 2009). Thus, knowledge about intestinal $Lgr5^+$ stem cells and their role in disease development has been known from early on (Barker, Ridgway et al. 2009). Still, the intestine remains an important research area, where organoid technology is applied frequently. Organoids are being used to study basic intestinal physiology (Yu, Hasan et al. 2017), but also pathophysiology as in the context of inflammatory bowel disease (Nishimura, Shirasaki et al. 2019) and associated molecules such as Tumor necrosis factor (TNF) alpha (α) (Grabinger, Bode et al. 2017, Howell, Kraiczy et al. 2017). Moreover, organoids have been in use to study host-pathogen interactions, not only in the intestine (In, Foulke-Abel et al. 2016) but also in the brain in the current topic of Zika virus research (Garcez, Loiola et al. 2016). Today, in basic research, organoids are used both to study healthy and malignant tissue (Lin and Barker 2011, Schwartz, Pehlivaner Kara et al. 2017, Sugimoto, Ohta et al. 2017). This is due to the fact that organoids can be handled as conventional cell culture cells (Fujii, Matano et al. 2015).

Furthermore, a wide range of state of the art technologies, including CRISPR/Cas9 and induced pluripotent stem cells (iPSCs) allow virtually any experiment imaginable, ranging from genome-editing to the targeted generation of neurologic disease models for e.g. Alzheimer's disease or kidney disease (Lancaster and Knoblich 2014, Freedman, Brooks et al. 2015, Raja, Mungenast et al. 2016, Schwank and Clevers 2016). Especially in oncology, organoids provide an interesting tool to study tumor-specific drug responses as well as tumor diversification *ex vivo* (Lee, Hu et al. 2018, Roerink, Sasaki et al. 2018). This is of special interest as it is evident that chemotherapy should not only be patient-specialized but also tumor or even cell-specific as "clonal" tumors show massive cellular diversity (Roerink, Sasaki et al. 2018). Pharmaceutical companies might incorporate organoids frequently in the future for toxicity testing but also in specific drug screening in patient-derived malignant tissue (Astashkina and Grainger 2014, Bulin, Broekgaarden et al. 2017, Kondo, Ekawa et al. 2018). Developments like this are very likely, as advantages of primary cells in comparison to conventional cell culture are evident and mice cannot be used for all experiments as they don't resemble all key aspects of human physiology (Leist and Hartung 2013).

Moreover, organoids have been shown, at least in a proof of principle study to function as a scaffold for transplantation. In mice, intestinal organoids were successfully transplanted into dextran sulfate sodium (DSS) -treated mice where they were able to restore damaged epithelium over 4-6 weeks (Yui, Nakamura et al. 2012).

Human colonoids (colon derived organoids) have been used to study the effects of investigational drugs in mucosal healing in an ulcerative colitis (UC)-like model (Nishimura, Shirasaki et al. 2019).

Additionally, with ever-expanding technologies and increasing computational power, systems biology is finding its way in the organoid field, opening completely new areas of investigation with unequaled depth of information (Lindeboom, van Voorthuijsen et al. 2018). Furthermore, as conventional 2D-culture tested drug-candidates fail in clinical trials, 3D organoids may also have a bright future ahead in this regard (Horvath, Aulner et al. 2016).

3.2.5 Perspectives of organoid research and ethical considerations

Together with genome-editing, organoids are seen by some as the future of personalized medicine (Sachs and Clevers 2014, Yin, Mead et al. 2016, Drost and Clevers 2017, Dutta, Heo et al. 2017). However, cultivation costs, residues from animal products and operating expenses are currently the largest drawbacks (Bartfeld and Clevers 2017, Drost and Clevers 2017). Moreover, before organoids really enter the clinics on a broad scale, society has to understand and accept the possible questions and perturbations this technology may cause (Figure 10) (Bredenoord, Clevers et al. 2017).

Together with specific genome editing there is the theoretical potential to “correct” genetic disorders and generally speaking “re-create” humanity to some extent. These topics require not only scientific and financial debates about feasibility and costs but more importantly ethical discussions on how far mankind wants to push this technology and field of science. In order to get a more or less binding vote, outcomes of this open debates should be manifested by EU or even better UN-law, as for example included in the human rights.

Moreover, cultivation of patient-derived organoids in complex setups of various organ-like structures on a chip, re-creating a human model-system, should give rise to further thoughts and limitations of organoid research (Sun, Luo et al. 2019).

Nevertheless, organoids harbor great potential to help improve specific treatment of patients. In order to do so, one is still in need to develop more techniques to quantitatively assess changes in organoids induced e.g. by chemotherapy, as only a few methods are described so far (Boehnke, Iversen et al. 2016, Grabinger, Delgado et al. 2016).

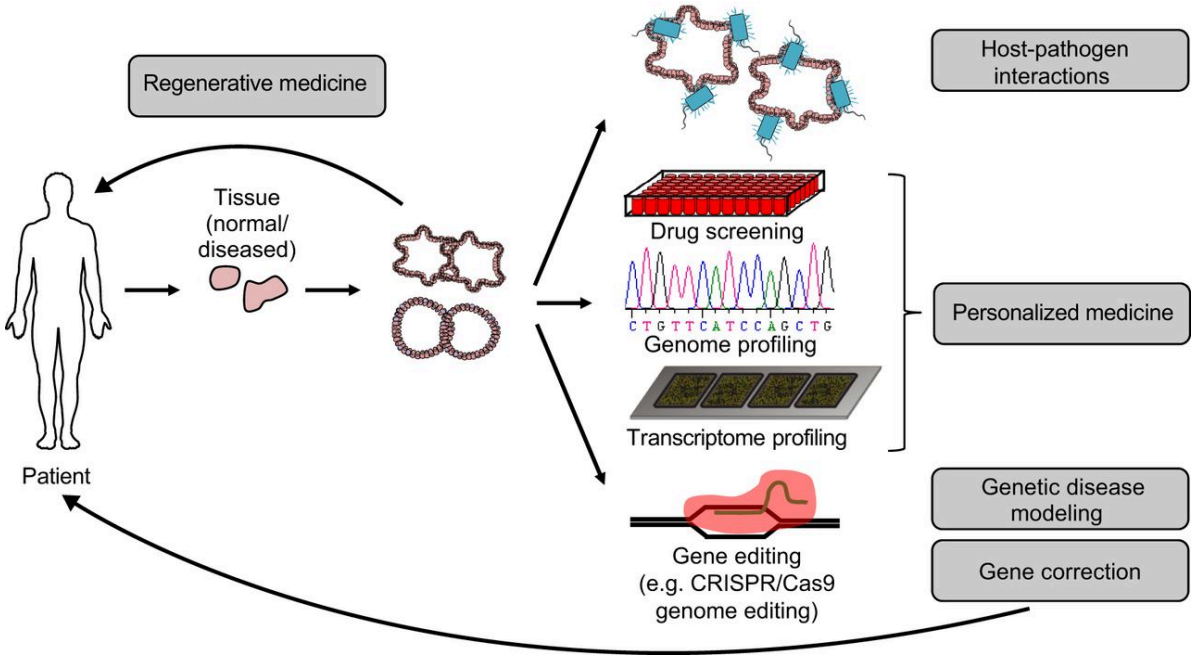

Figure 10: Future applications of organoid technology

Future applications of organoid technology ranging from basic research, as depicted by host-pathogen interactions, to applied research. Here, personalized medicine is the biggest area of application. Organoid usage ranges from specific treatment plans adapted to expression and transcriptome profiling, to directed drug screening. Moreover, genome editing opens the possibility for *ex vivo* gene correction and re-transplantation of corrected tissue. Figure adapted from (Drost and Clevers 2017).

3.3 TNF-signaling

TNFα has been described as a factor being able to induce necrosis in tumor cells (Carswell, Old et al. 1975). By now, more than a dozen ligands of the TNF receptor (TNFR) superfamily are described (Wajant, Pfizenmaier et al. 2003). All of them initiate pro-inflammatory signaling. TNF, by itself exists both in a soluble and a membrane bound form. Both versions fulfill different functions, as soluble TNF can access all areas of the body whereas membrane

bound TNF is restricted to cell-cell based interactions. Both forms of TNF are found as homo-trimers. A key feature to activate TNFR-signaling (Grell 1995).

Upon binding of TNF to its receptor two different signaling platforms can arrange, namely complex I and complex II which fulfill distinct functions. Simplified, complex I-formation is the principal TNF-response, leading to NFκB-activation. In TNF-signaling, complex I is comprised of TNFR-associated death domain (TRADD), TNFR-associated factor-2 (TRAF2), cellular inhibitor of apoptosis 1 and 2 (cIAP1& 2), the linear ubiquitin chain assembly complex (LUBAC), and the receptor interacting serine-threonine kinase 1 (RIPK1) (Micheau and Tschopp 2003). Opposing this, complex II forms secondarily, resulting in apoptosis. Here, TRADD detaches from the TNFR and binds to Fas-associated protein with death domain (FADD). Additionally, pro-cysteine-dependent aspartate-directed protease 8 (pro-caspase 8), and cellular FLICE-inhibitory protein (cFLIP) are being recruited, forming the complex IIa (Lavrik, Mock et al. 2008, Wang, Du et al. 2008, Ting and Bertrand 2016). Furthermore, yet another variation of complex II, namely complex IIb, also termed the Necrosome, can be formed, which will eventually lead to necroptosis (Vandenabeele, Declercq et al. 2010, Delgado and Brunner 2019).

3.3.1 Receptor types

TNFα has two major receptors, namely TNFR1 and TNFR2. Soluble TNF mostly binds and activates TNFR1, whereas membrane bound TNFα can activate both TNFR1& 2. By binding to TNFR1, TNFα can induce NFκB-, mitogen activated kinase (MAPK)-signaling and apoptosis (Wajant, Pfizenmaier et al. 2003). Binding to TNFR2 was thought not to play a role in apoptosis induction, as the receptor lacks the death domains. However, it was reported that if TNFR2 was overexpression in HeLa cells, these would solely respond to TNFR2 activation (Bigda, Beletsky et al. 1994).

Generally, TNFR1 signaling is well characterized, whereas the role and physiological as well as pathophysiological function of TNFR2-signal still remains to be fully elucidated. Experimentally, murine TNFR1, can be selectively triggered by human TNFα (hTNFα) which specifically binds to the latter. Murine TNFR2 on the other hand can be activated by a recombinant nonameric version of murine (m) TNFα, termed “selective TNF-based agonist of

receptor 2" (STAR2) - mimicking a membrane bound version of mTNFα (Rauert, Wicovsky et al. 2010, Fischer, Maier et al. 2011, Lang, Fullsack et al. 2016).

3.3.2 Role in inflammation

TNFα is a key pro-inflammatory cytokine (Mannel and Echtenacher 2000). Activation through NFκB and MAPK-signaling result in the upregulation of various pro-inflammatory target genes, including TNFα itself (Hayden, West et al. 2006). Moreover, TNFα is critically involved in numerous chronic inflammatory disorders, such as IBD (Maloy and Powrie 2011) or rheumatoid arthritis, where neutralizing antibodies are being used to ameliorate TNFα-induced tissue damage (Sode, Vogel et al. 2014). Bacterial lipopolysaccharides (LPS) were found to stimulate glucocorticoid-production via TNFα (Noti, Corazza et al. 2010).
In turn, TNFα, was also described to "suppress acute intestinal inflammation by inducing local glucocorticoid synthesis" (Noti, Corazza et al. 2010).

3.3.3 The role of TNF in the intestine

In the intestine, TNFα has a special role as it can directly induce apoptosis of intestinal epithelial cells by itself. A capability that is unpreceded in other tissues where TNFα will mostly lead to activation MAPK- and NFκB-signaling (Piguet, Vesin et al. 1999). Due to its important role in regulation of the inflammatory state in IBD, therapeutic antibodies are being used to block TNF, but also IL-6, another crucial pro-inflammatory cytokine (Atreya and Neurath 2008). Unlike other tissues, in the intestine, levels of cellular Inhibitor of Apoptosis 1 (cIAP1) determine, whether an intestinal epithelial cell will undergo cell death or survive upon encounter with TNF (Grabinger, Bode et al. 2017). This is of major importance, as TNFα as well as IAPs play a crucial role in pathophysiological IBD conditions (Maloy and Powrie 2011, Pedersen, LaCasse et al. 2014). Importantly, TNF can also contribute to an anti-inflammatory response by inducing local glucocorticoid production, and to differentiation as well as proliferation in the intestinal epithelium (Cima, Corazza et al. 2004, Mueller, Cima et al. 2006, Delgado and Brunner 2019).

3.3.4 Inhibitor of Apoptosis Proteins

Inhibitor of apoptosis proteins (IAPs) were discovered in baculovirus. Here, IAPs were found to work as caspase inhibitors (Gyrd-Hansen and Meier 2010). In mammals, cIAP1 and 2, X-linked IAP (XIAP), neuronal IAP (NIAP) and Survivin have been described (Silke and Vucic 2014). XIAP is well-known to block effector cysteine-dependent aspartate directed proteases (caspases), whereas cIAP1/2 interfere with NFκB –activation and cell death induction through their E3 domain, ubiquitinating thereby target proteins and leading to their subsequent proteasomal degradation (Bertrand, Milutinovic et al. 2008, Mahoney, Cheung et al. 2008, Silke and Vucic 2014). Second mitochondria-derived activator of caspases (Smac), a mitochondrial protein, and caspase 8 can bind to IAPs and block their death-inhibitory potential. Thus, great efforts have been made in order to generate small molecules targeting IAPs, to push cell death - especially, in cancer, an often-desired scenario (Varfolomeev, Blankenship et al. 2007, Vince, Wong et al. 2007). These, so called “Smac-mimetics” target the baculoviral repeat (BIR) domains and lead to autoubiquitination and subsequent proteasomal degradation of IAPs (Wang 2011, Sun, Lu et al. 2014, El-Mesery, Shaker et al. 2016). The most prominent small molecule IAP inhibitors, such as LCL161 or BV6 are widely used in research and have been tested in clinical studies mostly against multiple myeloma (Weisberg, Ray et al. 2010, Bai, Smith et al. 2014, Balakrishnan, Fu et al. 2016). The efficacy of Smac-mimetics has additionally been shown in cell lines from solid tumors, such as breast or pancreatic cancer (Hannes, Abhari et al. 2016). In these conditions however, it is on the molecular level only partly understood how Smac-mimetics lead to cell death (Schmidt, Kowald et al. 2019).

3.4 Cell death

Cell death is crucial in the life of any multicellular organism. For example, in *Caenorhabditis elegans*, a nematode, 131 cells die programmed during development (Peden, Killian et al. 2008). In mammals, the immune system is in part regulated by cell death, to prevent the development of autoreactive lymphocytes and overshooting immune responses (Owen and Jenkinson 1992, Brunner, Mogil et al. 1995). Moreover, cell death is crucial in the homeostasis of the intestinal epithelium (Delgado, Grabinger et al. 2016). On the other hand, in tumors, malignant cells often find ways to escape the intrinsic capacity to undergo cell death (Igney

and Krammer 2002). However, a cell has many ways to die (Galluzzi, Vitale et al. 2018). Until today, more than ten forms of regulated cell death have been described, which contribute to different extents to the tightly regulated homeostasis of multicellular organisms (Figure 11).

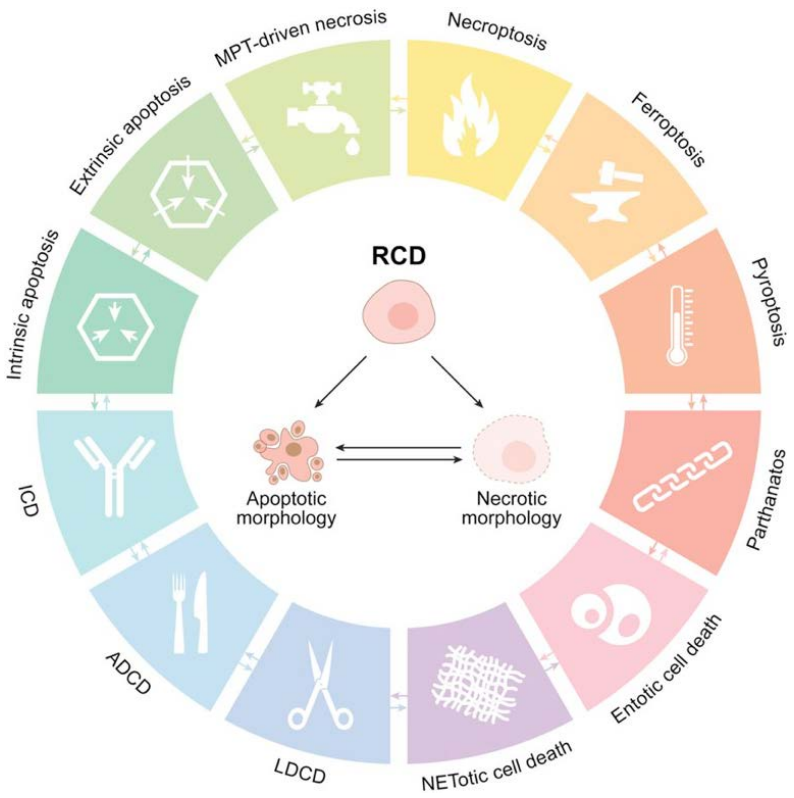

Figure 11: Different forms of Regulated Cell Death

Overview of the current ten described forms of regulated cell death. Forms of cell death with necrotic phenotype are depicted on the right side of the circle, whereas apoptotic phenotypes are depicted on the right. Figure adapted from (Galluzzi, Vitale et al. 2018)

3.4.1 Apoptosis

Apoptosis is a highly-regulated, energy dependent, and highly controlled form of cell death occurring in all multicellular organisms. It plays a crucial role during embryonic development as well as in normal physiology and is found altered in several pathophysiological conditions, most prominently in cancer (Igney and Krammer 2002, Elmore 2007). During apoptosis, cells undergo cell shrinkage and membrane blebbing, accompanied by the condensation of the nucleus (pyknosis) followed by the fragmentation of the nucleus (karyorrhexis) leading to so called apoptotic bodies. By displaying various phagocytotic molecules (“eat-me signals”), like phosphatidylserine on the surface, apoptotic bodies attract macrophages and neutrophils to

be taken up by those cells (Li, Sarkisian et al. 2003, Ravichandran 2011). Molecularly, apoptosis depends on the activation of a specific type of proteases, so called caspases (Galluzzi, Lopez-Soto et al. 2016). Activation of effector caspases, especially caspase 3, is considered a characteristic feature of apoptosis. Active caspase 3, has a multitude of well characterized targets, such as inhibitor of caspase-activated DNAse (ICAD). Removal of ICAD through caspase 3 results in the release of caspase-activated DNAse and subsequent DNA fragmentation (Enari, Sakahira et al. 1998). Moreover, caspase 3 activation induces the cleavage of poly(ADP-ribose) polymerase (PARP) and indirectly lamin A (Lazebnik, Kaufmann et al. 1994, Ruchaud, Korfali et al. 2002), and leads to the "flipping" of phosphatidylserine to the outside of the cell membrane (Mandal, Mazumder et al. 2005). Together, these events represent relevant processes in the execution of apoptosis – all of which can be detected for cell death analysis (Elmore 2007).

However, to start with, apoptosis in cells, can be initiated by two major pathways, being the intrinsic and the extrinsic pathway (Bohm and Schild 2003).

The intrinsic pathway

The intrinsic pathway is mainly triggered by toxins, viral infections, chemo- or radiation-induced DNA damage leading to p53 mediated-damage response and activation of Bcl-2 family members (Miyashita and Reed 1995). These can be further divided into pro- (Bax, Bak) and anti-apoptotic (Bcl-2, Bcl A1, Mcl-1 Bcl-w, Bcl-xL) Bcl-2 family members as well as sensitizers, also referred to as BH3-only proteins (Bid, Bim, Bad, Puma, Noxa, and others) (Volkmann, Marassi et al. 2014). Moreover, general cell-stress related signaling pathways, such as MAPK/extracellular signal-regulated protein kinase (ERK)-signaling, NF-κB-signaling, and c-Jun N-terminal kinase (JNK)-signaling are related to the intrinsic apoptosis pathway (Xia, Dickens et al. 1995, Davis 2000, Karin, Cao et al. 2002). How these stress-related pathways are molecularly interconnected with the intrinsic pathway of apoptosis is still an ongoing field of research (Tournier, Hess et al. 2000, Dhanasekaran and Reddy 2008, Win, Than et al. 2018). Eventually, the intrinsic pathway will lead to mitochondrial outer membrane permeabilization (MOMP), followed by cytochrome c and Smac/direct IAP binding protein with low pI (DIABLO) release (Goldstein, Waterhouse et al. 2000), recruitment of apoptotic protease activating factor 1 (Apaf1) and pro-caspase 9, resulting in the apoptosome complex (Acehan, Jiang et al.

2002). Activated caspase 9 will further activate effector caspases such as caspase 3/7 (Lakhani, Masud et al. 2006).

The extrinsic pathway

The extrinsic pathway, as the name implies, is initiated by extracellular molecules binding to "Death receptors" belonging to the TNFR superfamily. Fas ligand (FasL), TNF, TRAIL, TWEAK (TNF-related weak inducer of apoptosis) are all ligands targeting receptors from TNFR superfamily. By doing so, receptors and downstream associated proteins, are multimerizing (Dickens, Powley et al. 2012). Subsequently, depending on the receptor being targeted, complex I (NFκB-activation) or II (apoptosis induction) in the case of TNFR activation (see also 3.3), or death inducing signaling complex (DISC), in the case of Fas receptor (FasR), are being formed (Dickens, Powley et al. 2012). Through interaction via death domains (DD) adapter molecules, such as Fas-associated protein with death domain (FADD), or tumor necrosis factor receptor type 1-associated DEATH domain protein (TRADD) will be recruited (Scott, Stec et al. 2009). These in turn will recruit initiator pro-caspase 8 via death effector domains (DED), leading to cleavage and activation of pro-caspase 8 (Kischkel, Hellbardt et al. 1995). Activated caspase 8 will subsequently cleave and thereby activate effector caspases, such as caspase 3 and caspase 7 (Riedl and Shi 2004). However, caspase 8 can also crosslink the intrinsic and the extrinsic pathway by cleaving Bid, resulting in truncated Bid (tBid), which then triggers MOMP through the activation of Bax/Bak (Li, Zhu et al. 1998). This crosstalk is essential to induce apoptosis in so-called "type II cells", such as hepatocytes. Cells, such as lymphocytes, which do not require Bid cleavage and subsequent MOMP in addition to an extrinsic death receptor stimulus are consequently referred to as "type I cells" (Scaffidi, Schmitz et al. 1999, Jost, Grabow et al. 2009).

3.4.2 Necrosis

Necrosis represents another form of cell death. In contrast to apoptosis it is often referred to as "uncontrolled" (Farber 1994). Thus, necrosis can be induced by physical damage, like mechanical or osmotic stress (Proskuryakov, Konoplyannikov et al. 2003, Broker, Kruyt et al. 2005). Necrosis is morphologically different to apoptosis. Specifically, membrane rupture and the release of cellular contents to the extracellular space is characteristic for this form of cell

death. This mainly induces an inflammatory response, by attracting surrounding immune cells, which will cause further cellular damage in the surrounding tissue (Rock and Kono 2008).

3.4.3 Necroptosis and others

Necroptosis has been established as an important form of cell death in development, the immune system as well as inflammatory response (Welz, Wullaert et al. 2011, Zhang, Zhou et al. 2011, Dillon, Weinlich et al. 2014, Rickard, O'Donnell et al. 2014). Necroptosis is a form of programmed cell death which is dependent on Receptor-interacting serine/threonine-protein (RIP)-Kinases 1 and 3, as well as mixed-lineage kinase domain-like pseudokinase (MLKL) (Green, Oberst et al. 2011). More specifically, it was shown that the kinase activity of RIPK-1 is necessary for RIPK-3 dependent necroptosis (Vanden Berghe, Linkermann et al. 2014). However, there are also studies showing that RIPK-1 can function as a scaffold, less dependent of its kinase activity to regulate RIPK-3 driven necroptosis (Dannappel, Vlantis et al. 2014). Experimentally, necroptosis is observed in cell culture when caspases are inhibited, for example with the pan-caspase Inhibitor N-benzyloxycarbonyl-Val-Ala-Asp-fluoromethylketone (zVAD-fmk), possibly also dependent on autocrine production of TNFα (Wu, Tan et al. 2011, Kim and Li 2013, Yuan, Najafov et al. 2016, Shan, Pan et al. 2018).
In vitro, Necroptosis can be blocked by selective targeting of the RIP-1/RIPK-1 complex by Necrostatin-1 (Nec-1) (Degterev, Hitomi et al. 2008, Cho, McQuade et al. 2011). Moreover, several distinct forms of regulated cell death have been described, as depicted in Figure 10. However, most of these only occur in very special circumstances and show either an apoptotic or a necrotic morphology (Bohm and Schild 2003). Recently, yet another form of cell death has been discovered. This caspase-independent process, which was found to be induced by reactive oxygen species (ROS) has been termed “Oxeiptosis” (Holze, Michaudel et al. 2018).

3.5 Cell death detection assays

The abovementioned forms of cell death can be analyzed by different methods. Some of these methods are more specific than others to be able to discriminate between different forms of cell death. However, multiple methods need to be combined in order to precisely determine, what sort of death a cell of interest undergoes. Classically, changes in cell morphology, as well as nuclear condensation can be observed by light microscopy or more elaborate microscopic

methods (Muppidi, Porter et al. 2004). Moreover, changes in cell surface markers can be detected via flow cytometry or fluorescence microscopy (van Engeland, Nieland et al. 1998). On protein level, upregulation of pro- and anti- apoptotic proteins as well as sensitizers can be observed (He, Huang et al. 2016). Furthermore, activation of pro- and effector caspases can be detected with classical Western Blot or plate reader-based fluorescence probes (Kaufmann, Lee et al. 2008). DNA fragmentation can be detected by a simple agarose gel, as well as by TUNEL assay (Loo 2011, Banfalvi 2017). Additionally, intracellular substances such as Lactate Dehydrogenase (LDH) (Chan, Moriwaki et al. 2013) or Cytokeratin 18 can be used to investigate cell death (Krysko, Vanden Berghe et al. 2008). More indirect ways to measure cell death are levels of intracellular ATP, (Boehnke, Iversen et al. 2016, Francies, Barthorpe et al. 2016) crystal violet absorbance (Feoktistova, Geserick et al. 2016), as well as intracellular 3-(4,5-dimethylthiazol-2-yl)-2,5-diphenyltetrazolium bromide (MTT)-reduction capacity (Lobner 2000). The latter has been described to work for intestinal organoids as well (Grabinger, Luks et al. 2014, Grabinger, Delgado et al. 2016).

3.6 Nuclear dyes

Nuclear dyes have been used throughout the last millennium and have enabled major discoveries in cell biology. Gentian violet as one of the first nuclear dyes being used, is still in everyday application as the famous gram-staining for bacteria as well a fast option to study eukaryotic cell viability (Ohlmacher 1897, Russell 1914, Feoktistova, Geserick et al. 2016). Today, a multitude of nuclear dyes is available, staining DNA on different sites, with properties such as membrane permeability or light emission with wavelengths nearly over the whole spectrum of visible as well as UV and near-IR light. This enormous dye diversity together with ever co-evolving analysis-instruments enabled the study of chromatin rearrangements, chromosomal segregation, nuclear morphology or counting the number of nucleated cells (Barbier, Nowlan et al. 2012, Kilgore, Dolman et al. 2013). In the following, two examples are explained in more detail, as they have been used primarily throughout this work.

3.6.1 Hoechst

Hoechst dyes have a history of more than five decades staining nucleic acids (Latt, Stetten et al. 1975). Today, a multitude of Hoechst variants exist, which all have their unique

fluorescence spectra. Figure 12, shows one example, Hoechst33342, the dye that has been used throughout this thesis. The cell membrane permeable dyes exhibit blue fluorescence upon binding to DNA. Thus, Hoechst has been used to examine DNA structure and amount microscopically as well as with flow cytometry (Downs and Wilfinger 1983, Sterzel, Bedford et al. 1985). All Hoechst dyes are derived from bisbenzimidazole and are selective for Adenine-Thymine (AT) in the minor-groove of DNA (Portugal and Waring 1988).

Moreover, Hoechst is used to determine a subset of cells – mostly stem cells – which are able to actively efflux the dye. These type of cells are known as the "side population" and can also be found in some cancers (Wu and Alman 2008). However, whenever using fluorescent DNA dyes, one has to be aware of the fact that all dyes will show fluorescence even when not bound to DNA. Furthermore, application of increasing concentrations of the dyes, can shift the fluorescence spectra mostly to a longer wavelength (Asbury, Esposito et al. 1996).

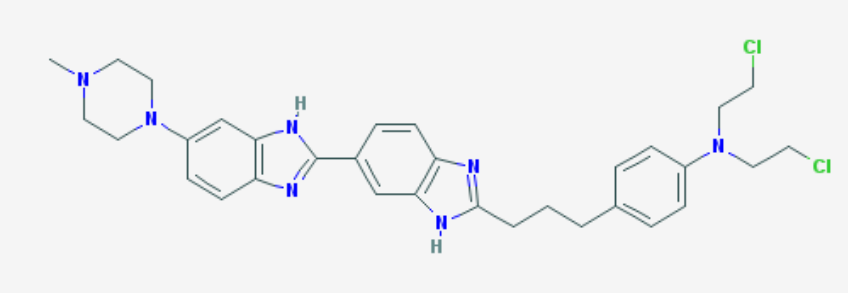

Figure 12: Hoechst33342 structure (https://pubchem.ncbi.nlm.nih.gov/)

3.6.2 Propidium Iodide

Propidium Iodide (PI) also stains nucleic acids (Figure 13 shows the structure of PI). However, in contrast to Hoechst dyes, PI is not able to pass an intact cell membrane. Therefore, PI has been largely used to discriminate apoptotic from necrotic cells (Darzynkiewicz, Bruno et al. 1992). Binding predominantly to Guanine-Cytosine (GC) bases, PI stains both RNA and DNA. Thus, tissue harboring large amounts of RNA, mostly show a cytoplasmic PI stain on top of the nuclear stain (Suzuki, Fujikura et al. 1997).

Nevertheless, Propidium Iodide has been used for a long time (Rieger, Nelson et al. 2011) and is still used today in flow cytometry to investigate cell death (Lincoln, Imig et al. 2018). Moreover, PI staining is used to discriminate between apoptosis and necroptosis in cell culture (Pietkiewicz, Schmidt et al. 2015).

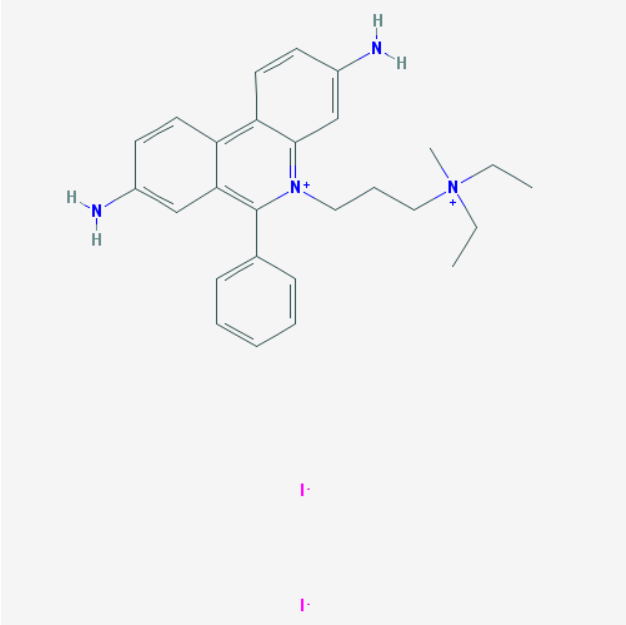

Figure 13: Propidium Iodide structure
https://pubchem.ncbi.nlm.nih.gov/

3.7 Chemotherapeutic drugs

In this study, the following two classical chemotherapeutic drugs have been used to induce cell death. However, any other chemotherapeutic drug or general cell death inducing compound could have been used, as only the outcome – cell death – was of interest in this study, not how the cells die.

3.7.1 Cisplatin

Cisplatin has been used for more about 50 years as a chemotherapeutic drug in a wide number of cancer types (Rancoule, Guy et al. 2017). Still, apart from crosslinking purine bases of DNA, its molecular mode of action is not entirely understood (Dasari and Tchounwou 2014). Thus, research of this highly prescribed chemotherapeutic drug is ongoing, approaching improved cancer targeting, reduced side-effects, basic molecular understanding as well as circumventing resistance formation (Hardie, Kava et al. 2016).

As all chemotherapeutics, cisplatin has several side-effects, ranging from nausea and hearing problems, to kidney failure and bone marrow suppression (Oun, Moussa et al. 2018).

3.7.2 5-Fluorouracil

Fluorouracil (5-FU) has been used for nearly 60 years, both systemically, but also topically (Heidelberger, Chaudhuri et al. 1957, Moore 2009). As an antimetabolite, 5-FU inhibits the thymidylate synthase (TS) and incorporates its metabolites into RNA and DNA (Longley, Harkin et al. 2003). Thus, 5-FU, as part of a combination of several drugs is a widely used chemotherapeutic, especially in colorectal cancer (Gamelin and Boisdron-Celle 1999, Saam, Critchfield et al. 2011). In addition to classical side-effects of chemotherapeutic drugs, treatment with 5-FU can lead to mania (Ha, Hwang et al. 2011).

4. Aim of the study

Organoids, as three-dimensional organ-like structures, comprising various primary epithelial cell types, resemble physiological key functions more closely than conventional two-dimensional cell culture. Thus, they are of interest for many research areas, bridging cell culture, animal experiments, and human patients. Since organoids can be grown from nearly all tissue types, biopsies enable the understanding of tissue-and even patient-specific physiological and pathophysiological conditions. In order to accurately analyze organoids with respect to drug treatments or genetic changes, adequate measurement technologies need to be available. Therefore, the aim of this thesis was to implement organoids as a test system for intestinal cell stress and cell death by establishing novel techniques to quantitatively measure intestinal cell death *ex vivo*. Therefore, at first the TNF-induced cell death was investigated in intestinal epithelial cells. Moreover, a fast and cheap fluorometric method, using the nuclear dyes Hoechst33342 and Propidium iodide to quantify organoid cell death was designed. PI, as a membrane-impermeable dye, only stains cells with a disintegrated membrane, whereas Hoechst, a membrane-permeable dye stains all cells serving as an internal normalization to total DNA. Generally, a simple technique was developed, which can be performed in any lab with organoid culture experience. With this, the aim was to support both basic research questions in the field of cell death, as well as analysis of patient material in mid- to large-scale screening approaches, drug development, toxicity testing, or individualized chemotherapy. Additionally, organoid technology was combined with a state-of-the-art quantitative protein detection method.

5. Results

5.1 Generation and development of murine intestinal organoids

Murine Organoids were generated as described previously (Grabinger, Delgado et al. 2016). In brief, C57BL/6 mice were sacrificed and the small intestine was removed, cut open and the villi removed by scraping with a microscope slide. Intestinal fragments were washed with cold PBS and subsequently incubated with 5 mM EDTA in PBS for 30 minutes. Then, the supernatant was exchanged to fresh PBS and the intestinal fragments were shaken several times to isolate crypts. Crypts were then seeded in Matrigel or basement membrane extract (BME) and cultured in complete crypt culturing medium. At the first day after isolation, crypts show rounded morphology and form spheres. Already at the second day, daughter cells give rise to new "crypt-like" regions start to form ("bud out") from the initial sphere, which continues with further cultivation (Figure 14). Growth and budding of intestinal organoids will continue over time. If being passaged, primary organoids can be kept in culture for long time periods (Matsui, Matsubayashi et al. 2018). In accordance with previous studies (Fatehullah, Appleton et al. 2013) we could show, by staining the epithelial actin-rich brush boarder with phalloidin (red), that primary murine intestinal organoids show polarization as observed *in vivo* (Figure 15).

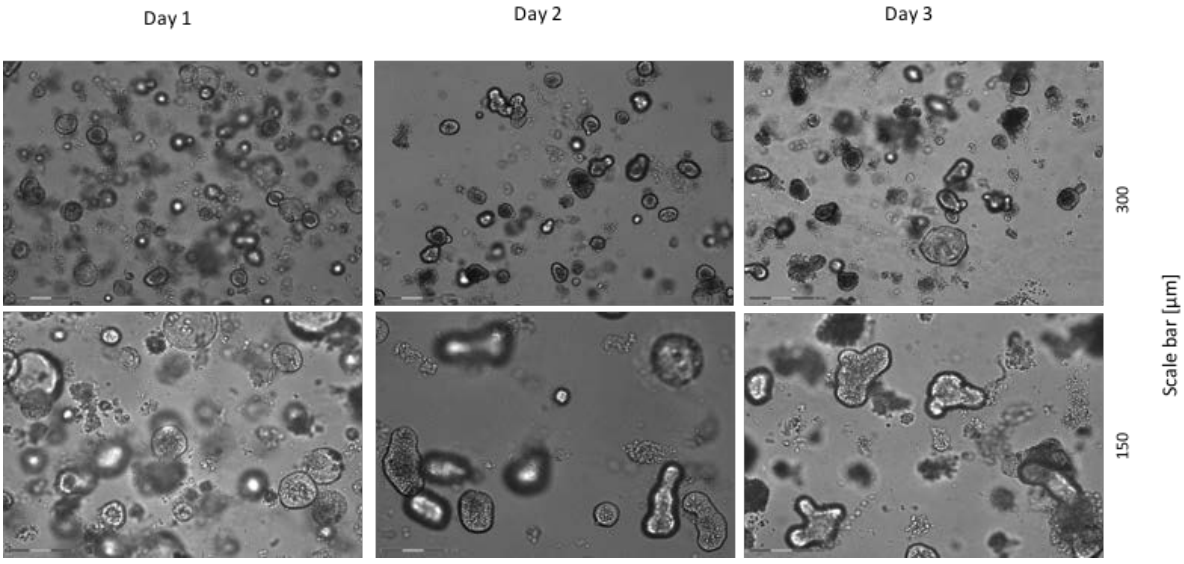

Figure 14: Growth of murine intestinal organoids

Brightfield images of isolated crypts with round morphology and sphere formation after one day of incubation in Matrigel. From day 2, after isolation, onwards, organoids grow and form new "crypt-like" regions. The classical morphology of murine small intestinal organoids can be observed at day 3 with fully developed microarchitecture, such as the novel "crypt-like" and interspaced "villus-like" regions. Scale bar: upper lane=300 µm, lower lane: 150 µm.

In fully developed intestinal organoids, enterocytes are facing with their brush-boarder to the apical side (inside) of the organoid lumen, whereas the nuclei (Hoechst staining= blue) are found at the basolateral side (Figure 15).

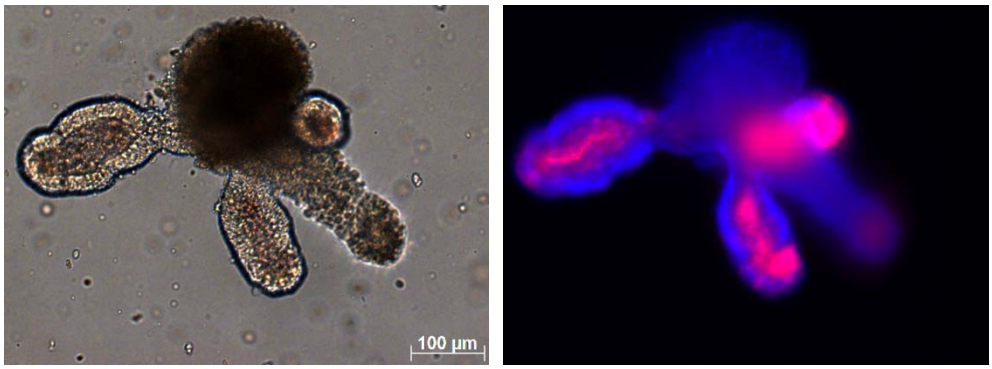

BF Hoechst Phalloidin

Figure 15: Murine intestinal organoids are polarized

Brightfield (BF) and fluorescence microscopic images from murine intestinal organoids show polarity similar to the structure of intestinal tissue *in vivo*. Phalloidin (red)-staining shows actin-rich brush boarders of epithelial enterocytes face the apical side of the organoid lumen. Cellular nuclei are stained Hoechst (blue). BF= brightfield. Scale bar= 100µm.

In vivo, intestinal epithelial cells are already being shed into the intestinal lumen after 3-5 days and subsequently transported out of the organism with the stool (Park, Kotani et al. 2016). However, in intestinal organoids, which resemble a closed system, dead cells accumulate in the lumen over prolonged cultivation time. This can happen to such an extent that after proximately a week after isolation and seeding of crypts, organoids are made up of living and dead cells to equal amounts (Figure 16).

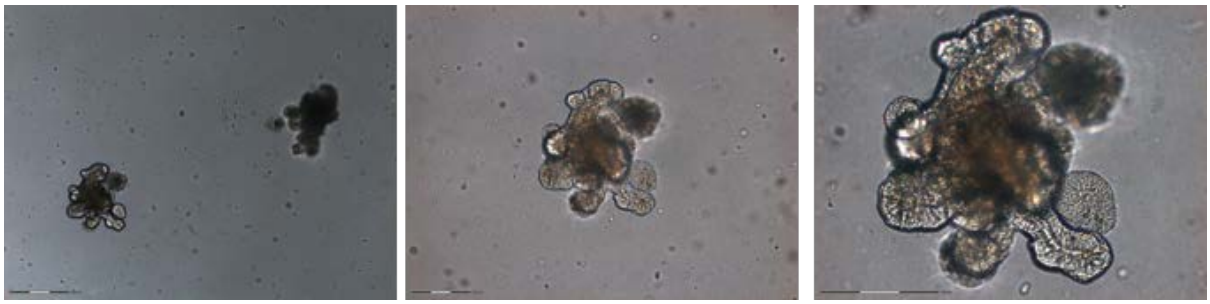

Figure 16: Murine intestinal organoids 7 days after crypt isolation

Brightfield images from murine intestinal organoids seven days after crypt isolation with medium exchange every other day. Scale bars show (from left to right): 300 µm, 150 µm, 75 µm.

5.2 Response of intestinal organoids to mTNFα treatment

Considering the increasing number of dead cells during organoid cultivation, organoids were analyzed at day one, two and three after crypt isolation. Therefore, organoids were treated overnight with increasing concentrations of mTNFα, as this cytokine was already known to exert cell death induction in primary intestinal epithelial cells (Piguet, Vesin et al. 1999, Grabinger, Bode et al. 2017). Specific organoid cell death was calculated the next day using the MTT reduction analysis. Here, independent of the time of treatment, intestinal organoids show a similar response to mTNFα-treatment (Figure 17). Only treatment after day three showed a lower overall cell death induction upon mTNFα-treatment.

This is again of importance, as cellular composition will relatively change over time of cultivation. The number of differentiated cells will proportionally increase compared to the $Lgr5^+$ ISCs and dead cells accumulating in the organoid lumen will contribute increasingly. Since it is still is not clear, which cells are most sensitive against mTNFα challenge, it was important to address this question here. With respect to signal to noise ratio from dead cells accumulating in the lumen, and thereby generating possible false positive signals, the time point of two or three days after isolation where chosen for all further experiments to treat organoids for cell death induction and analysis. Here, a good balance between overall cell number, leading to increased MTT reduction, and dead cells per total cells were obtained.

5.2.1 Comparison of different TNF variants

As described earlier, mTNFα can bind to both TNFR1 AND TNFR2, whereas hTNFα, only binds to TNFR1, and STAR2 a recombinant nonamer of mTNFα, binds selectively to TNFR2 (Rauert, Wicovsky et al. 2010, Fischer, Maier et al. 2011, Lang, Fullsack et al. 2016). In order to investigate whether one or the other TNFR plays a more important role in cell death induction in the intestinal epithelium, organoids from wild type (wt), $TNFR1^{-/-}$ and $TNFR2^{-/-}$ mice were treated overnight with increasing concentrations of mTNFα, hTNFα and STAR2. Specific cell death induction was calculated the following day with data obtained from a MTT reduction assay. Intestinal organoids generated from wt mice responded strongest to mTNFα treatment (Figure 18, A, upper panel). In contrast, treatment with hTNFα showed a reduced cell death induction, whereas STAR2 treatment was shown to have the lowest cell death induction capacity. Organoids generated from $TNFR1^{-/-}$ and $TNFR2^{-/-}$ mice displayed heterogeneous

response to all types of TNFα treatment (Figure 18 A, middle panel). Here, specific effects of TNFR1/2 in cell death signaling were not observed. However, overall assay performance was more inconclusive than in wt organoids. Furthermore, mRNA levels of TNFR1 and TNFR2 in freshly isolated crypts of wt, as well as TNFR1$^{-/-}$ and TNFR2$^{-/-}$ mice were analyzed. Here, wt mice display equal amounts of TNFR1/2. However, expression of TNFR2 in TNFR1$^{-/-}$ mice was shown to be elevated, whereas TNFR1 was not detectable. On the other hand, TNFR2$^{-/-}$ mice displayed no expression of TNFR1 and reduced expression of TNFR2, thus representing a phenotype resembling more of a double-KO of TNFR1 and TNFR2 (Figure 18, B).

Thus, until now, it is unclear which of the two receptor subtypes is more important in intestinal epithelial cell death induction.

Therefore, referring to Figure 18, A, both TNFR1 and TNFR2 play a role in TNFα induced cell death in the intestinal epithelium (Figure 18).

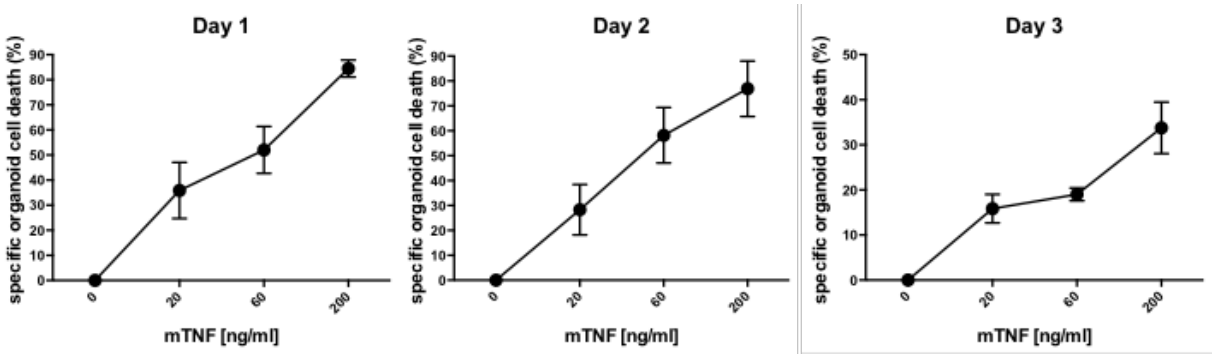

Figure 17: Cell death induction in intestinal organoids with mTNF

Organoids were treated at day 1, 2 and 3 after crypt isolation, with increasing concentrations of mTNFα overnight. Specific cell death was calculated the next day from MTT reduction potential of organoids. Dots represent mean ± standard deviation (SD) of three technical replicates. Representative data of two independent experiments are shown.

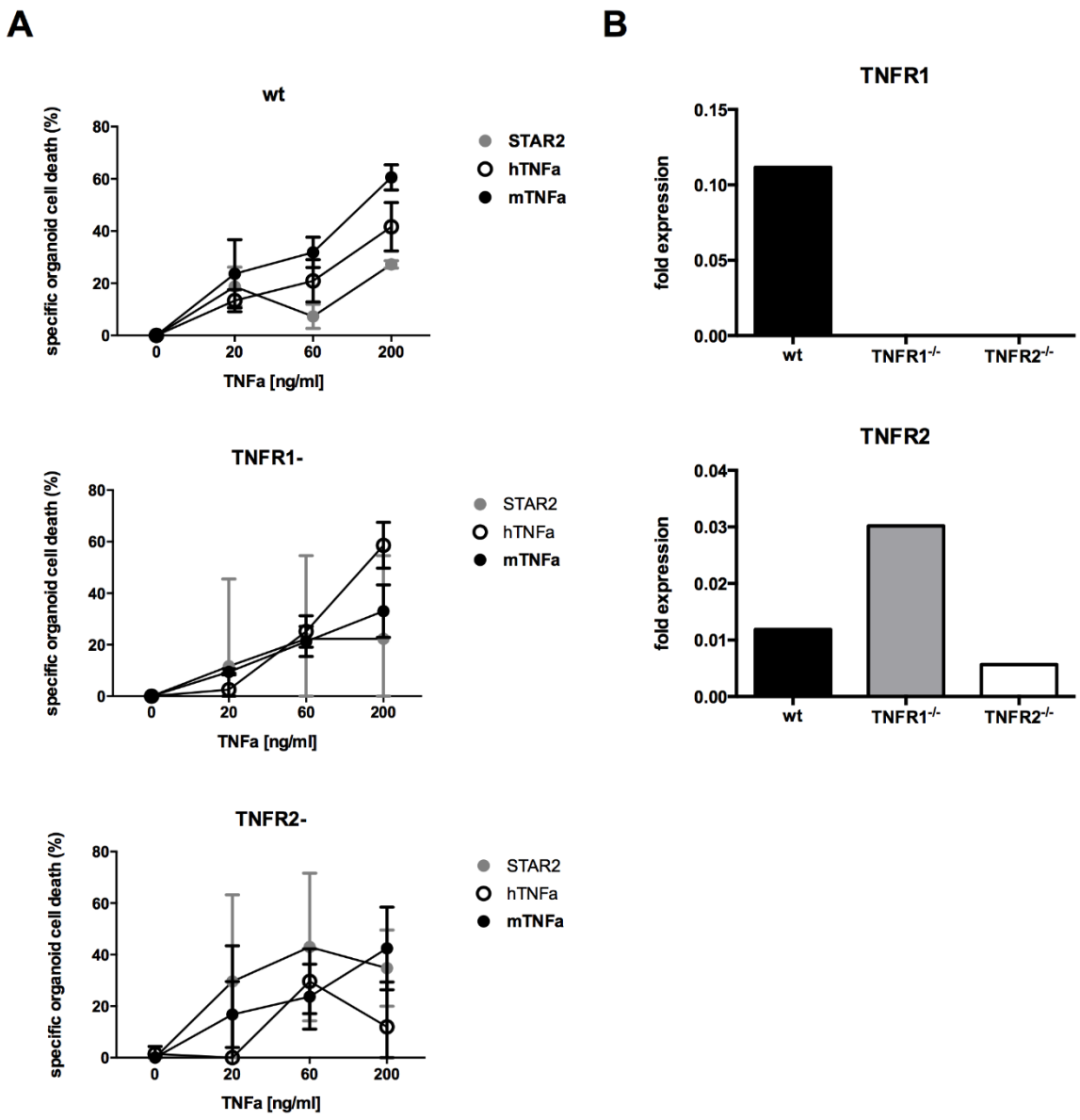

Figure 18: TNFR stimulation in intestinal organoids from wt, TNFR1-/-, and TNFR2-/- mice

(A) Organoids were generated from wt, TNFR1$^{-/-}$ and TNFR2$^{-/-}$ mice and treated with mTNFα, hTNFα or STAR2 at indicated concentrations. Specific organoid cell death was quantified from MTT reduction assay. Dots represent mean ± S.D. of three technical replicates. Representative data of two independent experiments are shown. (B) Expression of TNFR1 and TNFR2 in freshly isolated crypts from TNFR1$^{-/-}$ and TNFR2$^{-/-}$ analyzed with quantitative real time PCR. Fold expression was normalized to the reference expression of *Actb*.

5.2.2 The role of TNF and IAPs in cell death induction or survival in intestinal epithelial cells

TNFα not only exerts cell death induction but also activates the NFκB signaling pathway (Van Antwerp, Martin et al. 1996, Van Antwerp and Verma 1996, Piguet, Vesin et al. 1999). Therefore, the role of murine and human TNFα +/- LCL161 was analyzed with respect to NFκB-activation. Thus, MC38 cells were transfected with a NFκB-Luciferase reporter and treated with murine or hTNFα +/- LCL161 in order to assess their capacity in either cell death induction or activation of the NFκB signaling pathway.

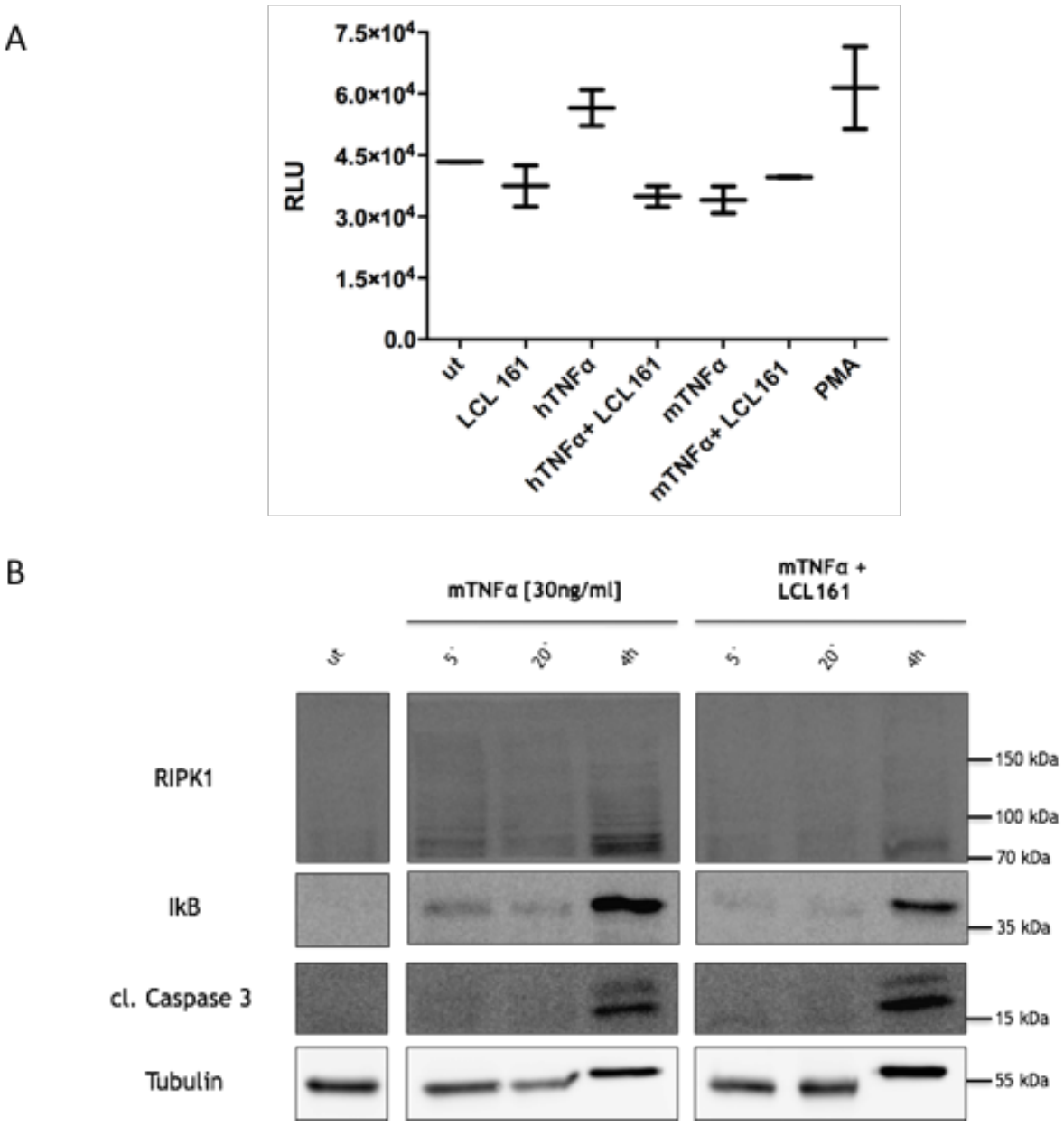

Figure 19: The Smac-mimetic LCL161 directs TNF-signaling towards cell death

(A) MC38 cells were transfected with NFκB-Luciferase reporter construct and treated with murine and hTNFα +/- LCL161 and relative luminescent units (RLU) recorded. (B) YAMC cells were treated with indicated concentrations of mTNFα +/- LCL161(2h pre-treatment) and PMA (Phorbol Myristate Acetate) as a positive control (Figure 19, A). Then, target proteins were analyzed by immunoblotting. Representative immunoblots of three independent experiments shown.

As reported recently, the protein level of cIAP1, a crucial regulatory protein in TNFα-induced cell death in the intestinal epithelium, is controlled by the SMAC mimetic LCL161 (Grabinger, Bode et al. 2017).

Treatment of transfected cells with hTNFα, led to increased RLUs, correlating with NFκB-activation. In contrast, combinatorial treatment of hTNFα and LCL161 led to a reduction of NFκB-activation, indicated an enhanced induction of the cell death pathway. This effect was not detected when cells were treated with mTNFα +/- LCL161 (Figure 19, A).

These observations were further analyzed in conditionally immortalized young adult mouse colon cell line (YAMC). Therefore, YAMCs were treated with +/- LCL161 for 5 and 20 minutes as well as for 4 hours. Cells were lysed after the indicated time points and proteins of interest were analyzed by immunoblot. Already after 5 and more prominently after 20 minutes, the NFκB –Inhibitor IκB was shown to be downregulated after mTNFα treatment. After 4 hours of treatment, IκB levels were drastically elevated. However, if cells were pre-treated with LCL161, the increase in IκB levels was impaired. Moreover, increased levels of cleaved caspase 3 were observed with the combinatorial treatment compared to the mTNFα treatment alone. Furthermore, an “ubiquitination smear” of RIPK1 was detected in mTNFα-treated YAMCs, but not in cells also treated with LCL161 indicating the proteasomal degradation of RIPK1 following mTNFα treatment (Figure 19, B).

In sum, these results indicate that TNF treatment alone initially induces the activation of NFκB and leads to cleavage of effector caspase 3. With the addition of the SMAC mimetic LCL161, NFκB activation was less prominent. Moreover, increased levels of cleaved caspase 3 were observed indicating enhanced cell death induction.

5.2.3 Cell death fate of intestinal epithelial cells after TNF-challenge

Until today, it is a highly-debated topic how intestinal epithelial cells die upon confrontation with TNF. As before mentioned, cIAP1 was discovered as a crucial regulator of TNF-induced intestinal epithelial cell death. Moreover, in large mouse studies, RIPK-1 was found to be essential in controlling intestinal homeostasis by hindering both apoptosis and necroptosis (Dannappel, Vlantis et al. 2014, Takahashi, Vereecke et al. 2014, Grabinger, Bode et al. 2017). Therefore, we investigated the death-inducing capacities of TNF in YAMC cells, by pharmacologically targeting RIPK-1. Thus, YAMCs were treated overnight in various combinations with mTNF, LCL161, the pan-caspase Inhibitor zVAD, Necrostatin-1 (Nec-1), and NaN_3 as a necrosis-inducing control. The next day, MTT-reduction capacity (Figure 20, A) and specific cell death (Figure 20, B) were assessed with the MTT-assay.

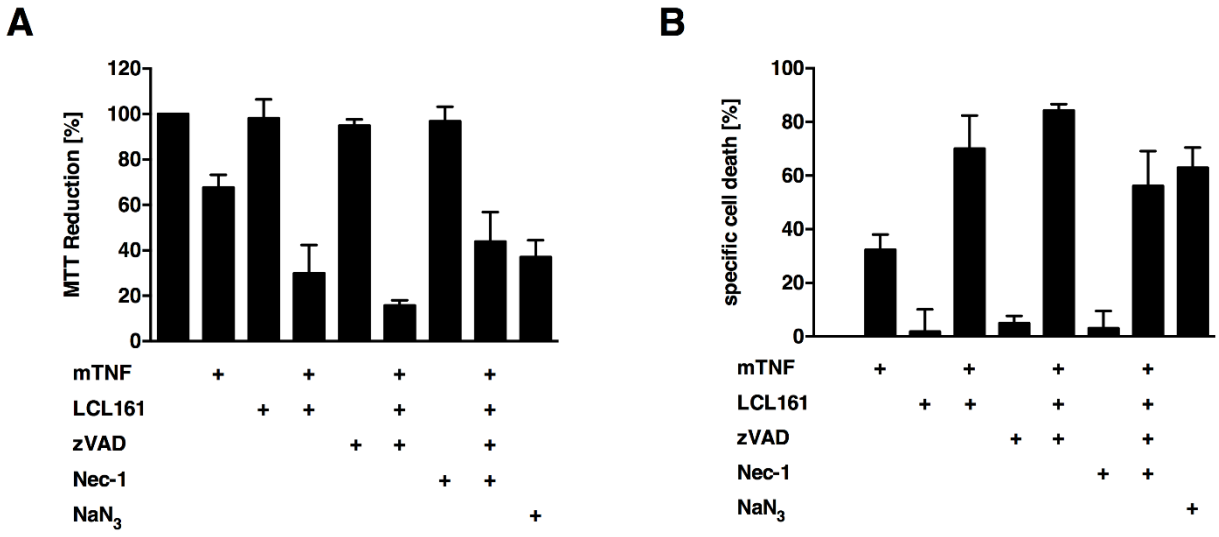

Figure 20: Blockage of caspases in TNF& LCL161-treated intestinal epithelial cells leads to necroptosis

YAMCs were treated with indicated combinations with mTNF (30 ng/ml), LCL161 (500 nM), zVAD (20 μM), Nec-1 (20 μM), and NaN_3 (20 mM) overnight. The next day, (A) MTT-reduction capacity and (B) specific cell death were analyzed using the MTT assay. Mean values of quadruplicates ± S.D. of three independent experiments are shown (unpaired *t*-test, untreated vs mTNF p=0,0006; mTNF vs mTNF+LCL p=0,0087; mTNF+LCL+zVAD vs mTNF+LCL+zVAD+Nec-1 p=0,0284).

Being used as single treatment, the small molecules LCL161, zVAD, and Nec-1 did not show an effect on MTT-reduction capacity or cell death induction (Figure 20, A& B). However, single treatment with mTNF lead to a contraction of MTT-reduction capacity and a corresponding increase of specific cell death as compared to the untreated control (Figure 20). Combined

with LCL161, mTNF treated YAMCs exhibited further diminished levels of MTT-reduction capacity and more increased levels of cell death induction were observed. If cells were additionally treated with zVAD on top of mTNF and LCL161, cell death would be elevated to 85-90%. At the same time, MTT-reduction capacity was correspondingly reduced to 10-15%. This strong cell death induction was ameliorated in cells which were also treated with Nec-1. Here, cell death was reduced to about 50% (Figure 20, B) and MTT-reduction capacity showed 50% of untreated control (Figure 20, A). In sum, the results show that pharmacological inhibition of RIPK-1 by Nec-1 reduced cell death around 30% in mTNF, LCL161 and, zVAD-treated YAMCs in comparison to cells treated only with mTNF, LCL161, and zVAD. With these results, the role of necroptosis in the intestinal epithelium in a situation where caspases are blocked was verified.

5.3 Staining kinetics of Propidium Iodide and Hoechst33342 in intestinal organoids

All previously shown data regarding the calculation of cell death were based on measuring MTT reduction capability of treated organoids. However, this has two major drawbacks. The first being that measuring MTT reduction will give an indication on the respiratory potential of the cell. Cell death can be correlated with this, but is not actually measured. If cells are metabolically inactive or arrested in cell cycle but not dead, MTT reduction measurements will yield in high numbers of false positive cells. The second problem is that MTT reduction is proportional to cell number per well (Grabinger, Luks et al. 2014). As organoids are hard to be seeded equally, variance in seeding drastically affects independent of any treatment the measurement outcome. Therefore, the idea was to develop a method which would address both topics: Directly measuring cell death and being more independent of cell number.

Thus, two nuclear dyes, namely Propidium Iodide (PI), a cell impermeable dye, and Hoechst33342 (Hoechst), a cell permeable dye, were used, which already proofed applicable for cell death detection in organoids (Jabs, Zickgraf et al. 2017).

To start with, staining kinetics of PI and Hoechst were determined. Therefore, intact and damaged organoids were stained with 10 μg/ml Propidium Iodide and Hoechst33342, respectively at timepoint=0. Subsequently, pictures were taken 5, 10 ,15 ,30, and 60 minutes after the dyes were added to the culture medium (Figure 21). An intact organoid is taking up Hoechst33342 already 5 minutes after Hoechst was added to the culture medium (Figure 21,

A). After 30 minutes a distinct Hoechst signal was detected. Uptake of PI in a damaged organoid was shown to be even faster than Hoechst in an intact one. Here, the PI signal was already observed after 15 minutes (Figure 21, B). In this case, Hoechst signal also appeared first at areas where PI signal was observed indicating the double staining of the cellular nuclei. According to the combined observations from intact and damaged organoids, the time point with 30 minutes staining time was chosen for the following experiments to quantify fluorescence of PI and Hoechst in treated organoids.

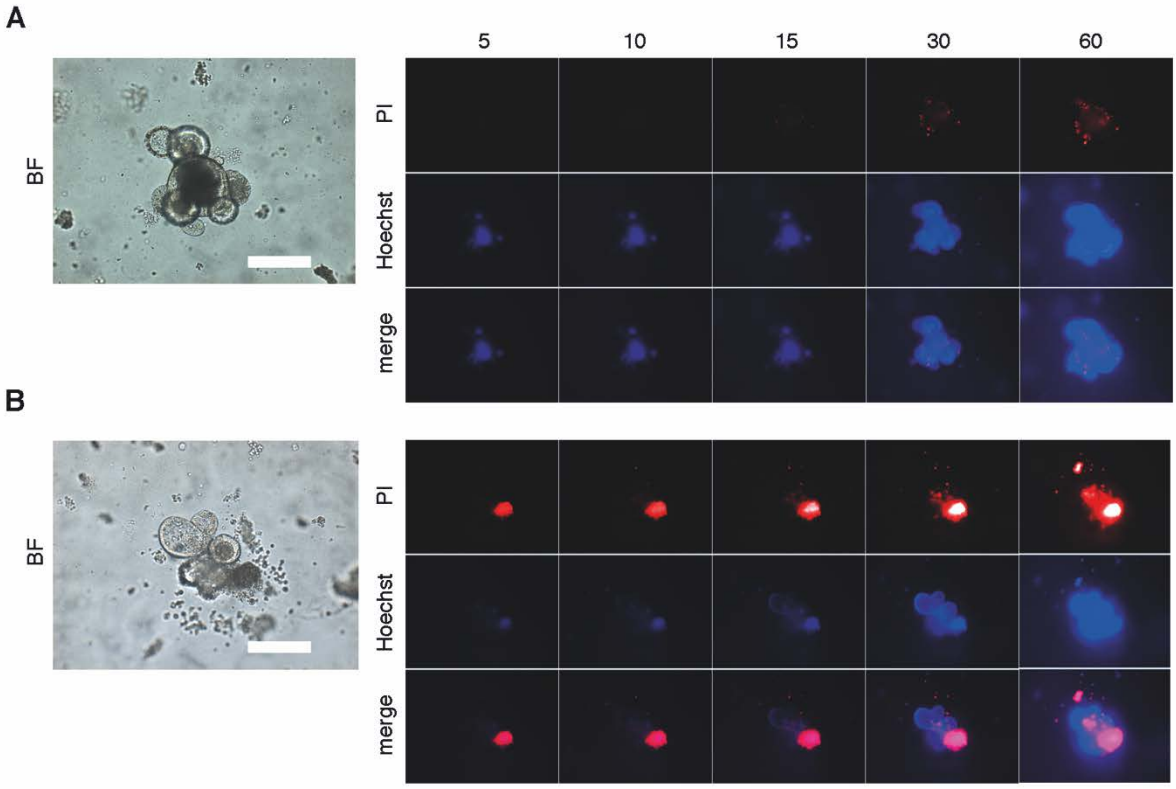

Figure 21: Staining kinetics of PI and Hoechst in murine intestinal organoids

Intact and damaged organoid were stained with 10 µg/ml Propidium Iodide and Hoechst33342, respectively at timepoint=0. Representative brightfield (BF) images were taken at timepoint 0. Subsequently, fluorescence microscopic images were taken from the same organoids 5, 10 ,15 ,30, and 60 minutes after the dyes were added to the organoid culture medium (scale bar = 100 µm).

5.4 Influence of extracellular matrix and growth medium on PI&H quantification

In order to grow in a three-dimensional environment, organoids need extracellular matrix substitutes. Most commonly, extract from a Engelbreth-Holm-Swarm (EHS) mouse sarcoma cell line is used. However, these basement membrane extracts (BME), like the frequently used Matrigel, but also Cultrex and all other EHS-extracts contain DNA (Corning). Therefore, it was tested, whether BME and growth medium would impair the fluorescence unit (FU) quantification through increasing the background fluorescence signal.

Thus, crypts (grown into organoids), BME and growth medium alone were stained with 10μg/ml Propidium Iodide and Hoechst33342 and subsequently, FUs were quantified.

The results show a strong background staining of BME, but also growth medium only exhibited fluorescence. This signal to background (S/B) effect was even stronger pronounced in growth medium with phenol red, than in medium without (w/o) phenol red (Figure 22, A and B). Unstained (ust) crypts in BME, BME alone, or growth medium only did not show high fluorescence (Figure 22). PI FUs showed higher differences in FUs than Hoechst when crypts in BME, BME alone, or growth medium only were compared (Figure 22, C and D).

For further measurements, ratio formation of total PI- and Hoechst-fluorescence per well was necessary, in order to normalize PI-positive ("dead" cells) to Hoechst-positive (all cells) cells in each well (see 5.6). Therefore, already at this stage, a simplified PI/H-ratio, based on FUs was calculated as the following, since it is the basis of cell death quantification in all following experiments:

$$\frac{PI}{Hoechst}\ (simplified) = \frac{FU\ (PI)}{FU\ (Hoechst)}$$

Considering the PI/H ratio, distinct differences between crypts in BME, BME alone, or growth medium only, were detected (Figure 22, E). Additionally, when background fluorescence (BME only) was subtracted from the crypt FU, stained crypts in phenol red-free growth medium showed twice the signal that was obtained in crypts grown in phenol red- containing medium (Figure 22, F).

In sum, these results made it clear that further PI&H quantification was performed in phenol-red-free medium in all following experiments. Moreover, background fluorescence of BME

alone was measured every other experiment and means subtracted from experimental crypt culture in BME FUs.

5.5 Staining medium vs new medium – differences in fluorescence?

BME, growth medium and phenol red influenced FU quantification of PI&H (Figure 22). Therefore, it was additionally tested, whether growth medium with the dyes PI and Hoechst, or its removal and replenishment with new medium would influence fluorescence quantification. Therefore, using the same experimental setup as in 5.4, FUs were analyzed and growth medium versus new medium was compared. Therefore, fluorescence was either directly quantified in staining medium or medium was exchanged to fresh phenol red free medium prior the measurement.

New medium opposed to growth medium resulted in overall lower FUs (Figure 23, A, left compared to Figure 22, A). Thus, signal to background (S/B) PI/H ratio were lower, too (Figure 23, B compared to Figure 22, E). This was also true in direct comparison for the individual dyes (Figure 23, C and D). Here, Hoechst fluorescence was reduced most prominently (Figure 23, C and D). PI fluorescence was reduced to a lower extent (Figure 23, C and D). Thus, the PI/H ratio in fresh phenol red-free medium (crypts in BME) was nearly one-third higher than in growth medium (Figure 23, E). This was also observed when the background fluorescence from BME and medium was subtracted (Figure 23, F).

As a result of this, growth medium in all following experiments was exchanged to new medium, before PI&H FUs were quantified.

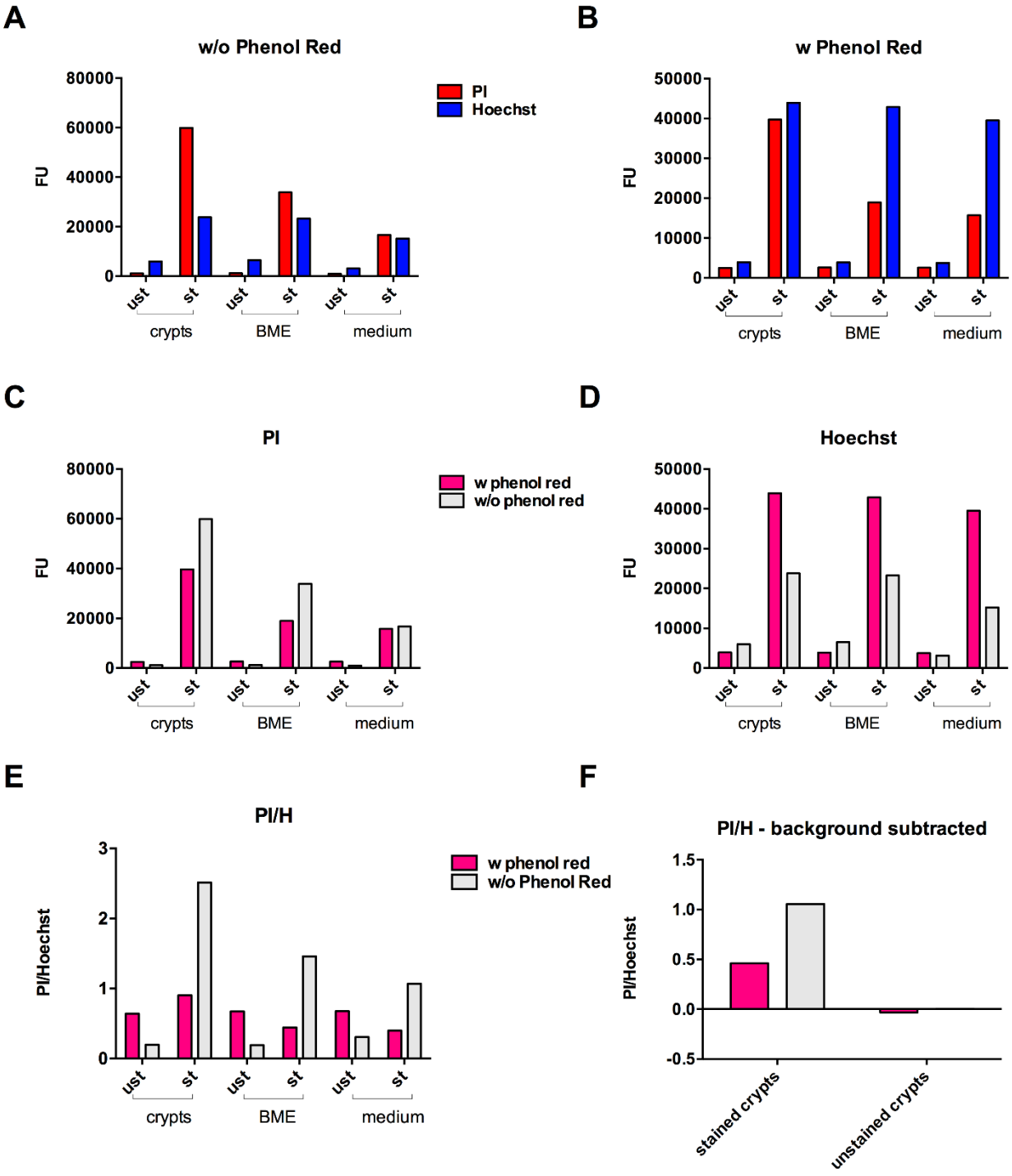

Figure 22: Influence of media and BME on PI&H FUs

Small intestinal crypts, BME only or culture medium were stained (st) or not (ust) in growth medium with 10 µg/ml Propidium Iodide and Hoechst33342 and fluorescence was detected. (A) signal to background (S/B) PI&Hoechst FUs in growth medium w/o phenol red. (B) S/B PI&Hoechst FUs in growth medium with phenol red. (C) S/B PI FUs in media w/o phenol red. (D) S/B Hoechst FUs in growth medium w/o phenol red. (E) S/B PI/H ratio in staining medium w/o phenol red. (F) PI/H ratio in media w/o phenol red (stained vs unstained crypts – background subtracted).

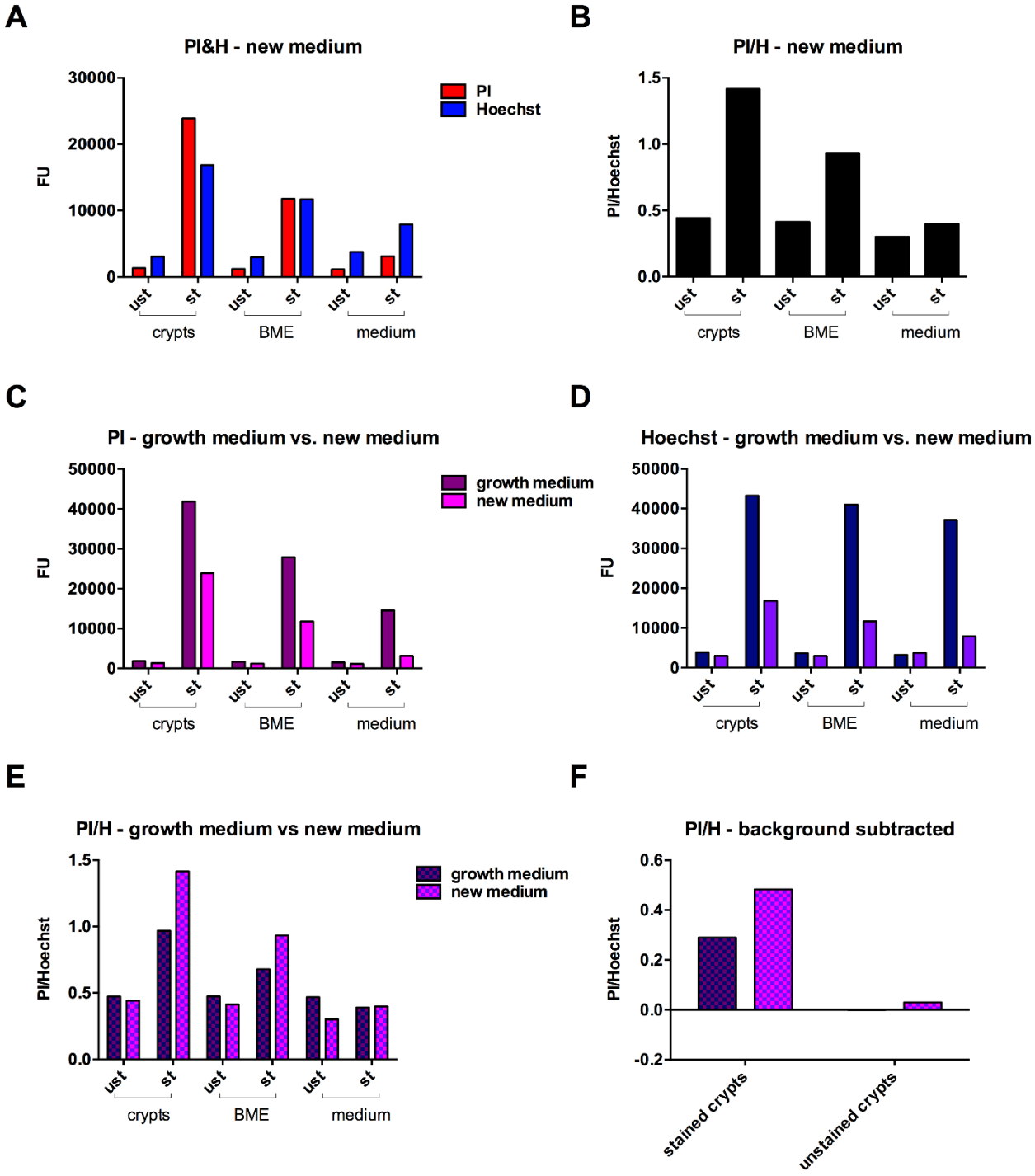

Figure 23: Staining medium vs. new medium influencing PI&H FUs

Small intestinal crypts, BME or medium were stained (st) or not (ust) in growth medium with 10 µg/ml Propidium Iodide and Hoechst33342 and fluorescence was detected in growth or new medium. (A) signal to background (S/B) PI&Hoechst FUs in new medium. (B) S/B PI/Hoechst ratio in new medium. (C) PI FUs in growth medium vs new medium. (D) Hoechst FUs in growth medium vs new medium. (E) PI/H ratio in staining medium vs new medium. (F) PI/H ratio in staining medium vs new medium (stained vs unstained crypts – background subtracted).

5.6 Quantification of Propidium Iodide and Hoechst 33342 fluorescence

PI and Hoechst show distant excitation and emission spectra. Therefore, they are suited to be used simultaneously for fluorescence quantification.

PI has an excitation peak at 535 nm and an emission peak at 617 nm. Hoechst33342 on the other hand, has its maximum excitation at 361 nm and an emission peak at 486 nm. Fluorescence units for both dyes were recorded at exactly these wavelengths using a monochromator (Tecan M200 Pro). As light shorter wavelengths leads to higher phototoxicity (Purschke, Rubio et al. 2010) than longer wavelengths (Laissue, Alghamdi et al. 2017), PI's fluorescence was analyzed first and Hoechst fluorescence afterwards. This has the additional advantage that fluorescence emitted from an excited Hoechst fluorophore does not excite neighboring PI fluorophores, leading to false positive dye excitations and fluorescence crossover (Simeonov and Davis 2004). In order to measure mean fluorescence intensity per well, the following setup within the i-control software (Tecan) was used (see also Figure 24):

- Multiple reads (12) per well to counteract uneven distribution of organoids
- A border of 1mm to the well border was set
- Gain was calculated from wells with highest expected fluorescence: PI Gain → positive control (Staurosporine), Hoechst33342 Gain → negative control (untreated/solvent)
- Number of flashes was set to 25
- Integration time was set to 20
- Between measurements of different dyes, 30 seconds' pause was introduced to reduce unspecific fluorescence and crossover

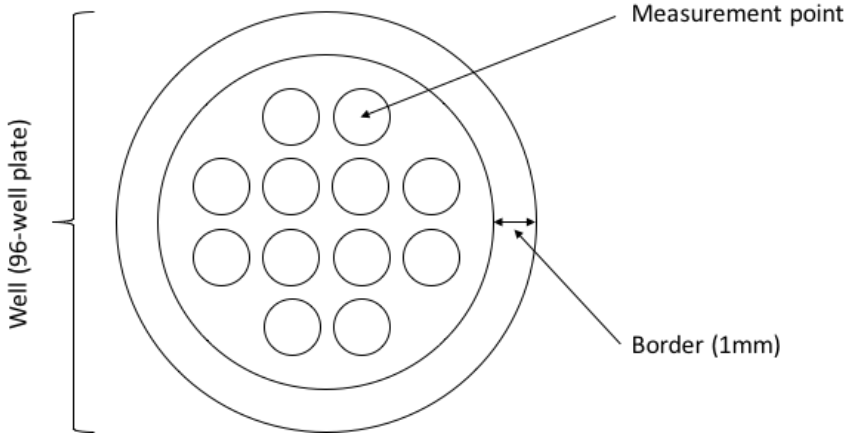

Figure 24: Layout - measurements/well

Measurement points/well + border (1 mm) in 1 exemplified well of a 96-well plate.

Murine intestinal organoids were generated as described before. After three days of cultivation, organoids were treated with increasing concentrations of the chemotherapeutic drug Cisplatin. Subsequently, treated organoids were stained with PI& Hoechst and analyzed microscopically before fluorescence was quantified as described above (Figure 25).

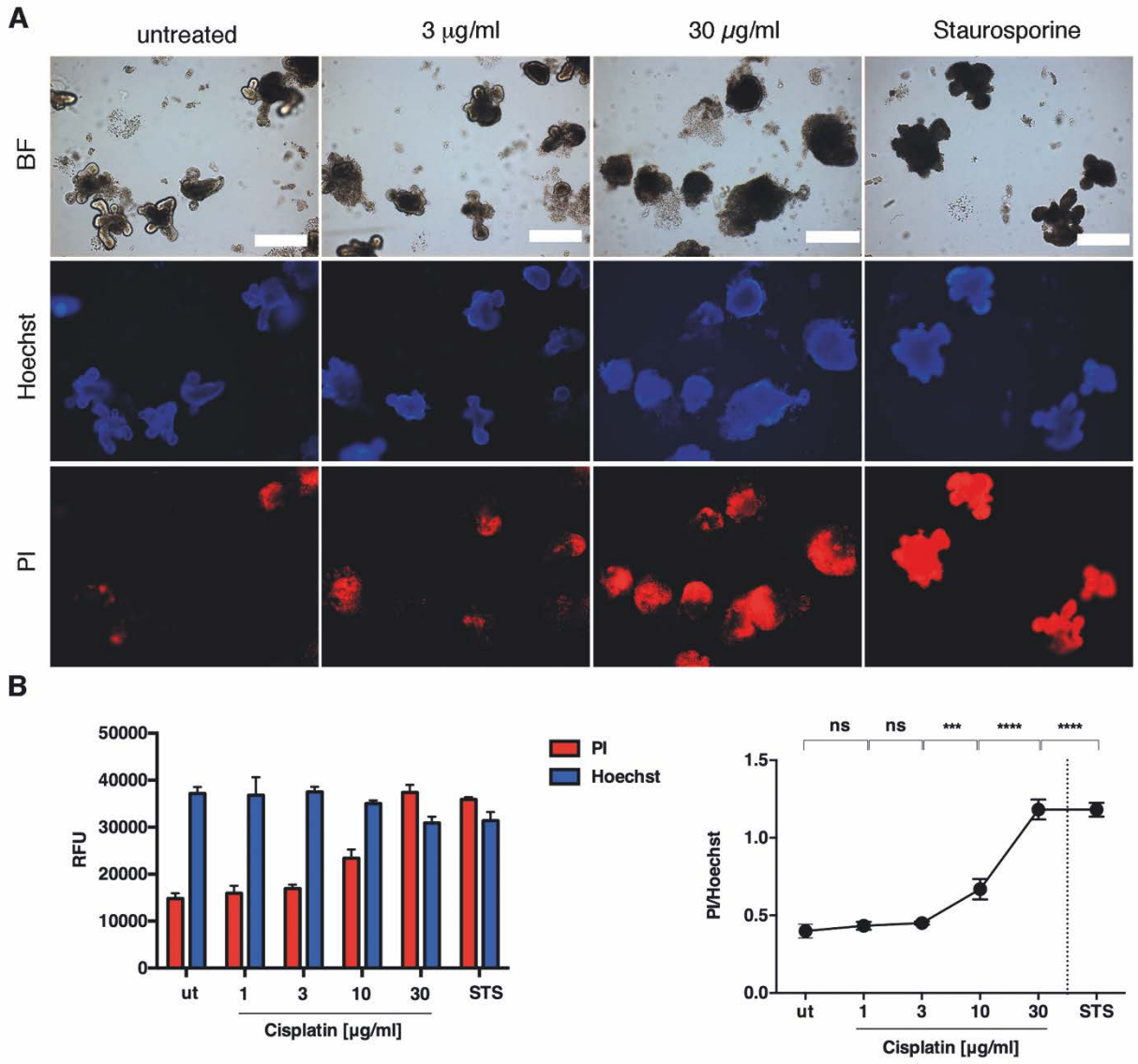

Figure 25: Quantification of Propidium Iodide and Hoechst33342 in 3D organoids

Organoids were treated with indicated concentrations of Cisplatin overnight. Then, organoids were stained with 10 µg/ml Propidium Iodide and Hoechst33342, respectively and fluorescence was detected after 30-minute incubation. (A) Representative brightfield (BF) and fluorescence microscopic images of treated organoids (scale bar = 200 µm). (B) Left side: relative fluorescence units (RFU) of PI and Hoechst after chemotherapeutic treatment. Right side: ratio of PI/H over the whole dose response. Mean ± S.D. of three independent experiments with technical triplicates are shown. One-way ANOVA with Dunnett's multiple comparisons test was performed. $p \leq 0.05$ (*), $p \leq 0.01$ (**), $p \leq 0.001$ (***), $p < 0.0001$ (****). Scale bar = 350 µm

Before the measurement, Gain and Z-position were determined using specific wells in which the maximum and minimum fluorescence signal of both dyes used, was expected. The maximum expected PI-fluorescence was recorded in wells with the cell death positive control (Staurosporine treatment), which would represent at the same time the minimal Hoechst-fluorescence. The maximum Hoechst-fluorescence was recorded in wells with the cell death negative control (untreated = solvent control), which would represent at the same time the minimal PI-fluorescence. The detected fluorescence units in each measurement where hence termed "relative fluorescence units" (RFUs), as Gain and Z-position were determined in reference wells and used throughout the measurement.

Resulting mean (of twelve individual values) fluorescence units per well for a dose-response of Cisplatin are shown in Figure 25 B. With increasing concentrations of Cisplatin, the PI RFUs are increasing whereas the corresponding Hoechst RFUs are decreasing at higher concentrations (Figure 25, B, left panel).

To evaluate the number of cells with an impaired cell membrane per total cell number measured, PI RFUs were divided by Hoechst RFUs as such:

$$\frac{PI}{Hoechst} = \frac{RFU\ (PI)}{RFU\ (Hoechst)}$$

Resulting values are termed "PI/H ratio" in the following. From 3 μg/ml Cisplatin and higher concentrations, significant differences compared to the untreated control were calculated (Figure 25, B, right panel).

The increase in PI signal and the stability of the Hoechst signal can also be seen by microscopy (Figure 25, A). Here, brightfield (BF) microscopy allowed to observe disintegration of organoids treated with 30 μg/ml Cisplatin and condensed structures for Staurosporine treated organoids. Fluorescence microscopy revealed that Hoechst staining remained stable throughout all concentrations of Cisplatin (Figure 25, A, middle panel). PI signal, however, is increasing with higher concentrations of Cisplatin (Figure 25, A, middle panel).

5.6.1 Independence of PI/H quantification from cell density

As mentioned above (5.3) MTT reduction of treated organoids is dependent on organoid number and the treatment itself. However, organoids show high well to well variability with regards to cell number, especially if they are generated from freshly isolated crypts. Here, seeding equal numbers of cells per well is impeded by the viscosity of extracellular-matrix derivate (e.g. Matrigel) needed for organoid culture.

Thus, the ratio of PI/H RFUs was tested on whether it would prove to be sufficient for controlling the cell density. Therefore, murine small intestinal crypts were isolated and seeded into different dilutions in Matrigel. After three days of organoid formation, organoids were analyzed through the measurement of intracellular ATP was analyzed using a commercial kit, CellTiterGlo® (in the following CellTiterGlo). Here, dependent on the dilution, relative luminescence units (RLU)-signal (corresponding to ATP) was significantly reduced from 200 seeded crypts/well onwards (Figure 26, A).

Additionally, tumoroids from $APC^{+/-}$ were diluted the same and analyzed by MTT-reduction assay. Microscopically, numbers of tumoroids in dilution were clearly reduced, thus also resulting in lower Formazan-staining (Figure 26, D). Therefore, absorbance values differed significantly from a dilution of 150 seeded crypts/well, onwards (Figure 26, B).

Moreover, in another experiment, crypts were seeded in the same dilutions as described before and grown into organoids for three days. Subsequently, they were treated with 10 μg/ml Cisplatin overnight to ensure decent amounts of PI-positive cells. On the next day, PI & Hoechst RFUs were quantified as described before (5.6). In this case, over the whole dilution series, no significant differences between PI/H ratios was detected. Thus, “internal normalization” of PI values (DNA of cells with disintegrated membrane) with Hoechst values (total DNA) proves to be sufficient in detecting the effects of treatment, being less dependent on equally seeded cell numbers, compared to assays assessing changes in cellular respiratory potential (Figure 26, C).

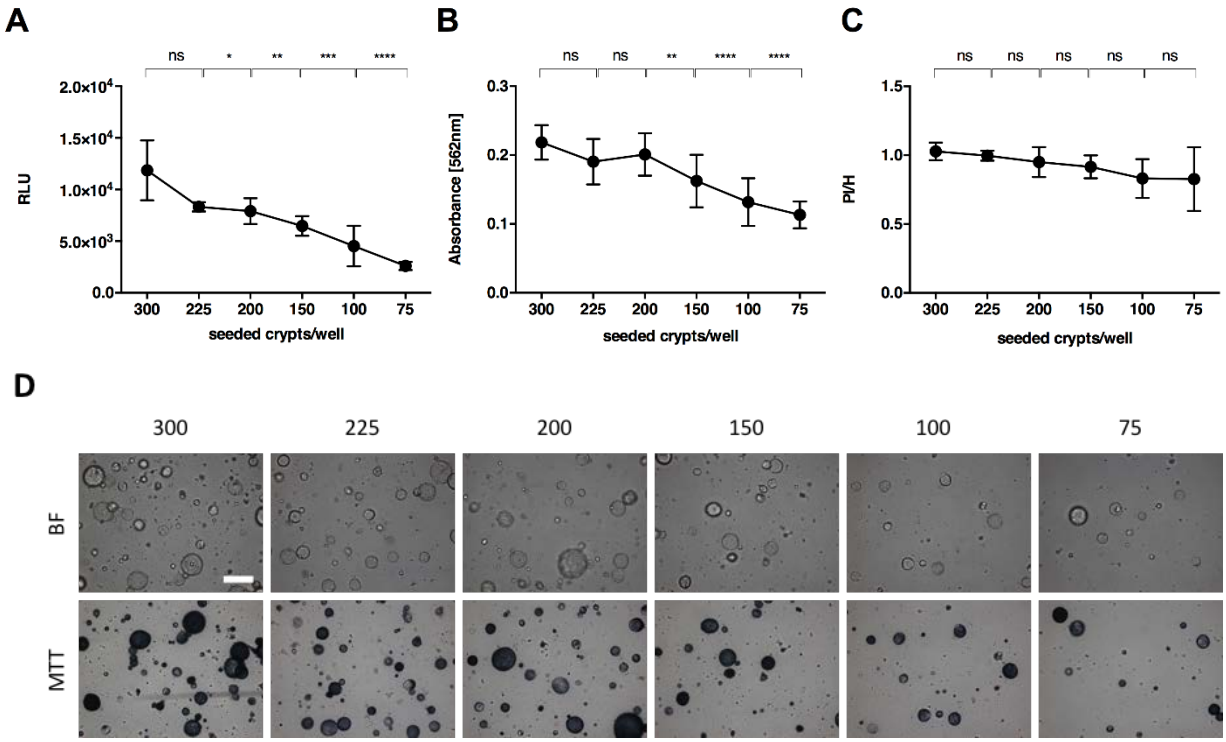

Figure 26: Fluorescence ratio is independent of crypt/organoid number

(A) Murine intestinal crypts from wt mice were seeded either directly in Matrigel or Matrigel/crypt mixtures were further diluted in Matrigel. Crypts were then grown for three days to form organoids. Then, CellTiterGlo was performed. (B) Tumoroids derived from $APC^{Min/+}$ mice were seeded in different dilutions and assessed with MTT reduction assay. (C) Three-day old organoids derived from wt mice were treated overnight with 30 μg/ml Cisplatin. The next day, organoids were stained with 10 μg/ml PI&Hoechst, respectively and fluorescence was quantified after 30-minute incubation and growth medium exchange. Mean ± S.D. of three independent experiments with technical triplicates are shown. One-way ANOVA with Dunnett's multiple comparisons test was performed. $p \leq 0.05$ (*), $p \leq 0.01$ (**), $p \leq 0.001$ (***), $p < 0.0001$ (****). (D) representative brightfield microscopic images of $APC^{Min/+}$-derived tumoroids in different dilutions, stained with MTT (same experiment as 26, B). (scale bar = 350μm)

5.7 Specific cell death can be calculated from fluorescence ratios

As quantification of fluorescence units from PI and Hoechst stained murine small intestinal organoids allowed significant distinction of different concentrations of chemotherapeutic drugs, namely Cisplatin (Figure 25, B, right panel), treatment-specific cell death was assessed the following way:

First, murine intestinal organoids were grown and treated overnight with increasing concentrations of the chemotherapeutic drugs Cisplatin, 5-FU, and Staurosporine (STS) as a cell death control. The next day, organoids were stained with PI and Hoechst. Subsequently, PI and Hoechst fluorescence values were quantified, and PI/H ratio calculated (Figure 27, A). Cisplatin allowed for a finer discrimination of ratios corresponding to increasing concentrations than 5-FU. Here, only the positive control showed a significantly different ratio than the untreated control.

In order to assess treatment-specific organoid cell death, each sample value was divided by the Staurosporine control and multiplied by one hundred. Additionally, untreated (ut) control was subtracted from all values, to take notice of background organoid death, hence enabling the calculation of treatment-specific organoid cell death (Figure 27, B).

To calculate treatment-specific organoid cell death, the following formula was used:

$$treatment-specific\ organoid\ cell\ death\ [\%] = \left[\frac{(sample)}{(STS)}\right] * 100 - (ut)$$

As a result of the calculation of treatment-specific organoid cell death, values for 5-FU and Cisplatin treatment can be discriminated further than using only PI/H ratio values (Figure 27, B).

Here, treatment-specific cell death values show significant differences compared to untreated control from 10 μg/ml Cisplatin, or 5-FU, respectively, onwards.

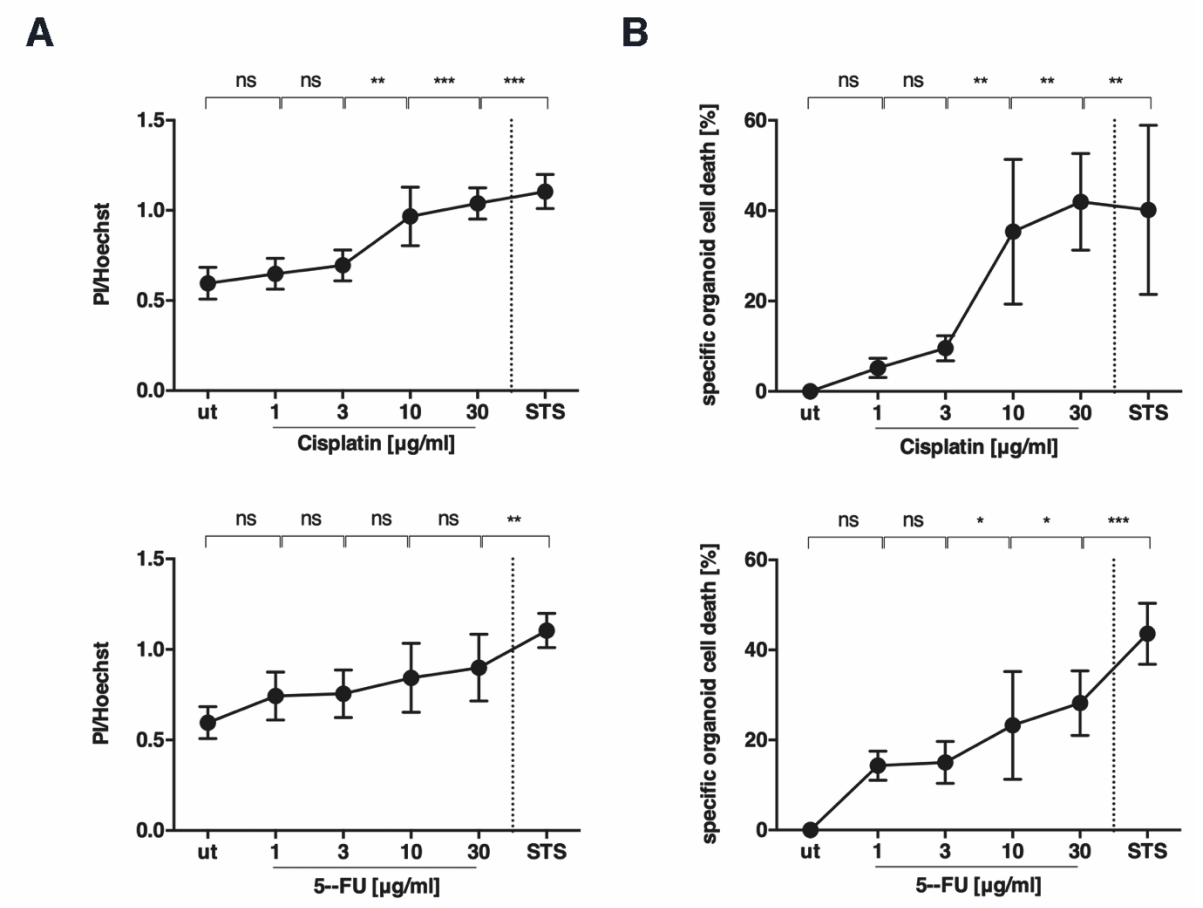

Figure 27: PI&H quantification allows treatment-specific organoid cell death determination

Organoids were treated overnight with indicated concentrations of Cisplatin (left panel) or 5-Fluorouracil (5-FU) (right panel). Then, organoids were stained with 10 µg/ml Propidium Iodide and Hoechst33342, respectively and fluorescence detected after 30minutes incubation. (A) PI/H ratios of DR for Cisplatin and 5-FU treatment. (B) Specific organoid cell death upon Cisplatin and 5-FU treatment. Mean ± S.D. of three independent experiments with technical triplicates are shown. One-way ANOVA with Dunnett's multiple comparisons test was performed. $p \leq 0.05$ (*), $p \leq 0.01$ (**), $p \leq 0.001$ (***).

5.7.1 Specific cell death calculated from Propidium Iodide/Hoechst33342 ratios is comparable to cell death determination from current methodologies

To show, that PI/H ratios and therefrom calculated treatment-specific organoid cell death holds true in comparison to current methodologies being used to assess organoid cell death, the latter were used for comparison.

Therefore, murine intestinal organoids were grown and treated with indicated concentrations of Cisplatin or 5-FU overnight. The next day, analysis was performed. Using the kit CellTiterGlo, intracellular ATP was quantified. The results show that the decrease in relative luminescent units (RLUs), corresponding to intracellular ATP, inversely correlates with data obtained from PI/H quantification (Figure 28, A compared to Figure 27, B).

Cleavage of effector caspases, namely caspase 3/7 was shown with a fluorescent probe, both microscopically as well as with plate reader quantification. Here, the signal for cleaved caspase 3/7 and PI do to some extent co-localize (Figure 28, B, left) and cleavage of caspases increased with higher concentrations of 5-FU confirming dose-dependent treatment-specific organoid cell death (Figure 28, B, right).

Moreover, Cisplatin and 5-FU treated organoids were used for protein analysis by Western Blot (WB). Therefore, after treatment, organoids were lysed after treatment and effector caspase 3, as well as Tubulin were analyzed. Treatment with chemotherapeutics lead to increase of the cleaved (active) form of Caspase 3, as observed in Figure 28, B (Figure 28, C). Additionally, densitometric analysis showed stronger cleavage of caspase 3/ tubulin (protein load) in Cisplatin treated organoids than in 5-Fluorouracil-treated ones. Staurosporine (STS) treated organoids did not show Caspase 3 activation here (Figure 28, D).

Combining these results, Cisplatin or 5-Fluorouracil treated organoids showed reduction of intracellular ATP levels, as well as cleavage of effector Caspases 3/7. The latter effect was observed microscopically, and assessed through fluorescence quantification and by protein analysis with Western Blot. Therefore, we concluded that increase in PI/H ratio following the same chemotherapeutic treatment resembled the reduction of intracellular ATP and cleavage of effector caspase 3/7 and thereby treatment-specific organoid cell death.

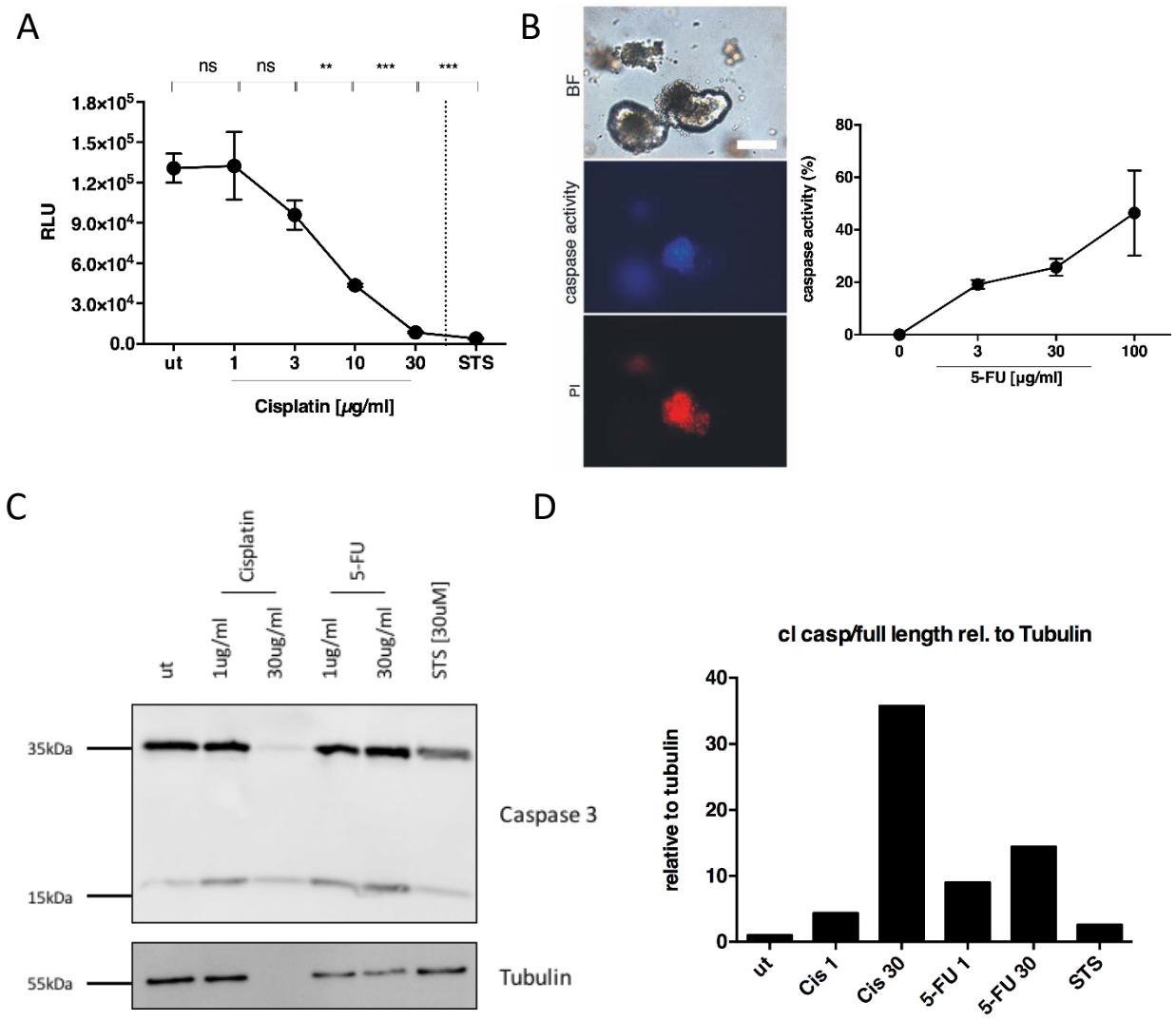

Figure 28: Verification of specific organoid cell death by PI/H quantification

Organoids were treated with indicated concentrations of Cisplatin or 5-FU and Staurosporine (STS) overnight. Analysis was performed the next day. (A) Cellular ATP content was analyzed using CellTiterGlo. Mean ± S.D. of three independent experiments with technical triplicates are shown. One-way ANOVA with Dunnett's multiple comparisons test was performed. $p \leq 0.05$ (*), $p \leq 0.01$ (**), $p \leq 0.001$ (***). (B) Representative brightfield (BF) and fluorescence images and quantification of fluorescent probe labeling cleaved caspse 3/7. (scale bar= 85 µm) (C) Western Blot of treated organoids. (D) Densitometric anaylsis of (C) using ImageJ.

5.8 Quantification of PI and Hoechst can be adapted to 2D cell culture

As the quantification of Propidium Iodide and Hoechst33342 was successful in three-dimensional small intestinal organoids, this methodology was transferred to conventional two-dimensional cell culture systems, to further broaden its application spectrum.

Therefore, murine (MC38) and human (Caco2) intestinal adenocarcinoma cell lines were treated with increasing concentrations of Cisplatin overnight. The next day, cells were stained with 5 μg/ml PI& Hoechst, respectively and after 30 minutes of incubation, fluorescence was measured in a plate reader. Here, minor adaptations to the abovementioned protocol were performed:

- Multiple reads (6x6) per well
- A distance range of 1.25 mm to the well border was set

Moreover, Gain setting was performed as for three-dimensional organoids, whereas Z-position was only determined once, as it was expected that cells would be more or less of the same height. The obtained values for Z-position and Gain for each cell line, were subsequently used for following measurements.

As already shown in Figure 25, PI&H fluorescence was detectable, enabling in well normalization to total DNA (Hoechst RFUs). Thereof, treatment-specific cell death could be calculated (Figure 29).

The response of Caco-2 cells towards cisplatin was detected from 3 μg/ml Cisplatin onwards, whereas the response of MC38 cell towards cisplatin was detected from 10 μg/ml Cisplatin onwards (Figure 29, A). Cisplatin treatment-specific cell death was calculated as described in 5.7, with the only difference that here, 100 μg/ml Cisplatin was included in the chemotherapeutic concentration range. Negative control (untreated) was the same as in 5.7.

Microscopic analyses revealed a similar picture as for murine intestinal organoids. Untreated cells (control) showed attached phenotype and confluent Hoechst33342 staining. MC38 cells treated with 30μg/ml Cisplatin overnight however, displayed a “roundish” morphology and increased PI staining together with reduced Hoechst staining (Figure 29, B). Moreover, detachment of dead cells and subsequent “floating” in the medium did reduce overall signal in high cisplatin concentrations (Figure 29, A).

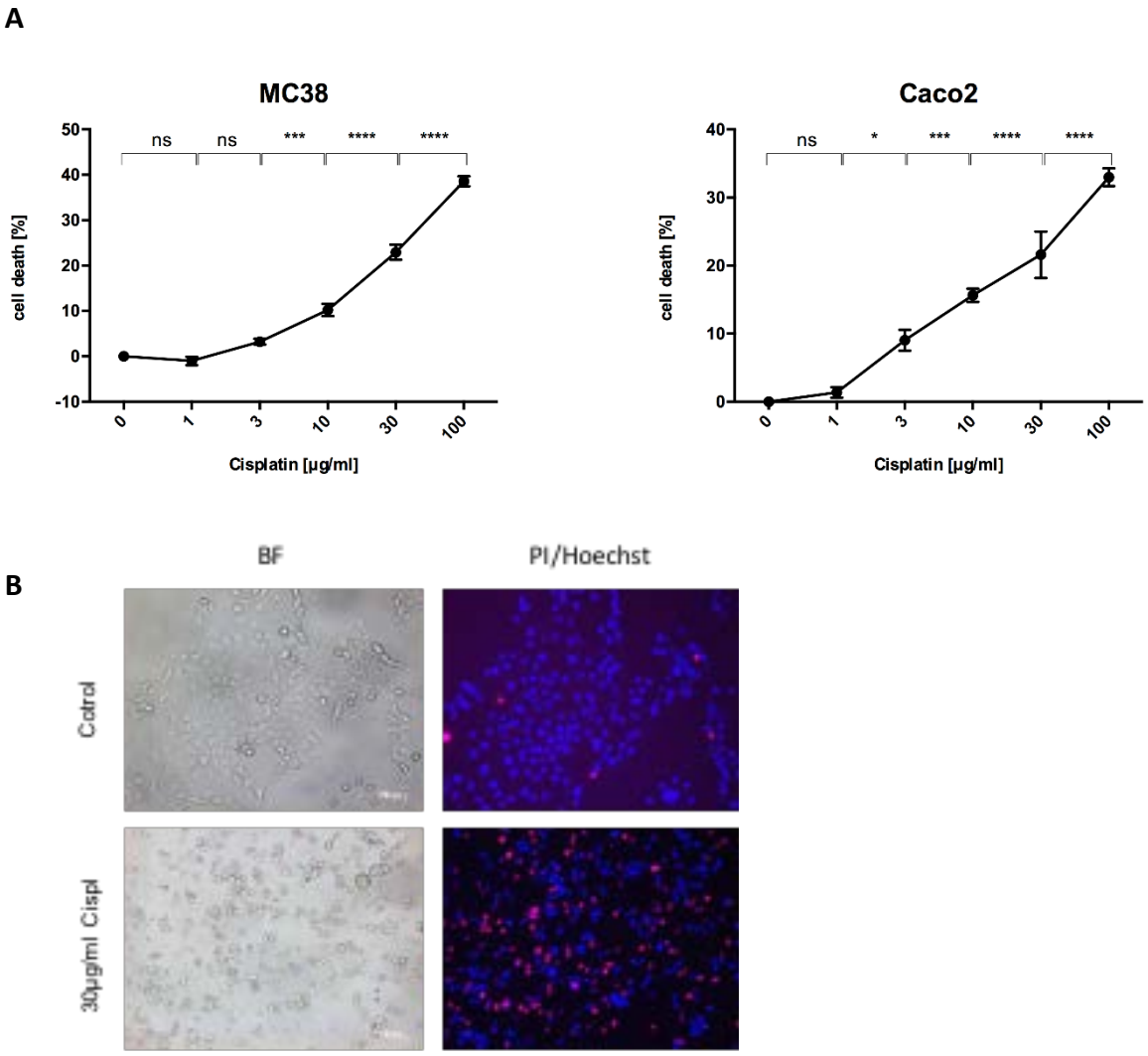

Figure 29: Cell death analyzed by PI/H quantification in MC38 and Caco2 cells

MC38 and Caco2cells were treated with indicated concentrations of Cisplatin overnight. The next day, cells were stained with 5 µg/ml Propidium Iodide and Hoechst33342, respectively and fluorescence was measured after 30-minute incubation. (A) Cell death induction measured using PI/H upon treatment with Cisplatin in MC38 cells (left) and Caco2 cells (right). Mean ± S.D. of three independent experiments with technical triplicates are shown. One-way ANOVA with Dunnett's multiple comparisons test was performed. $p \leq 0.05$ (*), $p \leq 0.01$ (**), $p \leq 0.001$ (***), $p < 0.0001$ (****). (B) Representative brightfield (BF) and fluorescence (PI/H-merge) images of untreated (control) MC38 cells or treated with 30 µg/ml Cisplatin overnight (scale bar = 100 µm). Representative images are shown from three independent experiments.

5.9 Multiplexing PI&H quantification with MTT reduction assay

Quantifying Propidium Iodide and Hoechst33342 fluorescence can be used to analyze cell death in three-dimensional organoids. However, this method does not allow to detect substances, that will not directly cause cell death but impair mitochondrial respiration. As this will eventually have fatal consequences, namely cell death as well, the idea was to combine PI&H quantification with the already established methodology of MTT reduction for three-dimensional organoids in a multiplex fashion (Grabinger, Delgado et al. 2016).

Therefore, organoids from $APC^{Min/+}$ mice jejunal tumors were grown. These so called "tumoroids" were treated overnight with 3, 30, and 100 μg/ml 5-Fluorouracil. The next day, PI&H staining and quantification was performed as described before (5.6). However, afterwards, tumoroids were incubated with MTT solution. Tumoroids being unharmed by treatment would reduce yellow MTT to purple formazan, whereas damaged organoids (5-FU treated) would do so less, if at all. Staining with potentially toxic dyes PI&H did not affect reducing capacity of untreated tumoroids (Figure 30, A). 5-FU treated tumoroids on the other hand, converted little MTT to formazan (Figure 30 B). Moreover, Hoechst and PI staining showed a similar staining pattern, as observed previously (Figure 25). Untreated tumoroids were Hoechst positive and PI negative, whereas 5-FU treated organoids were both Hoechst and PI positive (Figure 30, A and B).

As staining with both fluorescence dyes and reduced formazan did not influence each other, also quantification of both PI& Hoechst fluorescence as well as formazan absorption was performed. Therefore, before mentioned tumoroids were quantitatively assessed using a plate reader as described before (see 5.6). PI&H fluorescence was analyzed first. Then, formazan absorption was measured at 562 nm (Figure 30, C). Staining with nuclear dyes PI& Hoechst did not impair tumoroid MTT reduction capacity (Figure 30, C, left axis). The multiplex assessment of treatment-specific organoid cell death using PI&H quantification, as well as MTT reduction showed similar responses compared to individually performed assays (compare Figure 27 and Figure 30).

Moreover, organoids derived from human jejunal biopsy were treated with indicated concentrations of 1, 3, 10, and 30 μg/ml Cisplatin and 5 μM Staurosporine (STS) overnight. Subsequently, treatment-specific organoid cell death and MTT reduction were analyzed in the abovementioned multiplex PI/H & MTT-assay. Again, treatment specific organoid cell death

(PI& Hoechst) inversely correlated with MTT reduction capacity of treated human jejunal organoids (Figure 30, D).

Thus, by combining quantification of PI&H fluorescence and formazan absorption, the information, obtained from one well increased from cell death only, to impairment of mitochondrial respiration as well. Therefore, combination of both methods is suggested in order to obtain maximum information.

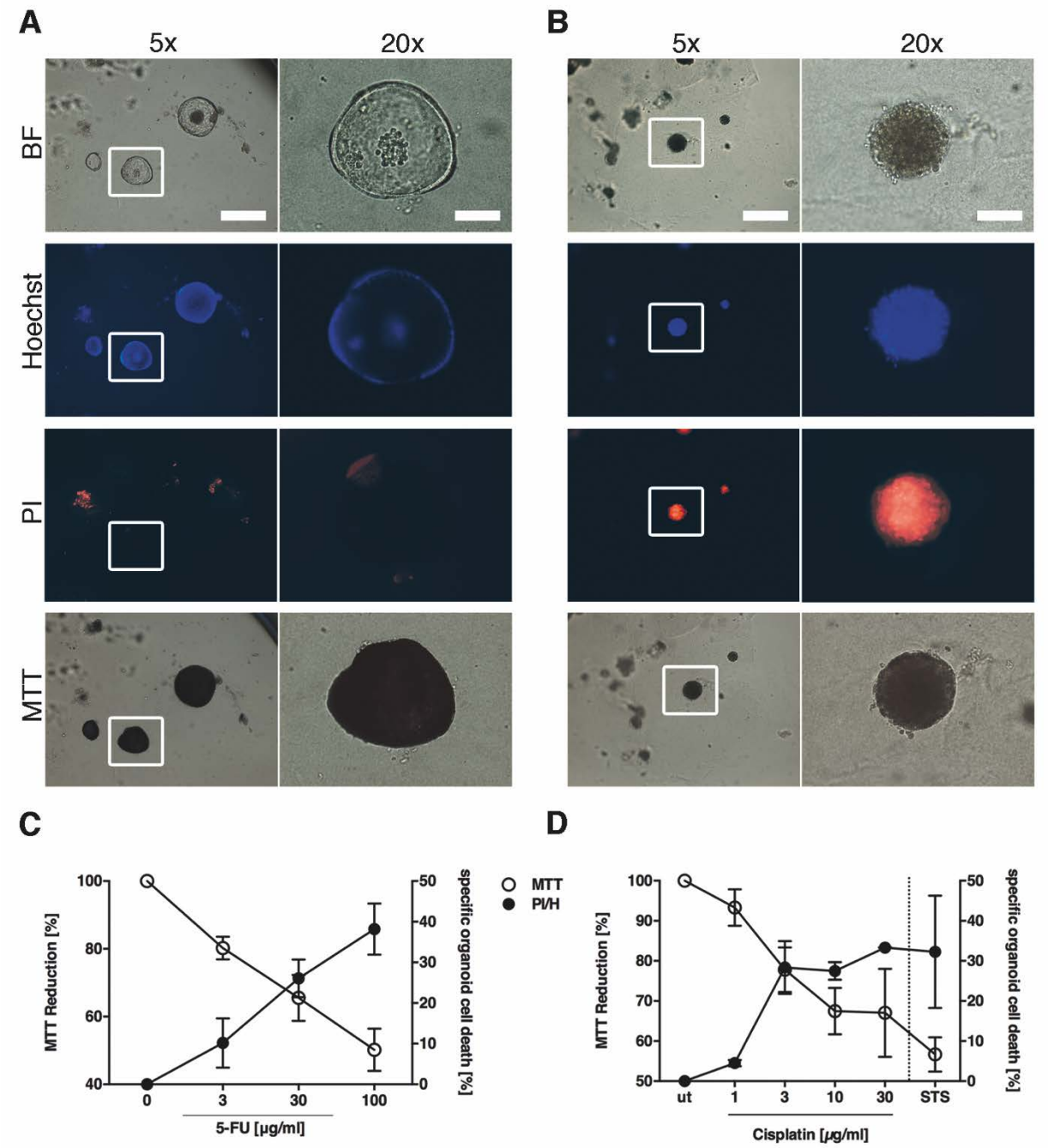

Figure 30: Multiplexing of PI/H and MTT staining in murine tumoroids and human organoids

Tumoroids grown from $APC^{Min/+}$ mice were treated with 5-FU overnight, stained with PI&H and fluorescence was quantified. Then, MTT solution was added and Formazan absorption was measured at 562 nm. Representative brightfield (BF) and fluorescence images of (A) untreated tumoroid staining positive for Hoechst and reduced Formazan, but not for PI and (B) 5-FU treated tumoroid, with impaired, condensed morphology, staining positive for Hoechst and PI, not for Formazan. (C) Quantification of tumoroid (A&B) treatment specific organoid cell death (right axis) and MTT reduction (left axis). (D) Human patient derived organoids were treated with cisplatin overnight. Then, PI&H fluorescence and Formazan absorption were measured and treatment specific organoid cell death as well as MTT reduction were calculated thereof. Scale bar (5x) = 350 μm, (20x) = 85 μm. Representative images and data from two independent experiments are shown.

5.10 Appendix: Investigating signal transduction in intestinal organoids on the protein level

Organoid technology has been in use for nearly two decades. Since its early beginnings, organoid research has focused on stem cell biology and the understanding of tissue development and architecture (Sato, Vries et al. 2009, Buske, Przybilla et al. 2012, Leushacke and Barker 2014, Date and Sato 2015, Sugimoto, Ohta et al. 2017). Recently, organoids have also been implicated in pre-clinical medicine where patient-derived organoids have already been used to screen for the most efficient chemotherapeutic drugs or for genomic alterations in various cancer tissues but also on a single cell level (Jabs, Zickgraf et al. 2017, Vlachogiannis, Hedayat et al. 2018, Nishimura, Shirasaki et al. 2019). However, until today organoids are rarely used to study signal transduction events on a protein level (Gonneaud, Asselin et al. 2017). As organoids closely resemble the tissue architecture and composition *ex vivo,* it is of great interest to also study signaling events and overall proteomic changes. Therefore, organoid technology was combined with a novel method, namely the digital western blot, to quantitatively determine protein levels – Digi West. The digital western blot (Digi West) is at first a common standard SDS-PAGE, followed by a western blot. Subsequently, the PVDF-membrane is separated into 96 molecular weight fractions. Proteins are then eluted and fixed on beads. Here, protein detection takes place using antibodies and a Luminex system (Treindl, Ruprecht et al. 2016). Usage of this technology allows to quantitatively assess changes in signal transduction pathways, e.g. upon treatment with very low amounts of protein. Thus, the ideal tool to investigate organoids.

5.10.1 Optimization of organoid recovery from BME

To start with, the bottleneck of protein analysis in organoids was assessed – BME. As the basement membrane extract (BME) is full of extracellular matrix proteins (see 3.2.3) it is a major drawback as they impair the analysis of proteins of interest. Therefore, organoid recovery from BME and substitutes was optimized in the first place, as initial trials with published protocols (Lindeboom, van Voorthuijsen et al. 2018) did not result in expected purities (Figure 31, A). In order to achieve the optimized organoid recovery, culture medium was removed and replaced with ice-cold PBS. Subsequently, organoids were incubated on ice for one hour. Then, BME was mechanically disrupted using a pipet tip and the BME-PBS

mixture was resuspended four times, before moving to a pre-cooled Eppendorf-tube. Next, organoids were centrifuged and intermittently washed according to the following table (Table 1). Resulting cell pellets were quick-frozen in liquid nitrogen, stored at -80°C, and shipped on dry ice.

Table 1: Optimized protocol for organoid recovery from BME

Step	Duration [min]	Centrifugation speed [x g]	Wash Volume [µl]
1	5	500	1000
2	5	1000	500
3	3	2000	300
4	2	3000	100

By optimizing the organoid recovery protocol, protein residues from BME with large molecular weight (98-183kDa) were strongly reduced in comparison to the published protocol used before (Figure 31, B compared to Figure 31, A). Therefore, further experiments used this protocol in order to obtain organoids from BME for subsequent protein analysis.

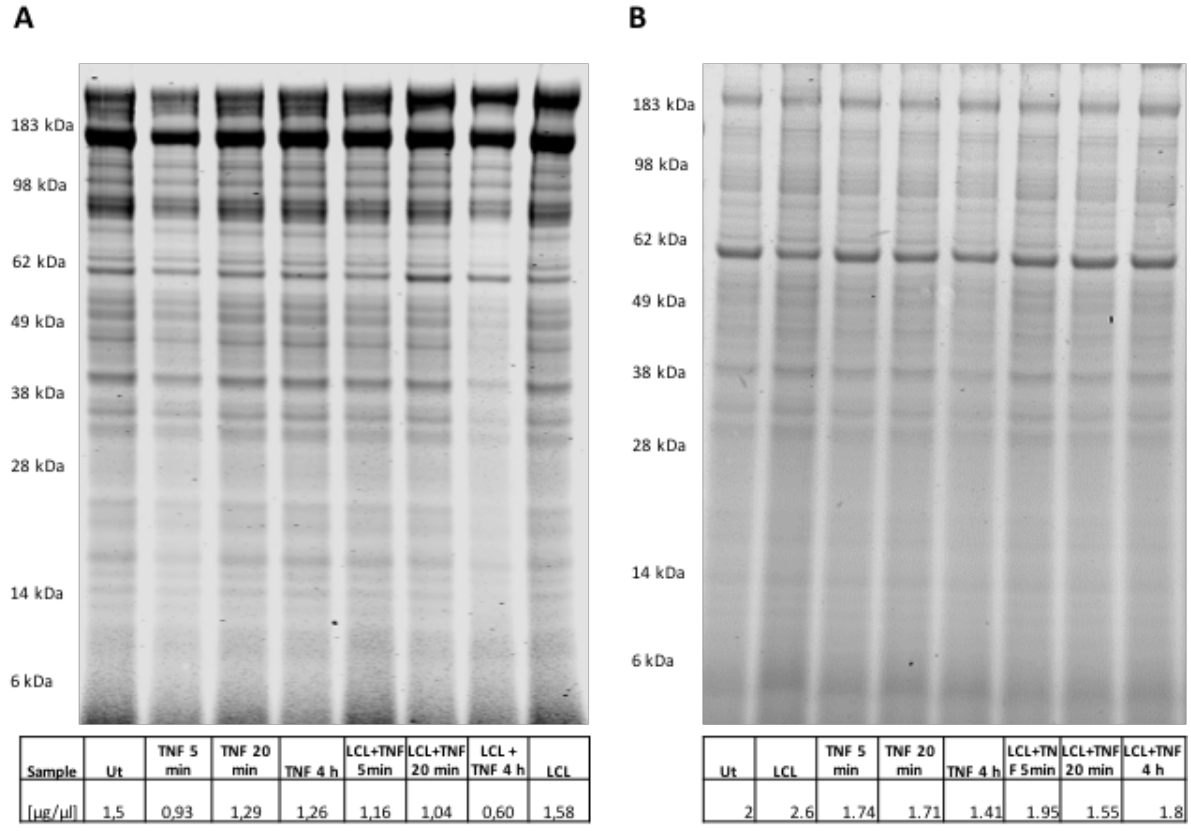

Figure 31: In-gel protein quantification of organoid samples

Murine intestinal organoids were treated with mTNF (30 ng/ml) ± LCL161 (500 nM) for the indicated time. Then, culture medium was removed, and organoids were recovered using ice-cold PBS. (A) Coomassie staining of SDS-PAGE run protein lysates from organoids recovered as described by (Lindeboom, van Voorthuijsen et al. 2018). (B) Coomassie staining of SDS-PAGE run protein lysates from organoids recovered using optimized recovery conditions (see Table 1). Protein lysates of two representative experiments shown. Images were taken and are the courtesy of Eugenia Salzmann, NMI, Reutlingen.

5.10.2 TNF- and LCL161-induced cell death in murine intestinal organoids

In the intestine, TNF plays a major role in cell stress and cell death signaling. Moreover, it was recently shown that cIAP1, represents a key level of decision taking to whether an intestinal epithelial cell will die upon TNF-encounter or not (Grabinger, Bode et al. 2017). Therefore, this highly important and well described field of study was used to combine organoid technology and Digi-West protein quantification to gain a deeper understanding of signaling events in primary epithelial cells. Building on the results from chapter 5.2.2 and 5.2.3, the aim was to investigate changes on the protein level in TNFR-signaling after mTNF and LCL161 treatment. Thus, two major experiments were set up. The first, resembling exactly the same conditions as described in chapter 5.2.2 (Figure 19, B). A kinetic where organoids were treated for 5 minutes, 20 minutes or 4 h with mTNF ± LCL161 (Figure 31). For the second experiment, organoids were analyzed at different time points after crypt isolation. Here, organoids were either left untreated or treated overnight with mTNF + LCL161 at one, three, five or seven days after crypts had been isolated. This experiment was accompanied by fluorescence microscopy and the MTT-reduction assay. In this scenario, organoid growth was monitored over the 8 days of the experiment. Notably, at day 7 after crypt isolation, organoids start to disintegrate and show increased PI-positive staining, even if untreated (Figure 32, A). However, organoids treated with mTNF + LCL161 showed disintegrated morphology already from day 1. Over the course of time, organoids responded similar to mTFN+LCL161 treatment (Figure 32, A). However, if MTT-reduction capacity of organoids was assessed, strong differences were observed. Whereas overall MTT-reduction capacity of untreated organoids increased until day 5, it was a massively decreased towards day 7. Here, MTT-reduction capacity was even reduced below day 1, similar to mTNF+LCL161 treated organoids (Figure 32, B). Overall, treatment of murine intestinal organoids with mTNF+LCL161 resulted in diminished MTT-reduction capacity, corresponding with cell death as indicated with PI^+-

stained cell (Figure 32, A). In sum, this confirmed the observations from 2D-cell culture, where mTNF+LCL161-treatment massively induced cell death (Figure 19, B and 20). The protein analysis using Digi-West technology was and is performed by Eugenia Salzmann at the NMI (Reutlingen). As the study is currently ongoing no Digi-West data is shown here.

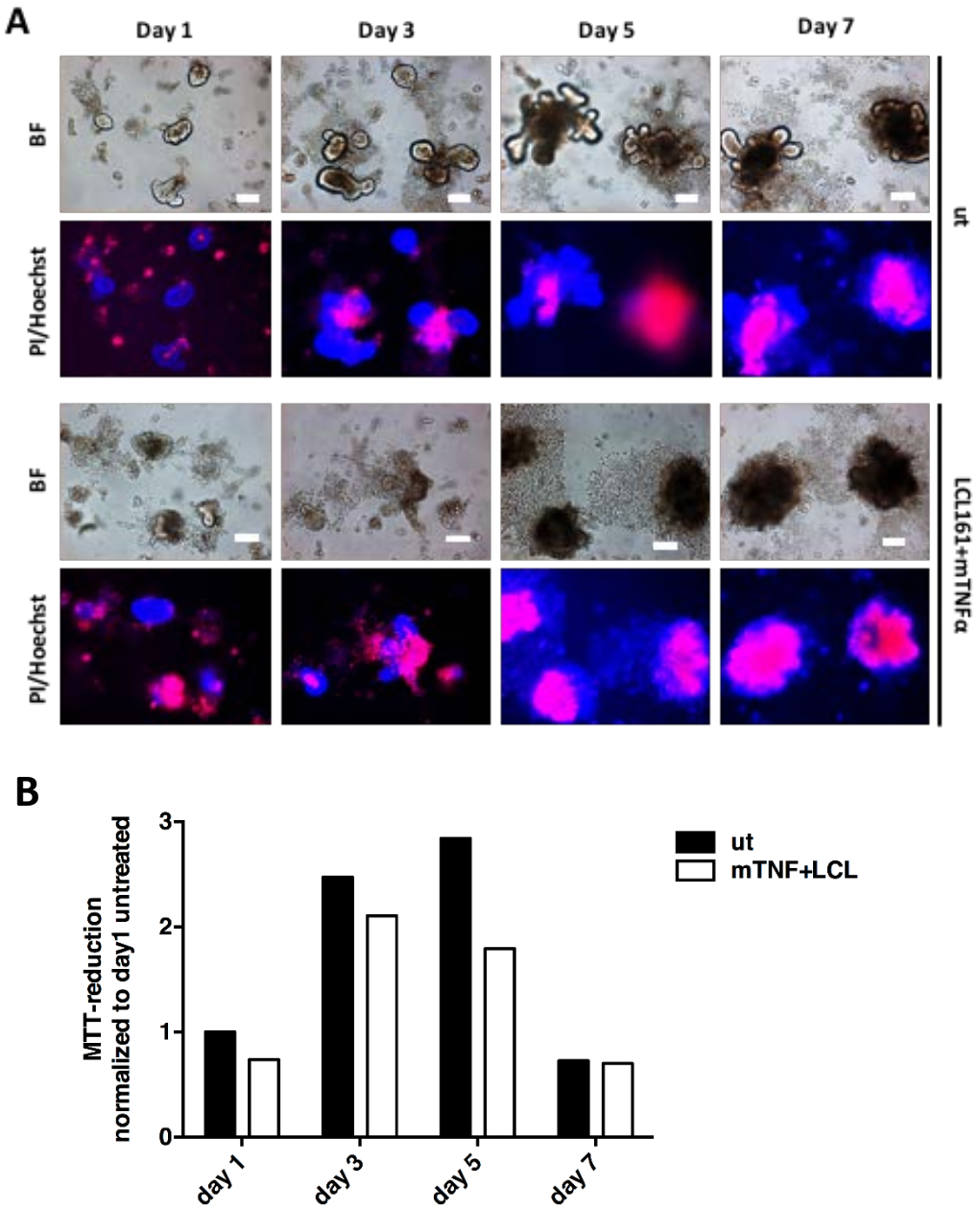

Figure 32: Functional analysis of intestinal organoids after mTNF- and LCL161-treatment

Organoids were grown from wt mice for 1, 3, 5, and 7 days. At indicated timepoints, organoids were not treated or treated with mTNF (30 ng/ml) and LCL161 (500 nM) overnight. (A) The next day, brightfield (BF) and fluorescence microscopy analysis was performed. (B) Afterwards, organoids MTT-reduction was assessed. Representative images and data from 4 independent experiments are depicted. Scale bar = 100 μm.

6. Discussion

6.1 Role of TNF in cell death induction in murine intestinal organoids

TNFα is a pro-inflammatory cytokine and known for its numerous roles in promoting inflammatory response and cell death. However, in most tissues, TNFα alone fails to induce cell death. The intestine is an exception (Piguet, Vesin et al. 1999). Here, levels of cIAP1 determine whether a cell will die upon encounter with TNFα, or not. However, it is not known until today, which intestinal epithelial cells die directly, and which receptor type (TNFR1/2) plays a role in cell death induction in the intestinal epithelium (Grabinger, Bode et al. 2017). Therefore, the role of TNF and its receptors in cell survival and cell death induction was further investigated in murine intestinal organoids.

At first, the response of murine organoids to murine TNFα (mTNFα) at different time points after crypt isolation was investigated. Here, organoids were treated at day 1,2, and 3 after crypt isolation with increasing concentrations of mTNFα and cell death was calculated from MTT reduction capacity (Figure 17). Independent of whether organoids were treated on day 1,2, or 3 after isolation, their cell death response was always similar (Figure 17). Thus, we concluded that all epithelial cell types are affected from TNFα treatment. At day 1, $Lgr5^+$ stem cells dominate the relative cellular composition of intestinal organoids. However, this shifts to more differentiated cells at day2, and is mostly comprised of fully differentiated enterocytes at day 3 after isolation (Murrow, Weber et al. 2017, Lindeboom, van Voorthuijsen et al. 2018, Thalheim, Quaas et al. 2018). Nevertheless, it has to be considered that bystander cells might have also died from anoikis. In this scenario, one cell type is specifically targeted by mTNFα and dies. Subsequently, cells in physical proximity may also die from anoikis as cohesion from their adjacent neighbors and adhesion to the extracellular matrix is being lost (Frisch and Francis 1994). Whether the first or the latter hypothesis holds true still has to be investigated. Most likely, a mixture of both actions will happen in the still more complex physiological situation, as also other cellular components such as the immune cells are involved.

Moreover, the role of TNFR1/2 in TNFα-mediated intestinal epithelial cell death was analyzed. Therefore, murine intestinal organoids were treated with mTNFα (targeting TNFR1/2), human TNFα (targeting TNFR1), and STAR2 (targeting TNFR2) (Wajant, Pfizenmaier et al. 2003). All variants of TNFα were shown to induce cell death in wt mice as measured by MTT reduction

(Figure 18, A). Mice lacking either TNFR1/2 however, did not show altered response to different TNF stimuli. Interestingly, mice lacking TNFR1 did die in response to hTNF-treatment which solely binds to TNFR1. The same effect was observed for TNFR2$^{-/-}$ were treatment with STAR2, which selectively targets TNFR2 also lead to cell death induction. The results have shown that specific organoid cell death was not altered from other TNF-stimuli (Figure 18, A). These unexpected results might be explained by the mRNA expression levels of TNFR in the mice used (Figure 18, B). Here, wt mice expressed both TNFR1&2. However, TNFR1$^{-/-}$ mice showed upregulated levels of TNFR2 in response to knockout (KO) of TNFR1, which might be a compensatory effect, also known from other KO-mouse models (Wang, Hummler et al. 2001, Sprossmann, Pankert et al. 2009). TNFR2$^{-/-}$ on the other hand, showed little expression of TNFR2, but absolutely none of TNFR1 as well. Hence, the TNFR2$^{-/-}$ mouse model used has more of the characteristics of a double KO of TNFR1&2 (Figure 18, B). Therefore, the KO-models used did not suffice to decipher the distinct functions of the two TNFRs. In sum, no direct link between cell death induction capacity and one or the other TNFR could be made. In conclusion, the results show that both TNFR1&2 play a role in cell death induction in the intestinal epithelium, whereas TNFR1 might be the predominant receptor for cell death signaling – a "classical" observation (Bigda, Beletsky et al. 1994).

6.1.2 Role of IAPs in intestinal epithelial TNF-signaling

As TNF does not exclusively induce cell death but also cell survival in the intestinal epithelium, activation of NFκB following TNFα treatment +/- LCL161 was analyzed (Van Antwerp, Martin et al. 1996, Van Antwerp and Verma 1996). As IAPs determine whether an intestinal epithelial cell will die upon TNF signaling, NFκB-activation was also investigated in cells treated either with TNF alone or in combination with the SMAC-mimetic LCL161.

Therefore, MC38 cells were transfected with a NFκB luciferase reporter construct and subsequently treated with m/hTNFα +/- LCL161. Treatment with hTNFα alone resulted in increased NFκB-activity, whereas combinatorial treatment with LCL161 leads to a reduction (Figure 19, A). Thus, in presence of a particular IAP, especially cIAP1, TNF triggers a pro-survival signal resulting in NFκB activation, whilst if cIAP1 is downregulated upon LCL161 treatment or genetically knocked out, TNF triggers cell death induction (Grabinger, Bode et al. 2017).

As abovementioned, the SMAC-mimetic LCL161 is known to downregulate IAPs. Cellular IAPs (cIAPs) in particular, are E3-ligases ubiquitinating RIPK1 at the TNFR1-complex. By doing so, ubiquitinated RIPK1 stabilizes NEMO and TAK1 and thus facilitates canonical NFκB- and MAPK-signaling (Vince, Wong et al. 2007, Mahoney, Cheung et al. 2008, Gyrd-Hansen and Meier 2010, Silke and Meier 2013, Silke and Vucic 2014). Additionally, regulation of RIPK-1 activity and its presence is tightly regulated not only by the abovementioned ubiquitination, but also by phosphorylation (Peltzer, Darding et al. 2016).

Moreover, RIPK-1 has a kinase-independent role, protecting from caspase 8-dependent apoptosis, in intestinal epithelial cells, adding another line of decision taking to cellular TNF response (Takahashi, Vereecke et al. 2014). This is of high interest, as it was reported, that colon cancer cells can be primed towards 5-FU-induced, RIPK1-driven, TNFα-dependent necroptosis if caspases were blocked (Oliver Metzig, Fuchs et al. 2016).

Taking into account the abovementioned, treatment of YAMC cells with mTNFα led to an "ubiquitination smear" of RIPK1 after 4 hours. However, if IAPs were downregulated by auto-ubiquitination due to LCL161 pre-treatment, this ubiquitination pattern was not detectable anymore (Figure 19, B). On the one hand, these observations confirm the before mentioned NFκB-activation (IκB downregulation) by the mTNFα treatment. Here, initial IκB-downregulation resulted in a drastic upregulation of IκB after 4h of treatment, indicating a negative feedback loop, a principle widely known in biology (Pan, Li et al. 2006, Bornstein, Winter et al. 2014). On the other hand, enhanced cell death induction through cleavage of effector caspase 3 was observed in samples treated with the combination of mTNFα and LCL161 (Figure 19, B). As a conclusion of these experiments, the role of cIAP as a key arbiter in TNF-induced cell death in the intestinal epithelium was further confirmed (Grabinger, Bode et al. 2017).

6.1.3 Cell death in intestinal epithelial cells

As mentioned before, TNFα can function as a double-edged sword in the intestinal epithelium. On the one hand, TNFα can elicit a strong pro-survival response via the NFκB pathway (Schutze, Wiegmann et al. 1995, Ghosh and Karin 2002, Wajant, Pfizenmaier et al. 2003). On the other hand, TNFα can act as a strong cell death signal, depending on levels of cIAP1 (Grabinger, Bode et al. 2017). How intestinal epithelial cells die upon TNFα encounter

on a molecular basis, is still a matter of debate. Independent of massive influence from the immune system in an *in vivo* situation, like IBD, where TNF plays an important role, both apoptosis as well as necroptosis are likely involved (Dannappel, Vlantis et al. 2014, Sode, Vogel et al. 2014, Takahashi, Vereecke et al. 2014, Francescone, Hou et al. 2015). Here, the death receptor-interacting RIP kinases play an important role, as they represent another major gatekeeper, implicated both in cell death pathways and TNF-induced NFκB-activation (Kelliher, Grimm et al. 1998, Green, Oberst et al. 2011). Building on these studies, the caspase-dependence of apoptosis and the RIPK-need of necroptosis was utilized in the experimental setup. By pharmacologically inhibiting both caspases and RIPK-1, the involvement of both forms of programmed cell death in the intestinal epithelium in TNF-induced epithelial damage was investigated. Therefore, YAMC cells were treated with mTNFα, LCL161, the pan-caspase Inhibitor zVAD, and the RIPK-1-specific inhibitor Nec-1 (see 5.2.3). Combinatorial treatment of YAMC cells with mTNF and LCL161 resulted in high levels of cell death. However, if caspases were blocked with the additional treatment of zVAD, cell death was not reduced but even enhanced. Inclusion of Nec-1 in the treatment ameliorated the cell death and lead to an increased MTT-reduction capacity compared to mTNF, LCL161, and zVAD-treatment (Figure 20, A& B). These results are in line with previous studies, where upon caspase-blockage, TNF-dependent necroptosis was observed in colon cancer and fibrosarcoma cells (Wu, Tan et al. 2011, Oliver Metzig, Fuchs et al. 2016). Moreover, studies in mice with conditionally deleted RIPK-1, show its importance *in vivo*, as these animals spontaneously develop intestinal inflammation and epithelial apoptosis. This drastic effect was partially rescued by additional deletion of RIPK-3 indicating the involvement of necroptosis in intestinal epithelial cell death. However, deletion of TNFR1 and even more pronounced deletion of caspase 8 diminished the RIPK-1-deletion-induced spontaneous inflammation. Hence, TNF and apoptosis play a major role in intestinal epithelial cell death (Takahashi, Vereecke et al. 2014). Moreover, another study showed the RIPK-1 deletion induced-apoptosis was rescued by additional ablation of FADD. However, this triggered RIPK-3 driven necroptosis (Dannappel, Vlantis et al. 2014). This is in line with our data, as we observed that treatment of YAMCs with mTNF and LCL161 lead to stabilization of RIPK1, due to downregulation of IAPs and cleavage of effector caspase 3 (Figure 19, B). However, if caspases were blocked, no decrease, but an increase in cell death was observed (Figure 20, B). This effect was partly restored, when cells were also treated with the RIPK-1 Inhibitor Nec-

1 (Figure 20, B). Therefore, we conclude that YAMC cells die by necroptosis if caspases are blocked. However, as usage of Nec-1 only partially restored the cell death induction, it is suggested that mTNF also elicits caspase-dependent apoptosis (Figure 19& 20, B). To be exclusively clear in these settings, one should use knock-out models of RIPK-1, Caspase 8, FADD and TNFR1 together with knock-in models restoring each component, in order to show the contributions of each programmed cell death pathways in intestinal epithelial cell death. *In vivo*, with the contribution of a complex microbiome and an intact immune system, the situation is quite likely even more complex.

6.2 Quantification of Propidium Iodide and Hoechst3342 as a measure for cell death

6.2.1 Overall considerations

For the past decades, researches have been using the nuclear dye Propidium Iodide to determine cell death in classical cell culture using flow cytometry (Riccardi and Nicoletti 2006). This technology has been recently adapted to assess cell death in dissociated patient-derived organoids (PDOs) (Steele, Chakrabarti et al. 2018). However, this methodology is labor-intensive, as organoids have first to be recovered from the extracellular-matrix substitute (e.g. Matrigel), and will yield in high numbers of false positives, if untreated with ROCK-Inhibitor as detached epithelial cells are prone to undergo anoikis (Zhang, Valdez et al. 2011). Therefore, only recently, a highly-sophisticated method assessing specific organoid cell death, using the nuclear dyes Propidium Iodide and Hoechst33342, has been described. This method however, is of great computational expenditure, and requires long-term organoid monitoring as well as high-content imaging equipment. Nevertheless, it enabled the monitoring of organoid-drug-response in the culture plate, and thereby reducing experimental complexity, as recovery of organoids from extracellular-matrix substitutes and subsequent dissociation were omitted (Jabs, Zickgraf et al. 2017).

Here, we adapted this method to work as a faster and simpler fluorometric method. By quantifying PI& Hoechst fluorescence with a conventional plate reader, experimental and financial expenditures are further decreased, thus making the here described method applicable for standard cell culture labs working with organoids. Additionally, by decreasing measurement time and reducing computational expenses in data evaluation, it has the

possibility to enable any of these labs quantification of cell death in intestinal or other organoids on a mid to large scale.

In summary, intestinal organoids were grown for three days after crypt isolation, treated overnight with chemotherapeutics and were then stained with the nuclear dyes Propidium Iodide and Hoechst33342. After growth-medium exchange to fresh phenol-red free medium, the fluorescence of both dyes was analyzed with a microplate reader (Figure 22).

At first, Gain and Z-position were optimized for highest and lowest expected fluorescence of each dye. With these settings, initial fluorescence units (FU) were converted into relative fluorescence units (RFU), as the signal detected was relative to the maximum Gain, obtained in the initial setting (see 5.6). Subsequently, RFUs of both dyes were used to calculate the PI/Hoechst ratios (Figure 25). Ongoing from these ratios, the treatment-specific organoid cell death was determined by setting the Staurosporine-treated organoids as one hundred percent dead. Afterwards, signal from untreated organoids was subtracted, to exclude background organoid cell death and to specifically show treatment-induced organoid cell death (see 5.6 and Figure 27). All experiments were controlled with the "gold standard" for cell death detection in organoids – MTT (Grabinger, Delgado et al. 2016) and the commercially available CellTiterGlo (Vlachogiannis, Hedayat et al. 2018). Results obtained with the PI/Hoechst staining were in line with CellTiterGlo, and cleavage of effector caspases 3/7, indicating that treatment of organoids with chemotherapeutics reduced intracellular ATP-levels and activated effector caspases (Figure 28).

These results confirm that the increase of treatment-specific organoid cell death derived from PI& H-fluorescence resembled reduced organoid viability (ATP) as well as increased organoid cell death (activation of effector caspases) (Figure 27 and 28).

An additional benefit of microplate-reader-based PI& Hoechst quantification in comparison to MTT-reduction or the intracellular ATP assessment (Figure 26, A, B), is its relative independence of cell number (Figure 26, C). As cell number strongly influences MTT reduction capacity per well (Grabinger, Luks et al. 2014), even plating of crypts/organoids is required – a condition hardly ever achieved with primary organoids. Quantification of PI& Hoechst on the other hand, allowed to internally "normalize" to total cell number in differing numbers of organoids (Hoechst positive organoids= total DNA), and therefore reduced the negative effect of uneven plating during crypt/organoid seeding (Figure 26, C).

However, using PI and Hoechst as readout for cell death does not allow to distinguish what form of cell death the organoid actually dies from. More specific assays e.g. quantifying activity of caspases (Kaufmann, Lee et al. 2008), presence of RIPK1 (He, Huang et al. 2016), or LDH release (Chan, Moriwaki et al. 2013) or more sophisticated "-omics" and high-throughput approaches may be more appropriate to assess the molecular type of cell death (Burkhart, Baker et al. 2018, Gunasekara, DiSalvo et al. 2018, Kondo, Ekawa et al. 2018, Lindeboom, van Voorthuijsen et al. 2018).

Nevertheless, this lack of information in the presented fluorometric method is compromised by its experimental speed, simplicity, low cost, and its internal normalization with the Hoechst stain (total DNA) (Figure 25 and 26). As abovementioned, this is addressing a fundamental problem in organoid technology, as abovementioned to seed equal number of organoids during plating. Therefore, the here presented method can be applied in practice, mostly to accompany and add to the MTT reduction test (Grabinger, Delgado et al. 2016).

As Jabs et al. showed, that staining of organoids with the nuclear dyes PI& Hoechst does not impair drug-induced cell death (Jabs, Zickgraf et al. 2017) it is expected that usage of both dyes is applicable for organoid cell death detection, especially if being used in a multiplexed system (Figure 30).

6.2.2 Comments on PI& Hoechst assay quality

With respect to fluorescence images, PI levels rise with increasing concentrations of chemotherapeutic treatment. However, Hoechst levels remain unaltered, independent of treatment (Figure 25, A). Quantification of PI& Hoechst RFUs follows the same pattern: with increasing concentrations of chemotherapeutic treatment increasing PI fluorescence units were detected, whilst Hoechst fluorescence units are only slightly diminished following chemotherapeutic treatment (Figure 25, B). Thus, forming the ratio of PI^+ / $Hoechst^+$ cells gives a good base for treatment-specific organoid cell death quantification (Figure 27, A, B).

However, fluorescence detection in the described assay system is not too robust, as standard deviations are quite high (Figure 25, 27). This, nonetheless is in part reflecting the *in vivo* situation. Inter-experiment variances might therefore be explained by mouse to mouse differences, as well as by varying qualities of crypt isolation. Moreover, quantification of PI&H RFUs is only significantly different from untreated control, if cell death can also be visually

observed with a microscope. Meaning, only from concentrations of 10µg/ml Cisplatin/5-FU onwards significant differences to the solvent control (untreated) can be measured (Figure 25, 27). Taking these results into consideration, it becomes evident that the quantification of the nuclear dyes PI& Hoechst in intestinal organoids with our described plate-reader based method, is not very sensitive. Therefore, the described PI&H-assay should mostly be used in cases were real end-point toxicity is the aim of detection as subtle effects cannot be differentiated from untreated control. Therefore, as for all novel methods, fields of application and experimental design have to be chosen with care (Leist and Hengstler 2018). Nevertheless, PI& Hoechst staining has been used effectively by other groups. However, in this case, PI& Hoechst-stained organoids were analyzed microscopically in Z-stacks and area of PI& Hoechst-stained organoids was used to calculate cytotoxic or cytostatic effects over time (Jabs, Zickgraf et al. 2017). Moreover, PI& Calcein-AM stained organoids were used for cell death quantification via microscopic analysis as well (Bulin, Broekgaarden et al. 2017). With regards to the two latter described methodologies, high-content imaging allows to get further information from the same image/well/sample, namely cytotoxic versus cytostatic effects, changes in organoid morphology, and the influence of organoid size on drug-response (Celli, Rizvi et al. 2014). Following these applications, the nuclear dyes PI& Hoechst are well suitable for quantification of organoid cell death.

However, in the setup used in this thesis, further drawbacks using the quantification of PI& Hoechst fluorescence have to be tightly monitored: As extracellular matrix substitutes, such as BME or Matrigel harbor DNA themselves (Corning), the background staining has to be taken into consideration (Figure 22& 23). Therefore, synthetic matrices will have the additional advantage to defined chemical composition of being DNA-free, thus reducing the background staining (Gjorevski, Sachs et al. 2016, Cruz-Acuna, Quiros et al. 2017, Tong, Martyn et al. 2017). In line with the before mentioned, a strong background for wells with BME only was observed (Figure 22& 23, A and B). This background was especially pronounced for the dye Hoechst33342. Strikingly, stained medium by itself, with no cellular DNA present, showed a strong unspecific background – an unexpected effect: Unbound Hoechst exhibits a lower fluorescence intensity than DNA-bound Hoechst33342, which emission peak is re-shifted by 50nm to lower wavelengths. Therefore, by using a monochromator (Tecan, M200 Pro), and setting a single specific wavelength to detect Hoechst emitting fluorescence,

detection of fluorescence being emitted from unbound dye can be avoided (Asbury, Esposito et al. 1996, Petersen, Ibrahim et al. 2004).

However, fluorescence from stained medium in this setup was still detectable as some kind of leakage must occur. By subtracting the BME-background signal from the actual signal (crypts/organoids in BME/Matrigel) the treatment-specific cell death was calculated. The resulting PI/H ratio was still at a considerably high level, showing that background staining does not falsify the readout or diminish it completely (Figure 22& 23, E and F). The usage of fluorescence-optimized media (phenol-red free) was taken into consideration as well as detection limits together with the spatial resolution of the plate reader being used (Figure 25). Another issue is the exchange/removal of growth medium and its replenishment with new phenol red-free medium for the measurement (Figure 23). Here, remarkable differences between staining medium and new medium were detected. Especially, the background (BME+ medium) was reduced if fluorescence was measured in new, phenol red-free medium and PI/H ratio (background subtracted) was increased in new medium in comparison to growth medium with the nuclear dyes PI and Hoechst (Figure 23, E and F). Investing into black-walled clear bottom plate with glass-like optical properties may additionally improve signal to noise ratio as well as sensitivity and robustness, as plate-usage can have drastic effects on measurement outcome (Cui, Gilda et al. 2014). Furthermore, assessing Z-stacks with the plate-reader could further improve assay-sensitivity. However, this goes with cost of experimental speed and would drastically complicate data evaluation.

Still, the presented method of PI& Hoechst quantification has further limitations with respect to applicability. For instance, this method is not suitable to determine short-term toxicity in organoids leading to mitochondrial damage and caspase activation, but can only be used for long-term treatment were necrosis, secondary necrosis, or any other form of cell death takes place. Moreover, the presented method does not allow to distinguish what form of cell death the treated organoids have actually died from. Taken together, only if cellular membrane integrity is disrupted, cellular DNA will stain PI positive and will allow treatment-induced cell death detection with PI& Hoechst quantification in organoids. This is of importance, as timing of endpoint/measurement and duration of treatment have a major impact on effects of drug-induced cell death (Troger, Fischel et al. 1992, Raymond, Hanauske et al. 1997, Vita, Nagachar et al. 2011).

6.2.3 Application of PI& Hoechst quantification

The method of quantifying PI& Hoechst fluorescence quantification presented here can be used not only for murine and human intestinal organoids as shown here, but it application can be extended to all types of organoids and three-dimensional-cell-structures, generated today (Ingber 2018). Moreover, quantification of PI&H fluorescence can be added to the already established MTT/MTS reduction assay (Grabinger, Delgado et al. 2016, Steele, Chakrabarti et al. 2018).

By multiplexing these two methods, cell death as well as effects on mitochondrial respiration can be assessed in the same plate, well and even single organoid if of interest (5.9, Fig 30). This allows not only to analyze murine intestinal organoids, as well as murine tumoroids (Figure 30, C), but also human, patient-derived organoids (PDOs) (Figure 30, D). By doing so, individual weaknesses of the different methods such as background signal (PI&H), cell number (MTT), and sensitivity (PI&H and MTT) are ameliorated and counterbalanced.

Furthermore, multiplexing PI& Hoechst and MTT reduction will lead to increased data generation and therefore information, from limited sample size, as already being done with two-dimensional cells (Duellman, Zhou et al. 2015). Thus, the given results suggest to use both methods in combination in order to obtain optimal information from experiments is highly recommended. However, considering the limitations discussed in 6.2.2, PI& Hoechst quantification, also in combination with the MTT-reduction assay, should be mostly used in screening approaches where a response or no response in the endpoint analysis is the aim of detection. To measure a real dose-response over a wide concentration range of a e.g. chemotherapeutic drug, PI& Hoechst and MTT-reduction, at least in the setup presented here, are not sensitive enough.

Nevertheless, quantifying cell death in organoids is needed in numerous research and future applicative fields. Cancer research is one of the most prominent examples. Here, in ductal pancreatic cancer, prostate cancer and gastrointestinal cancer a lot of progress has been made to utilize PDOs to model drug response of certain tumor types (Gao, Vela et al. 2014, Huang, Holtzinger et al. 2015, Hubert, Rivera et al. 2016, Wills and Drenth 2017, Perkhofer, Frappart et al. 2018, Vlachogiannis, Hedayat et al. 2018). This is of especially great interest, as it was shown in gastrointestinal cancer-derived PDOs, that 96% of the parental and the PDO mutational spectrum would overlap, on top of histological similarities. Closely

resembling the *in vivo* situation, these PDOs made progress in stepping further towards individualized cancer medicine (Vlachogiannis, Hedayat et al. 2018). Moreover, an organoid-like 3D-primary cell culture model has been effectively used to screen 306 emerging oncology compounds on their efficacy towards influencing cell survival and corresponding drug-sensitivity score (Saeed, Rahkama et al. 2017). This is due to the fact that already since 2016, protocols for mid- and large-scale screening approaches based on luminescent readouts using the commercially available CellTiterGlo, are well described and used (Francies, Barthorpe et al. 2016, Li, Francies et al. 2018). In order to push organoid technology towards translational research for bench-to-bedside application, further expansion of specialized analysis technology, as the here presented method of PI& Hoechst quantification is definitely needed (Fan, Davidson et al. 2015, Boehnke, Iversen et al. 2016, Walsh, Cook et al. 2016, Bulin, Broekgaarden et al. 2017, Jabs, Zickgraf et al. 2017, Saeed, Rahkama et al. 2017, Steele, Chakrabarti et al. 2018).

6.2.4 Translational usage of PI& Hoechst quantification

Also, classical cell culture can benefit from the quantification of PI& Hoechst fluorescence, as the method is applicable in MC38 and Caco2 cells (Figure 29). Here, murine MC38 as well as human Caco2 cells responded with increasing PI/H ratios to increasing concentrations of the chemotherapeutic cisplatin (Figure 29). However, standard deviation is – as often observed in cell culture – a lot smaller than in primary organoids (Figure 29, A). Moreover, in Caco2 cells, sensitivity was higher than in organoids, as already 3µg/ml Cisplatin generated significant differences to untreated control (Figure 29, A). However, this effect was not seen in MC38 cells (Figure 29, A). Although of less importance in 2D, as there are other well-established methods to quantify cell death (e.g. Annexin-V/PI, TUNEL, DEVD-assay) there might be still applications for our presented method of plate reader-based quantification of PI& Hoechst fluorescence (van Engeland, Nieland et al. 1998, Kaufmann, Lee et al. 2008, Loo 2011, Lekshmi, Varadarajan et al. 2017).

6.3 Concluding remarks & Future perspectives

Cell stress and cell death detection in three-dimensional organoids is until today limited as only few complex and expert-knowledge requiring methods exist. Established assays being

frequently used in the field, mostly rely on measuring lowered mitochondrial respiration or require specialized equipment and extensive computational power. This has obvious limitations, as assessment of mitochondrial activity does only in part reflect cell death, and lengthy, highly complex methods that can only be used in a selected number of laboratories, limit world-wide broad-scale applications. As organoids harbor great potential to be used in the future not only in basic research question and pharmaceutical companies for drug development, but also in personalized medicine, robust methods that allow direct assessment of specific organoid cell death, are necessary. Considering that these kind of experiments, or rather clinical/personalized diagnostics will require mid- to high- throughput analysis, it is straightforward that assays need to be easily applicable. Additionally, as costs for organoid cultivation and subsequent patient treatment with biologicals will reach unpreceded levels, everyday analysis should be inexpensive. This includes not only consumables, but also instruments, staff, and server systems. Moreover, transferability as well as user-friendliness need to be taken care of, as diagnostics of such kind might be performed throughout the world. Therefore, the presented methodology quantifying fluorescent nuclear dyes in a plate reader, especially multiplexed with already established methods like MTT reduction or analysis of intracellular ATP, assessing changes in mitochondrial respiration, is an important step in the ongoing process of bringing organoids from bench-to-bedside.

Taken together these applications, there is an obvious need for further technologies as already published ones to quantify cell stress and cell death in organoids. By using two already established nuclear dyes, PI& Hoechst, but simplifying and dramatically increasing the read-out and analysis speed, by reducing cost and experimental equipment at the same time, the described PI& Hoechst quantification in a plate reader holds potential to be used as a first in line method to quickly assess chemo/radiation or general drug-induced cell death in basic research and PDOs.

7. Materials and methods

7.1 Materials

7.1.1 Cell culture ware

Cell culture ware	Abbreviation/Synonym	Catalog Number	Manufacturer
6-well plate	6-well plate	83.3920	Sarstedt
24-well plate	24-well plate	83.3922	Sarstedt
96-well plate	96-well plate	83.3924	Sarstedt
Easystrainer 70µm		542070	Greiner Bio-one
Cell culture flask T75cm2		83.3911.002	Sarstedt
Cell culture flask T175cm2		83.3912.002	Sarstedt
5ml pipet		861.253.001	Sarstedt
10ml pipet		861.254.001	Sarstedt
25ml pipet		861.685.001	Sarstedt
10 µl pipet tip		70.760.002	Sarstedt
200 µl pipet tip		70.1130	Sarstedt
1000 µl pipet tip		70.762.411	Sarstedt
15ml Falcon Tube	15ml Falcon	62.554.502	Sarstedt
50ml Falcon Tube	50ml Falcon	62.547.004	Sarstedt

7.1.2 Media/supplements

Media/Supplements	Abbreviation/Synonym	Catalog Number	Manufacturer
Trypsin EDTA	Trypsin	T3924	Sigma
L-Glutamine	Glutamine	G7513	Sigma

Dulbecco's Modified Eagle's Medium - high glucose	DMEM	D5796	Sigma
Dulbecco's Modified Eagle's Medium - high glucose Phenol red free	DMEM – phenol red free	D1145	Sigma
Iscove's Modified Dulbecco's Medium	IMDM	I3390	Sigma
Dulbecco's Modified Eagle's Medium F12	DMEM-F12	D6421	Sigma
RPMI-1640 Medium	RPMI	R8758	Sigma
Phosphate buffered saline	PBS	D8537	Sigma
Trypan Blue solution	Trypan Blue	93395	Sigma
N2 supplement	N2	17502-048	Fisher Scientific
B27 supplement	B27	17504-044	Fisher Scientific
Gentle Cell Dissocoation Reagent		07174	Stemcell
BD Matrigel Basal membran matrix	Matrigel	734-0269	VWR
Cultrex® Reduced Growth Factor Basement Membrane Matrix, Type 2 (BME 2)	BME	3533-010-02	Trevigen
Geltrex™ LDEV-Free Reduced Growth Factor Basement Membrane Matrix	Cultrex	12053569	Fisher Scientific
Fetal Bovine Serum low in Endotoxin	FBS	F7524	Sigma

Insulin-Transferrin-Sodium Selenite Supplement	ITS	11074547001	Roche
Penicillin/Streptomicin	PenStrep	P4333	Sigma
Gentamicin	Genta	G1397	Sigma

7.1.3 Chemicals/Solutions

Chemicals/solutions	**Abbreviation/Synonym**	**Catalog Number**	**Manufacturer**
Bovine Serum Albumine	BSA	T844.3	Roth
HEPES		9105.3	Roth
TEMED (N, N, N´, N´ Tetramethylethylenediamin)		411019	Sigma
Hydrogen peroxide (30%)		8597	MERCK
Rotiphorese® Gel 30	Acrylamide	3029.1	Roth
PageRuler Plus Prestained Protein Ladder		26616	Fisher Scientific
p-Coumaric acid		C-9008	Sigma
Luminol		A8511	Sigma
NP-40		i3021	Sigma
Triton X-100		T8787	Sigma
Natriumdeoxycholate		6504	MERCK
SDS pellets		CN30.3	Roth
Trizma hydrochloride	Tris-HCl	T5941	Sigma
Sodium Cloride	NaCl	S9888	Sigma
Ammoniumperoxodisulfate	APS	9592.2	Roth
Y-27632 Dihydrochloride	ROCK-Inhibitor	Y0503	Sigma

cis-Diammineplatinum(II) dichloride	Cisplatin	P4394	Sigma
5-Fluorouracil	5-FU	F6627	Sigma
Penicillin-Streptomycin	PenStrep	P4333	Sigma
Gentamicin solution	Gentamicin	G1272	Sigma
LCL161		A11928-10	AdooQ Bioscience
Z VAD FMK	zVAD	ALX-260-020-M001	Enzo
Propidium Iodide 1mg/ml solution	PI	P3566	Fisher Scientific
Hoechst 33342, Trihydrochloride, Trihydrate	Hoechst	H1399	Fisher Scientific
Dimethylsulfoxid	DMSO	7029.2	Carl Roth
Staurosporine		ALX-380-014-C250	Enzo Life Sciences
SB202190		1624	Enzo Life Sciences
A83-01		2939	Tocris
CHIR-99021 (CT99021)	CHIR	S1263	Selleckchem
Nicotinamide		N3376	Sigma
[Leu15]-Gastrin I	Gastrin	G9145	Sigma
N-acetyl-cysteine	NAC	A9165	Sigma
3-(4,5-Dimethylthiazol-2-yl)-2,5-diphenyltetrazoliumbromid	MTT	M2128	Sigma
Tetramethylrhodamine, Methyl Ester, Perchlorate	TMRM	T668	Sigma
peqGOLD TriFast reagent		30-2010	PeqLab

7.1.4 Growth factors/Cytokines

Growth factors / cytokines	Abbreviation/Synonym	Catalog Number	Manufacturer
mEGF		315-09	Peprotech
mNoggin		250-38	Peprotech
hR-Spondin 1		120-38	Peprotech
mTNFα		315-01A	Peprotech
mIFNγ		315-05	Peprotech
hTNFα			Kind gift of H.Wajant, Würzburg
STAR2	Nonameric TNFα		Kind gift of H.Wajant, Würzburg

7.1.5 Cell lines

Cell line	Abbreviation/Synonym	Catalog Number	Manufacturer
Human embryonic kidney 293	Hek293		Courtesy of T.Brunner, Konstanz
Human embryonic kidney 293 T	Hek293 T		Courtesy of T.Brunner, Konstanz
Murine colon carcinoma 38	MC38		Courtesy of T.Brunner, Konstanz
Human caucasian colon-2	Caco-2		Courtesy of T.Brunner, Konstanz
Immortalized Mouse Colonic Epithelial Cells-Conditionally	YAMC		Courtesy of T.Brunner, Konstanz

7.1.6 Antibodies

Primary Antibodies	**Abbreviation/Synonym**	**Catalog Number**	**Manufacturer**
anti-PARP (46D11)		9532S	Cell Signaling
anti-cIAP1 (D5G9)		7065S	Cell Signaling
anti-cIAP2 (58C7)		3130S	Cell Signaling
anti-XIAP (3B6)		2045S	Cell Signaling
anti-Tubulin		T5168	Sigma
anti-Caspase 3 (proform+active subunits)		9662S	Cell Signaling
Secondary Antibodies (HRP-conjugated)	**Abbreviation/Synonym**	**Catalog Number**	**Manufacturer**
Peroxidase AffiniPure Goat Anti-Mouse IgG (H+L)	Anti-mouse	115-035-003	Jackson Immuno Research
Peroxidase AffiniPure Goat Anti-Rabbit IgG	Anti-rabbit	111-035-144	Jackson Immuno Research

7.1.7 Kits

Kit	**Abbreviation/Synonym**	**Catalog Number**	**Manufacturer**
CellTiter-Glo® 3D Cell Viability Assay	CellTiter-Glo	G9681	Promega
Cell Meter™ Live Cell Caspase 3/7 Assay Kit		20250	AAT Bioquest
Pierce™ BCA Protein Assay Kit	BCA assay	23225	Fisher Scientific
FAST SYBR Green Master Kit		4385612	Applied Biosystems
cDNA Reverse Transcription Kit		4368814	Applied Biosystems

7.1.8 Equipment

Equipment	Abbreviation/Synonym	Catalog Number	Manufacturer
Tecan Infinite M200 Pro - Platereader	Tecan		Tecan
Axio Observer.Z1	Fluorescence Microscope		Zeiss
ImageQuant LAS 4000			General Electric
HeraCell CO_2/O_2-Incubator	Incubator		Fisher Scientific
HeraSafe Laminar Flow			Fisher Scientific
Megafure 2.0 R			Heraeus
Thermomixer F1.5			Eppendorf
Centrifuge 5804 R			Eppendorf
Centrifuge 5427 R			Eppendorf
NanoDrop 2000	NanoDrop		Fisher Scientifc - Peqlab
TissueLyser II			Quiagen
StepOnePlus Real-time PCR system			Applied Biosystems

7.1.9 Software

Software	Abbreviation/Synonym	Catalog Number	Manufacturer
Graphpad Prism			Graphpad Software
ImageJ			NIH
AxioVision 4.8.2			Zeiss
PalmRobo			Zeiss
MS Office			Microsoft
i-control 2.0.10			Tecan
Adobe Photoshop CS6			Adobe

7.2 Methods

7.2.1 Mice

C57BL/6, TNFR1$^{-/-}$, and TNFR2$^{-/-}$ mice were bred and kept in individually ventilated cages at the central animal facility of the University of Konstanz. APC$^{Min/+}$ mice were a kind gift of Jan Paul Medema, Amsterdam.

7.2.2 Generation of murine intestinal organoids

Intestinal crypts were isolated as described previously with minor changes (Sato, Vries et al. 2009, Grabinger, Luks et al. 2014). Shortly, the small intestine of 8- to 16-week-old C57BL/6 wild-type was cut open in length. Then, villi were removed by scraping with a microscope slide. Afterwards, the intestine was cut into 3-4 cm pieces, washed three times with cold PBS (Ca^{2+} and Mg^{2+} free) and incubated with 2 mM EDTA in PBS for 30 minutes at 4°C on a rotating wheel. All subsequent steps until seeding were performed on ice. Supernatant was restored with fresh PBS, shaken to remove residual villi, and again replaced by fresh PBS. Each fraction was checked for crypt/villus ratio under the microscope. Up to four crypt-fractions were pooled, filtered through a 70 µm cell strainer (BD Biosciences), centrifuged at 100 × g (3 minutes, 4°C) and resuspended in 5 ml PBS for crypt counting under the microscope. Required amounts of crypts were centrifuged at 80 x g (3 minutes, 4°C) and the pellet resuspended in Matrigel (BD Biosciences) or in Basement Membrane Extract (BME), Type II (R&D). Two hundred to 300 crypts were seeded per well in 8 µl Matrigel or BME on a 96-well flat-bottom plate (Sartstedt), or 1000-1200 crypts in 40 µl Matrigel or BME per well on a 24-well plate (Sarstedt). Seeded crypts were incubated for 20 minutes at 37°C to let Matrigel/BME solidify. Then, 80 µl or 400 µl of complete crypt culture medium per well was added gently (ADF medium: advanced DMEM/F12 (Sigma), 0.1 % BSA (PAA), 2 mM L-glutamine (Sigma), 10 mM HEPES (Sigma), 100 U/ml penicillin (Sigma), 100 µg/ml streptomycin (Sigma), 1 mM N-acetyl cysteine (Sigma), 1× B27 supplement (Invitrogen), 1× N2 supplement (Invitrogen), 50 ng/ml mEGF (Peprotech), 100 ng/ml mNoggin (Peprotech)). hR-Spondin-1 was added as conditioned medium of hR-spondin-1-transfected Hek 293T cells to a final volume of 25% (v/v) to crypt culture medium (see Appendix, 9.2). Organoids were cultured at 37 °C in a 5% CO_2 atmosphere for 1-3 days before cell death induction.

7.2.3 Generation of murine tumoroids

Organoids from murine tumors (tumoroids) were generated similar as described previously with slight modifications (Xue and Shah 2013). Briefly, the small intestine of $APC^{Min/+}$ mice was cut open in length. Tumors were isolated from intestinal tissue with scissors and forceps and cut into small pieces. Subsequently, tumor fragments were washed thrice with ice cold PBS (Ca^{2+} and Mg^{2+} free). Then, tumor fragments were incubated in digestion buffer (DMEM, 2.5% FBS, 100 U/ml penicillin (Sigma), 100 µg/ml streptomycin (Sigma), 200 U/ml Collagenase IV (Sigma), 125 µg/ml Dispase II (Corning, Bedford, USA)) for 1 h at 37°C, 5% CO_2. Cell suspension was shaken every 15 minutes. After 1 h, tumor fragments were allowed to settle for one minute. Subsequently, supernatant was taken and centrifuged at 200xg for 3 minutes. The pellet was washed with 5ml PBS and then filtered through 70µm and then through a 40µm cell strainer (Greiner). After centrifugation (200xg for 3 minutes), cells were resuspended in 500 µl PBS and counted. Cell numbers were adjusted to $1.5x10^4$ cells/50 µl Matrigel/BME. Complete growth medium with only 50 ng/ml mEGF (Peprotech) was added. Medium was exchanged every 4 days. Tumoroids were split according to density but mostly every week. Therefore, medium was removed and tumoroids were incubated in cold PBS for 1 h on ice. Subsequently, Matrigel was dissociated mechanically with a pipet tip and resuspended in cold PBS. Then, tumoroids were centrifuged at 200 x g for 3 minutes and the pellet resuspended in TrypLE Express (Thermo Fisher Scientific) for 15 minutes at RT. Tumoroid fragments were then centrifuged at 350 x g for 3 minutes and split in a 1:4 ratio for further culture.

7.2.4 Cultivation of human intestinal organoids

Human intestinal organoids were a kind gift from Dr. Marcus Metzger, TERM (Tissue Engineering and Regenerative Medicine), University of Würzburg and were cultivated as described previously (Schweinlin, Wilhelm et al. 2016). Briefly, organoids were thawed and cultured in a mixture of 50% basal medium containing 500 ng/ml hR-Spondin-1, 50 ng/ml mEGF, 100 ng/ml mNoggin, 10 nM [Leu15]-Gastrin I, 10 mM Nicotinamide, 500 nM A83-01 (TGFβ-Inhibitor), 10 µM SB202190 (p38/MAPK-Inhibitor), 10 µM Y-27632 (ROCK-Inhibitor), and 50% (v/v) Wnt3A-conditioned medium. Growth medium was replenished every 2^{nd} to 3^{rd} day, and organoids were passaged weekly.

7.2.5 Staining with PI and Hoechst

Intestinal organoids were stained with PI (Sigma) and Hoechst 33342 (Thermo Fisher Scientific) at a final concentration of 10 μg/ml in a 96-well plate. Staining solution (dyes in PBS) was directly added to culturing medium after treatment. Organoids were stained for 30 minutes at 37°C, 5% CO2. Then, medium with staining solution was removed and replaced by fresh phenol-red-red free DMEM-medium (Sigma). Subsequently, fluorescence was analyzed in plate with a plate reader (Tecan) or by fluorescence microscopy (Zeiss). Caco2 and MC38 cells were stained with 5 μg/ml PI and Hoechst.

7.2.6 Fluorometric quantification of cell viability and death in intestinal organoids

Fluorescence of stained organoids was quantified in clear culturing 96-well plates in a microplate reader (Tecan). Measurements were taken from top. Before measuring, staining medium was replaced with fresh phenol-red-free medium (DMEM). First, the Gain was set to the wells for the highest expected cell death (PI) and the lowest expected cell death (Hoechst) and was checked for values between 115 and 160. Then, Z-position was determined automatically from the corresponding wells and was checked for values between 1.5 x 10^6 and 1.6 x 10^6 μm. Subsequently, fluorescence was measured with 25 flashes, with an integration time of 20 μs. Lag and settle time were set to 0s. Per well, four times four measurements were taken with a boarder of 1mm around measurement points. Excitation and emission wavelengths for PI were 535 nm and 617 nm, respectively. For Hoechst, 361 nm and 486 nm were used as excitation and emission wavelengths. During the measurement, first all wells were measured for PI fluorescence and after a 30 s wait timer for Hoechst fluorescence. For Caco2 and MC38 cells, fluorometric quantification was performed the same, with minor modifications. Here, 6 x 6 multiple reads were performed. Moreover, the border was extended to 1.25 mm. Gain setting was performed as for 3D organoids, whereas Z-plane was only determined once for each cell type and subsequently used for all follow-up experiments.

7.2.7 Determination of organoid viability and death with MTT reduction

Organoid viability was assessed by MTT reduction as described in detail earlier (Grabinger, Luks et al. 2014). Briefly, after cell death induction, MTT (Sigma) solution was added to the

organoid culture to a final concentration of 500 µg/ml for 1 h at 37°C, 5% CO_2. Then, medium was discarded and 20 µl of 2% SDS (Sigma) solution in H_2O was added per well to solubilize the Matrigel/BME (1 h, 37 °C). Subsequently, 80 µl of DMSO per well were added for 1 h (37 °C) to solubilize the reduced MTT and the OD was measured at 562 nm in a plate reader (Tecan). Specific cell death was calculated as described before using the following formula (Grabinger, Delgado et al. 2016):

$$specific\ cell\ death\ (\%) = \left[1 - \frac{OD\ (sample)_{562nm}}{OD\ (control)_{562nm}}\right] * 100$$

For 2D cells, cell viability and cell death were analyzed the same. However, the step including SDS-solubilization was omitted. Here, specific cell death was calculated as above. Moreover, MTT-reduction capacity was calculated as follows:

$$MTT - reduction\ (\%) = \left[\frac{OD\ (sample)_{562nm}}{OD\ (control)_{562nm}}\right] * 100$$

7.2.8 Cell culture

The human colorectal tumor cell line Caco-2 was cultured in IMDM (Sigma) supplemented with 10% fetal calf serum (FCS, PAA), 4 mM L-glutamine and 50 µg/ml gentamycin (Sigma) at 37 °C and 5% CO_2 (Grabinger, Luks et al. 2014). The murine colon adenocarcinoma cell line MC38 was cultured in DMEM (Sigma), supplemented with 10% FCS (PAA), 2mM l-Glutamine and 10,000 U penicillin/ml and 10 mg streptomycin/ml (Sigma) at 37 °C and 5% CO_2. The human embryonic kidney 293T (Hek293T) cell line was cultured in DMEM (Sigma), supplemented with 10% FCS (PAA), 2mM l-Glutamine and 10,000 U penicillin/ml and 10 mg streptomycin/ml (Sigma) at 37 °C and 5% CO_2. The conditionally immortalized young adult mouse colon (YAMC) cell line (gift of R. Whitehead, Vanderbuilt University)(Whitehead, VanEeden et al. 1993) was cultured at 32°C with 5% CO_2 in RPMI 1640 medium (Sigma), supplemented with 5% FCS, ITS solution (Gibco), 50 µg/ml Gentamicin (Sigma) and 5 U/ml mIFNγ. For experiments, incubation of YAMCs at 32°C was changed to 37°C and cells were subsequently treated in culture medium without mIFNγ.

7.2.9 SDS-PAGE and Immunoblotting

For organoids, complete medium was removed. Then, Matrigel/BME was dissolved in 200 µl Cell Recovery Solution (Corning) for 1 h on ice. Samples were then centrifuged at 1000 x g at 4°C for 5 minutes, washed once with cold PBS and centrifuged at 1000 x g at 4°C for 5 minutes. Organoid pellets were lysed for 20 minutes in RIPA lysis buffer (150 mM NaCl, 1% NP-40, 0.5% Natriumdeoxycholate, 0.1% Sodium dodecyl sulfate (SDS), 50 mM Tris-HCl, pH 8.0) on ice. Lysates were centrifuged at 20000 x g for 20 minutes at 4°C and the supernatant was collected. For cell culture, cells were scraped in medium using cell scrapers (Sarstedt). Cells were then centrifuged at 400 x g, RT for 5 minutes and the pellet was subsequently lysed for 20 minutes in RIPA lysis buffer on ice. Lysates were centrifuged at 20000 x g for 20 minutes at 4°C and the supernatant was collected. Total protein concentration was determined using BCA assay (Pierce) following manufacturer's guidelines. Samples were boiled with SDS sample buffer (95°C, 5 minutes), resolved on SDS polyacrylamide gel electrophoresis gels (12%) and transferred to a polyvinylidene difluoride membrane (PVDF) at 350 mA for 60-120 minutes, depending on the proteins being analyzed. Immunoblot analyses were performed using specific unlabeled primary antibodies. For that, PVDF membranes were incubated with primary antibodies for 1 hour at RT or at 4°C overnight. Then, membranes were washed three times in TBS-T and incubated for one hour at room temperature with HRP-labeled secondary antibody. Proteins of interest were afterwards visualized using ECL and H_2O_2 (1000:1) with a biomolecular imager (ImageQuant LAS4000). Densitometry analysis was performed using ImageJ (National Institutes of Health).

7.2.10 Fluorescence microscopy

Intestinal organoids were stained as described above (7.2.5) and fluorescence was subsequently analyzed in Matrigel or BME in plate on a Axio Observer.Z1 microscope (Zeiss). Brightfield images were taken with Palm-ROBO and fluorescence images were taken with AxioVision Software (Zeiss).

7.2.11 Determination of intracellular ATP

Intracellular ATP, was detected by usage of CellTiter-Glo® 3D Cell Viability Assay (Promega), according to manufacturer instruction with minor modifications. Briefly, organoids were

treated in a 96-well plate. After treatment, supernatant of organoids was removed and collected. Subsequently, organoids in Matrigel domes were lysed in 100 µl pre-warmed (RT) CellTiter-Glo® 3D solution. Then, lysed cells were incubated for 30 minutes in the dark whilst gently shaking. Afterwards, luminescence was recorded using a plate reader (Tecan).

7.2.12 Analysis of activated effector caspases

Activated effector caspases were analyzed using the Cell Meter™ Live Cell Caspase 3/7 Assay Kit according to manufacturer instructions. In short, medium of treated organoids was removed and replaced by 100 µl, 1:500 caspase 3/7 staining solution diluted in Hank's Balanced Salt solution (HBSS). Fluorophores were excited at 350 nm and emission was detected at 470 nm using a plate reader (Tecan).

7.2.13 Transient transfection of eukaryotic cells

Hek293T cells were seeded the day before transfection. On the day of transfection, medium was removed from the cells, and fresh medium added. Then, two tubes were prepared: Tube 1 containing 50 µl $CaCl_2$ 2.5M, H_2O until 200 µl total volume and 5 µg of plasmid of interest. Tube 2 containing 200 µl 2x HBS buffer. Afterwards, DNA/$CaCl_2$ solution (Tube 1) was dropwise added to Tube 2 whilst gently vortexing. Then, DNA precipitate was incubated for 30 minutes at RT and added dropwise to the cells. Medium was exchanged after 6-8 hours or overnight.

7.2.14 Generation of hRSpondin-1 conditioned medium

Hek293T cells were transfected with pcDNA3.1 containing hRSpondin1, inserted by EcoRI-HF and BamHI-HF (New England Biolabs). Media was exchanged for three days after transfection and subsequently pooled, centrifuged at 400 x g at RT and supernatant, termed "conditioned medium" was used to culture primary murine intestinal organoids (see 9.2, Figure 31).

7.2.15 Statistical analysis

Statistical analysis was performed using GraphPad Prism. Unless denoted otherwise, experiments were performed three times independently, n=3 with technical triplicates. One-

way ANOVA, with Dunnett's multiple comparisons test was performed, with $p \leq 0.05$ (*), $p \leq 0.01$ (**), $p \leq 0.001$ (***), $p < 0.0001$ (****). Furthermore, unpaired t-test was performed with $p \leq 0.05$ (*), $p \leq 0.01$ (**), $p \leq 0.001$ (***), $p < 0.0001$ (****).

7.2.16 Luciferase reporter assay

Luciferase reporter assay was performed as described previously with minor modifications (Schwaderer, Gaiser et al. 2017). MC38 cells were transiently transfected with expression and NKκB-luciferase reporter plasmids. Co-transfection with β-galactosidase expression plasmid served as an internal normalization. One day after transfection, cells were either control treated, treated with different concentrations of m/hTNFα +/- (30 ng/ml / 100 ng/ml) overnight, pre-treated with LCL161 [500 nM] for 2 h, or with PMA [10 ng/ml] overnight. Then, cells were lysed (100 mM K_2HPO_4, 0.2% Triton X-100, pH 7.8) for 15 minutes on ice. Lysates were then centrifuged at 500 x g for 10 minutes at RT and supernatants used for luciferase measurement. Therefore, 30 µl lysate was mixed with 50 µl ATP-solution (10 mM ATP, 20 mM $MgCl_2$, 35 mM Glycyl-glycine) and 50 µl Luciferin-solution (270 µM Co-Enzyme A (Li-salt), 470 µM Luciferin (K-salt), 20 mM $MgCl_2$, 35 mM Glycil-Glycine). β-galactosidase activity was measured by combining 30 µl lysate with 0.2 mg/ml O-nitrophenyl β-D- galactopyranoside (ONPG) in 60 mM Na_2HPO_4, 40 mM NaH_2PO_4, 10 mM KCl, 1 mM $MgSO_4$, and 50 mM β-mercaptoethanol. Luciferase and β-galactosidase activity was measured in cell lysates with a plate reader at 37°C (Tecan).

7.2.17 Reverse Transcription and quantitative PCR

Reverse transcription and quantitative PCR (qPCR) were performed as described previously with minor modifications (Schwaderer, Gaiser et al. 2017). To isolate RNA, freshly isolated small intestinal crypts from wt (C57BL/6), $TNFR1^{-/-}$ and $TNFR2^{-/-}$ mice were lysed in 1 ml peqGOLD TriFast (PeqLab) through homogenization using the TissueLyser II (Quiagen). Subsequently, RNA was isolated following the manufacturers protocol. Then, one microgram of RNA was reverse transcribed using the High-Capacity cDNA Reverse Transcription Kit (Applied Biosystems). Afterwards, cDNA was used for gene expression analysis by quantitative real-time PCR using FAST SYBR Green Master Kit and a StepOnePlus Real-time PCR system (Applied Biosystems) with primers stated in Table 2.

Table 2: Primers for qPCR of TNFR1/2

TNFR1 (5' → 3')	
fwd	GGCTCTGCTGATGGGGATAC
rev	GCTTTCCAGCCTTCTCCTCTT
TNFR2 (5' → 3')	
fwd	CCACCGCATCTGTAGCATCC
rev	TCCTGAGAGAAGGGGACCTG

7.2.18 Generation of Wnt-conditioned medium

Wnt-secreting L-WRN cells were a kind gift of Marco Metzger (TERM, Würzburg). In brief, Wnt-conditioned medium was produced as described earlier (Miyoshi and Stappenbeck 2013). Briefly, cells were cultivated in DMEM, supplemented with 10% FCS (PAA), 2mM l-Glutamine and 10,000 U penicillin/ml and 10 mg streptomycin/ml (Sigma) at 37 °C and 5% CO_2. Two generate Wnt-conditioned medium, supernatants were collected for three days, centrifuged at 400 x g for 5 min at room temperature and pooled afterwards. Supernatants were then tested for organoid forming and growth capacity (see also 9.2, Figure 31).

8. References

Acehan, D., X. Jiang, D. G. Morgan, J. E. Heuser, X. Wang and C. W. Akey (2002). "Three-dimensional structure of the apoptosome: implications for assembly, procaspase-9 binding, and activation." Mol Cell **9**(2): 423-432.

Alison, M. R. and C. E. Sarraf (1994). "The role of growth factors in gastrointestinal cell proliferation." Cell Biol Int **18**(1): 1-10.

Asbury, C. L., R. Esposito, C. Farmer and G. van den Engh (1996). "Fluorescence spectra of DNA dyes measured in a flow cytometer." Cytometry **24**(3): 234-242.

Astashkina, A. and D. W. Grainger (2014). "Critical analysis of 3-D organoid in vitro cell culture models for high-throughput drug candidate toxicity assessments." Adv Drug Deliv Rev **69-70**: 1-18.

Atreya, R. and M. F. Neurath (2008). "New therapeutic strategies for treatment of inflammatory bowel disease." Mucosal Immunol **1**(3): 175-182.

Ayabe, T., D. P. Satchell, P. Pesendorfer, H. Tanabe, C. L. Wilson, S. J. Hagen and A. J. Ouellette (2002). "Activation of Paneth cell alpha-defensins in mouse small intestine." J Biol Chem **277**(7): 5219-5228.

Bai, L., D. C. Smith and S. Wang (2014). "Small-molecule SMAC mimetics as new cancer therapeutics." Pharmacol Ther **144**(1): 82-95.

Balakrishnan, K., M. Fu, F. Onida, W. G. Wierda, M. J. Keating and V. Gandhi (2016). "Reactivation of smac-mediated apoptosis in chronic lymphocytic leukemia cells: mechanistic studies of smac mimetic." Oncotarget.

Banfalvi, G. (2017). "Methods to detect apoptotic cell death." Apoptosis **22**(2): 306-323.

Barbier, V., B. Nowlan, J. P. Levesque and I. G. Winkler (2012). "Flow cytometry analysis of cell cycling and proliferation in mouse hematopoietic stem and progenitor cells." Methods Mol Biol **844**: 31-43.

Barker, N. (2014). "Adult intestinal stem cells: critical drivers of epithelial homeostasis and regeneration." Nat Rev Mol Cell Biol **15**(1): 19-33.

Barker, N. and H. Clevers (2010). "Leucine-rich repeat-containing G-protein-coupled receptors as markers of adult stem cells." Gastroenterology **138**(5): 1681-1696.

Barker, N., R. A. Ridgway, J. H. van Es, M. van de Wetering, H. Begthel, M. van den Born, E. Danenberg, A. R. Clarke, O. J. Sansom and H. Clevers (2009). "Crypt stem cells as the cells-of-origin of intestinal cancer." Nature **457**(7229): 608-611.

Barker, N., J. H. van Es, J. Kuipers, P. Kujala, M. van den Born, M. Cozijnsen, A. Haegebarth, J. Korving, H. Begthel, P. J. Peters and H. Clevers (2007). "Identification of stem cells in small intestine and colon by marker gene Lgr5." Nature **449**(7165): 1003-1007.

Bartfeld, S. and H. Clevers (2017). "Stem cell-derived organoids and their application for medical research and patient treatment." J Mol Med (Berl) **95**(7): 729-738.

Bas, T. and L. H. Augenlicht (2014). "Real time analysis of metabolic profile in ex vivo mouse intestinal crypt organoid cultures." J Vis Exp(93): e52026.

Bayrer, J. R., H. Wang, R. Nattiv, M. Suzawa, H. S. Escusa, R. J. Fletterick, O. D. Klein, D. D. Moore and H. A. Ingraham (2018). "LRH-1 mitigates intestinal inflammatory disease by maintaining epithelial homeostasis and cell survival." Nat Commun **9**(1): 4055.

Benton, G., I. Arnaoutova, J. George, H. K. Kleinman and J. Koblinski (2014). "Matrigel: from discovery and ECM mimicry to assays and models for cancer research." Adv Drug Deliv Rev **79-80**: 3-18.

Bertrand, M. J., S. Milutinovic, K. M. Dickson, W. C. Ho, A. Boudreault, J. Durkin, J. W. Gillard, J. B. Jaquith, S. J. Morris and P. A. Barker (2008). "cIAP1 and cIAP2 facilitate cancer cell survival by functioning as E3 ligases that promote RIP1 ubiquitination." Mol Cell **30**(6): 689-700.

Beumer, J. and H. Clevers (2016). "Regulation and plasticity of intestinal stem cells during homeostasis and regeneration." Development **143**(20): 3639-3649.

Bigda, J., I. Beletsky, C. Brakebusch, Y. Varfolomeev, H. Engelmann, J. Bigda, H. Holtmann and D. Wallach (1994). "Dual role of the p75 tumor necrosis factor (TNF) receptor in TNF cytotoxicity." J Exp Med **180**(2): 445-460.

Boehnke, K., P. W. Iversen, D. Schumacher, M. J. Lallena, R. Haro, J. Amat, J. Haybaeck, S. Liebs, M. Lange, R. Schafer, C. R. Regenbrecht, C. Reinhard and J. A. Velasco (2016). "Assay Establishment and Validation of a High-Throughput Screening Platform for Three-Dimensional Patient-Derived Colon Cancer Organoid Cultures." J Biomol Screen.

Bohm, I. and H. Schild (2003). "Apoptosis: the complex scenario for a silent cell death." Mol Imaging Biol **5**(1): 2-14.

Bornstein, C., D. Winter, Z. Barnett-Itzhaki, E. David, S. Kadri, M. Garber and I. Amit (2014). "A negative feedback loop of transcription factors specifies alternative dendritic cell chromatin States." Mol Cell **56**(6): 749-762.

Botrugno, O. A., E. Fayard, J. S. Annicotte, C. Haby, T. Brennan, O. Wendling, T. Tanaka, T. Kodama, W. Thomas, J. Auwerx and K. Schoonjans (2004). "Synergy between LRH-1 and beta-catenin induces G1 cyclin-mediated cell proliferation." Mol Cell **15**(4): 499-509.

Bredenoord, A. L., H. Clevers and J. A. Knoblich (2017). "Human tissues in a dish: The research and ethical implications of organoid technology." Science **355**(6322).

Broker, L. E., F. A. Kruyt and G. Giaccone (2005). "Cell death independent of caspases: a review." Clin Cancer Res **11**(9): 3155-3162.

Brunner, T. (2009). "Living on the edge: immune cells and immunopathology in the intestinal mucosa." Semin Immunopathol **31**(2): 143-144.

Brunner, T., D. Arnold, C. Wasem, S. Herren and C. Frutschi (2001). "Regulation of cell death and survival in intestinal intraepithelial lymphocytes." Cell Death Differ **8**(7): 706-714.

Brunner, T., R. J. Mogil, D. LaFace, N. J. Yoo, A. Mahboubi, F. Echeverri, S. J. Martin, W. R. Force, D. H. Lynch, C. F. Ware and et al. (1995). "Cell-autonomous Fas (CD95)/Fas-ligand interaction mediates activation-induced apoptosis in T-cell hybridomas." Nature **373**(6513): 441-444.

Bulin, A. L., M. Broekgaarden and T. Hasan (2017). "Comprehensive high-throughput image analysis for therapeutic efficacy of architecturally complex heterotypic organoids." Sci Rep **7**(1): 16645.

Bullen, T. F., S. Forrest, F. Campbell, A. R. Dodson, M. J. Hershman, D. M. Pritchard, J. R. Turner, M. H. Montrose and A. J. Watson (2006). "Characterization of epithelial cell shedding from human small intestine." Lab Invest **86**(10): 1052-1063.

Burkhart, R. A., L. A. Baker and H. Tiriac (2018). "Testing Susceptibility of Patient-Derived Organoid Cultures to Therapies: Pharmacotyping." Methods Mol Biol **1787**: 253-261.

Buske, P., J. Przybilla, M. Loeffler, N. Sachs, T. Sato, H. Clevers and J. Galle (2012). "On the biomechanics of stem cell niche formation in the gut--modelling growing organoids." FEBS J **279**(18): 3475-3487.

Canfora, E. E., J. W. Jocken and E. E. Blaak (2015). "Short-chain fatty acids in control of body weight and insulin sensitivity." Nat Rev Endocrinol **11**(10): 577-591.

Capeling, M. M., M. Czerwinski, S. Huang, Y. H. Tsai, A. Wu, M. S. Nagy, B. Juliar, N. Sundaram, Y. Song, W. M. Han, S. Takayama, E. Alsberg, A. J. Garcia, M. Helmrath, A. J. Putnam and J. R. Spence (2018). "Nonadhesive Alginate Hydrogels Support Growth of Pluripotent Stem Cell-Derived Intestinal Organoids." Stem Cell Reports.

Carswell, E. A., L. J. Old, R. L. Kassel, S. Green, N. Fiore and B. Williamson (1975). "An endotoxin-induced serum factor that causes necrosis of tumors." Proc Natl Acad Sci U S A **72**(9): 3666-3670.

Celli, J. P., I. Rizvi, A. R. Blanden, I. Massodi, M. D. Glidden, B. W. Pogue and T. Hasan (2014). "An imaging-based platform for high-content, quantitative evaluation of therapeutic response in 3D tumour models." Sci Rep **4**: 3751.

Chan, F. K., K. Moriwaki and M. J. De Rosa (2013). "Detection of necrosis by release of lactate dehydrogenase activity." Methods Mol Biol **979**: 65-70.

Cho, Y., T. McQuade, H. Zhang, J. Zhang and F. K. Chan (2011). "RIP1-dependent and independent effects of necrostatin-1 in necrosis and T cell activation." PLoS One **6**(8): e23209.

Cima, I., N. Corazza, B. Dick, A. Fuhrer, S. Herren, S. Jakob, E. Ayuni, C. Mueller and T. Brunner (2004). "Intestinal epithelial cells synthesize glucocorticoids and regulate T cell activation." J Exp Med **200**(12): 1635-1646.

Clevers, H. (2013). "The intestinal crypt, a prototype stem cell compartment." Cell **154**(2): 274-284.

Clevers, H. (2016). "Modeling Development and Disease with Organoids." Cell **165**(7): 1586-1597.

Clevers, H., K. M. Loh and R. Nusse (2014). "Stem cell signaling. An integral program for tissue renewal and regeneration: Wnt signaling and stem cell control." Science **346**(6205): 1248012.

Clevers, H. C. and C. L. Bevins (2013). "Paneth cells: maestros of the small intestinal crypts." Annu Rev Physiol **75**: 289-311.

Coste, A., L. Dubuquoy, R. Barnouin, J. S. Annicotte, B. Magnier, M. Notti, N. Corazza, M. C. Antal, D. Metzger, P. Desreumaux, T. Brunner, J. Auwerx and K. Schoonjans (2007). "LRH-1-mediated glucocorticoid synthesis in enterocytes protects against inflammatory bowel disease." Proc Natl Acad Sci U S A **104**(32): 13098-13103.

Crapo, P. M., T. W. Gilbert and S. F. Badylak (2011). "An overview of tissue and whole organ decellularization processes." Biomaterials **32**(12): 3233-3243.

Crosnier, C., D. Stamataki and J. Lewis (2006). "Organizing cell renewal in the intestine: stem cells, signals and combinatorial control." Nat Rev Genet **7**(5): 349-359.

Cruz-Acuna, R., M. Quiros, A. E. Farkas, P. H. Dedhia, S. Huang, D. Siuda, V. Garcia-Hernandez, A. J. Miller, J. R. Spence, A. Nusrat and A. J. Garcia (2017). "Synthetic hydrogels for human intestinal organoid generation and colonic wound repair." Nat Cell Biol **19**(11): 1326-1335.

Cui, Z., J. E. Gilda and A. V. Gomes (2014). "Crude and purified proteasome activity assays are affected by type of microplate." Anal Biochem **446**: 44-52.

D'Aquila, T., Y. H. Hung, A. Carreiro and K. K. Buhman (2016). "Recent discoveries on absorption of dietary fat: Presence, synthesis, and metabolism of cytoplasmic lipid droplets within enterocytes." Biochim Biophys Acta **1861**(8 Pt A): 730-747.

Danielsen, E. M. and G. H. Hansen (2008). "Lipid raft organization and function in the small intestinal brush border." J Physiol Biochem **64**(4): 377-382.

Danielson, K. G., A. Martinez-Hernandez, J. R. Hassell and R. V. Iozzo (1992). "Establishment of a cell line from the EHS tumor: biosynthesis of basement membrane constituents and characterization of a hybrid proteoglycan containing heparan and chondroitin sulfate chains." Matrix **12**(1): 22-35.

Dannappel, M., K. Vlantis, S. Kumari, A. Polykratis, C. Kim, L. Wachsmuth, C. Eftychi, J. Lin, T. Corona, N. Hermance, M. Zelic, P. Kirsch, M. Basic, A. Bleich, M. Kelliher and M. Pasparakis (2014). "RIPK1 maintains epithelial homeostasis by inhibiting apoptosis and necroptosis." Nature **513**(7516): 90-94.

Darzynkiewicz, Z., S. Bruno, G. Del Bino, W. Gorczyca, M. A. Hotz, P. Lassota and F. Traganos (1992). "Features of apoptotic cells measured by flow cytometry." Cytometry **13**(8): 795-808.

Dasari, S. and P. B. Tchounwou (2014). "Cisplatin in cancer therapy: molecular mechanisms of action." Eur J Pharmacol **740**: 364-378.

Date, S. and T. Sato (2015). "Mini-gut organoids: reconstitution of the stem cell niche." Annu Rev Cell Dev Biol **31**: 269-289.

Davis, R. J. (2000). "Signal transduction by the JNK group of MAP kinases." Cell **103**(2): 239-252.

De Iudicibus, S., R. Franca, S. Martelossi, A. Ventura and G. Decorti (2011). "Molecular mechanism of glucocorticoid resistance in inflammatory bowel disease." World J Gastroenterol **17**(9): 1095-1108.

de Lau, W., W. C. Peng, P. Gros and H. Clevers (2014). "The R-spondin/Lgr5/Rnf43 module: regulator of Wnt signal strength." Genes Dev **28**(4): 305-316.

Degterev, A., J. Hitomi, M. Germscheid, I. L. Ch'en, O. Korkina, X. Teng, D. Abbott, G. D. Cuny, C. Yuan, G. Wagner, S. M. Hedrick, S. A. Gerber, A. Lugovskoy and J. Yuan (2008). "Identification of RIP1 kinase as a specific cellular target of necrostatins." Nat Chem Biol **4**(5): 313-321.

Dekkers, J. F., C. L. Wiegerinck, H. R. de Jonge, I. Bronsveld, H. M. Janssens, K. M. de Winter-de Groot, A. M. Brandsma, N. W. de Jong, M. J. Bijvelds, B. J. Scholte, E. E. Nieuwenhuis, S. van den Brink, H. Clevers, C. K. van der Ent, S. Middendorp and J. M. Beekman (2013). "A functional CFTR assay using primary cystic fibrosis intestinal organoids." Nat Med **19**(7): 939-945.

Delgado, M. E. and T. Brunner (2019). "The many faces of tumor necrosis factor signaling in the intestinal epithelium." Genes Immun.

Delgado, M. E., T. Grabinger and T. Brunner (2016). "Cell death at the intestinal epithelial front line." FEBS J **283**(14): 2701-2719.

Dhanasekaran, D. N. and E. P. Reddy (2008). "JNK signaling in apoptosis." Oncogene **27**(48): 6245-6251.

Dickens, L. S., I. R. Powley, M. A. Hughes and M. MacFarlane (2012). "The 'complexities' of life and death: death receptor signalling platforms." Exp Cell Res **318**(11): 1269-1277.

Dillon, C. P., R. Weinlich, D. A. Rodriguez, J. G. Cripps, G. Quarato, P. Gurung, K. C. Verbist, T. L. Brewer, F. Llambi, Y. N. Gong, L. J. Janke, M. A. Kelliher, T. D. Kanneganti and D. R. Green (2014). "RIPK1 blocks early postnatal lethality mediated by caspase-8 and RIPK3." Cell **157**(5): 1189-1202.

DiMarco, R. L., R. E. Dewi, G. Bernal, C. Kuo and S. C. Heilshorn (2015). "Protein-engineered scaffolds for in vitro 3D culture of primary adult intestinal organoids." Biomater Sci **3**(10): 1376-1385.

Downs, T. R. and W. W. Wilfinger (1983). "Fluorometric quantification of DNA in cells and tissue." Anal Biochem **131**(2): 538-547.

Drost, J. and H. Clevers (2017). "Translational applications of adult stem cell-derived organoids." Development **144**(6): 968-975.

Dubois-Camacho, K., P. A. Ottum, D. Franco-Munoz, M. De la Fuente, A. Torres-Riquelme, D. Diaz-Jimenez, M. Olivares-Morales, G. Astudillo, R. Quera and M. A. Hermoso (2017). "Glucocorticosteroid therapy in inflammatory bowel diseases: From clinical practice to molecular biology." World J Gastroenterol **23**(36): 6628-6638.

Duellman, S. J., W. Zhou, P. Meisenheimer, G. Vidugiris, J. J. Cali, P. Gautam, K. Wennerberg and J. Vidugiriene (2015). "Bioluminescent, Nonlytic, Real-Time Cell Viability Assay and Use in Inhibitor Screening." Assay Drug Dev Technol **13**(8): 456-465.

Dutta, D., I. Heo and H. Clevers (2017). "Disease Modeling in Stem Cell-Derived 3D Organoid Systems." Trends Mol Med **23**(5): 393-410.

Eastwood, G. L. (1977). "Gastrointestinal epithelial renewal." Gastroenterology **72**(5 Pt 1): 962-975.

El-Mesery, M., M. E. Shaker and A. Elgaml (2016). "The SMAC mimetic BV6 induces cell death and sensitizes different cell lines to TNF-alpha and TRAIL-induced apoptosis." Exp Biol Med (Maywood).

Elmore, S. (2007). "Apoptosis: a review of programmed cell death." Toxicol Pathol **35**(4): 495-516.

Enari, M., H. Sakahira, H. Yokoyama, K. Okawa, A. Iwamatsu and S. Nagata (1998). "A caspase-activated DNase that degrades DNA during apoptosis, and its inhibitor ICAD." Nature **391**(6662): 43-50.

Endres, C. H., A. Roth and T. B. Bruck (2018). "Modeling Microalgae Productivity in Industrial-Scale Vertical Flat Panel Photobioreactors." Environ Sci Technol **52**(9): 5490-5498.

Fan, Y. Y., L. A. Davidson, E. S. Callaway, G. A. Wright, S. Safe and R. S. Chapkin (2015). "A bioassay to measure energy metabolism in mouse colonic crypts, organoids, and sorted stem cells." Am J Physiol Gastrointest Liver Physiol **309**(1): G1-9.

Farber, E. (1994). "Programmed cell death: necrosis versus apoptosis." Mod Pathol **7**(5): 605-609.

Fatehullah, A., P. L. Appleton and I. S. Nathke (2013). "Cell and tissue polarity in the intestinal tract during tumourigenesis: cells still know the right way up, but tissue organization is lost." Philos Trans R Soc Lond B Biol Sci **368**(1629): 20130014.

Feoktistova, M., P. Geserick and M. Leverkus (2016). "Crystal Violet Assay for Determining Viability of Cultured Cells." Cold Spring Harb Protoc **2016**(4): pdb prot087379.

Finkbeiner, S. R. and J. R. Spence (2013). "A gutsy task: generating intestinal tissue from human pluripotent stem cells." Dig Dis Sci **58**(5): 1176-1184.

Fischer, R., O. Maier, M. Siegemund, H. Wajant, P. Scheurich and K. Pfizenmaier (2011). "A TNF receptor 2 selective agonist rescues human neurons from oxidative stress-induced cell death." PLoS One **6**(11): e27621.

Francescone, R., V. Hou and S. I. Grivennikov (2015). "Cytokines, IBD, and colitis-associated cancer." Inflamm Bowel Dis **21**(2): 409-418.

Francies, H. E., A. Barthorpe, A. McLaren-Douglas, W. J. Barendt and M. J. Garnett (2016). "Drug Sensitivity Assays of Human Cancer Organoid Cultures." Methods Mol Biol.

Freedman, B. S., C. R. Brooks, A. Q. Lam, H. Fu, R. Morizane, V. Agrawal, A. F. Saad, M. K. Li, M. R. Hughes, R. V. Werff, D. T. Peters, J. Lu, A. Baccei, A. M. Siedlecki, M. T. Valerius, K. Musunuru, K. M. McNagny, T. I. Steinman, J. Zhou, P. H. Lerou and J. V. Bonventre (2015). "Modelling kidney disease with CRISPR-mutant kidney organoids derived from human pluripotent epiblast spheroids." Nat Commun **6**: 8715.

Frisch, S. M. and H. Francis (1994). "Disruption of epithelial cell-matrix interactions induces apoptosis." J Cell Biol **124**(4): 619-626.

Fujii, M., M. Matano, K. Nanki and T. Sato (2015). "Efficient genetic engineering of human intestinal organoids using electroporation." Nat Protoc **10**(10): 1474-1485.

Fujii, M., M. Shimokawa, S. Date, A. Takano, M. Matano, K. Nanki, Y. Ohta, K. Toshimitsu, Y. Nakazato, K. Kawasaki, T. Uraoka, T. Watanabe, T. Kanai and T. Sato (2016). "A Colorectal Tumor Organoid Library Demonstrates Progressive Loss of Niche Factor Requirements during Tumorigenesis." Cell Stem Cell **18**(6): 827-838.

Galluzzi, L., A. Lopez-Soto, S. Kumar and G. Kroemer (2016). "Caspases Connect Cell-Death Signaling to Organismal Homeostasis." Immunity **44**(2): 221-231.

Galluzzi, L., I. Vitale, S. A. Aaronson, J. M. Abrams, D. Adam, P. Agostinis, E. S. Alnemri, L. Altucci, I. Amelio, D. W. Andrews, M. Annicchiarico-Petruzzelli, A. V. Antonov, E. Arama, E. H. Baehrecke, N. A. Barlev, N. G. Bazan, F. Bernassola, M. J. M. Bertrand, K. Bianchi, M. V. Blagosklonny, K. Blomgren, C. Borner, P. Boya, C. Brenner, M. Campanella, E. Candi, D. Carmona-Gutierrez, F. Cecconi, F. K. Chan, N. S. Chandel, E. H. Cheng, J. E. Chipuk, J. A. Cidlowski, A. Ciechanover, G. M. Cohen, M. Conrad, J. R. Cubillos-Ruiz, P. E. Czabotar, V. D'Angiolella, T. M. Dawson, V. L. Dawson, V. De Laurenzi, R. De Maria, K. M. Debatin, R. J. DeBerardinis, M. Deshmukh, N. Di Daniele, F. Di Virgilio, V. M. Dixit, S. J. Dixon, C. S. Duckett, B. D. Dynlacht, W. S. El-Deiry, J. W. Elrod, G. M. Fimia, S. Fulda, A. J. Garcia-Saez, A. D. Garg, C. Garrido, E. Gavathiotis, P. Golstein, E. Gottlieb, D. R. Green, L. A. Greene, H. Gronemeyer, A. Gross, G. Hajnoczky, J. M. Hardwick, I. S. Harris, M. O. Hengartner, C. Hetz, H. Ichijo, M. Jaattela, B. Joseph, P. J. Jost, P. P. Juin, W. J. Kaiser, M. Karin, T. Kaufmann, O. Kepp, A. Kimchi, R. N. Kitsis, D. J. Klionsky, R. A. Knight, S. Kumar, S. W. Lee, J. J. Lemasters, B. Levine,

A. Linkermann, S. A. Lipton, R. A. Lockshin, C. Lopez-Otin, S. W. Lowe, T. Luedde, E. Lugli, M. MacFarlane, F. Madeo, M. Malewicz, W. Malorni, G. Manic, J. C. Marine, S. J. Martin, J. C. Martinou, J. P. Medema, P. Mehlen, P. Meier, S. Melino, E. A. Miao, J. D. Molkentin, U. M. Moll, C. Munoz-Pinedo, S. Nagata, G. Nunez, A. Oberst, M. Oren, M. Overholtzer, M. Pagano, T. Panaretakis, M. Pasparakis, J. M. Penninger, D. M. Pereira, S. Pervaiz, M. E. Peter, M. Piacentini, P. Pinton, J. H. M. Prehn, H. Puthalakath, G. A. Rabinovich, M. Rehm, R. Rizzuto, C. M. P. Rodrigues, D. C. Rubinsztein, T. Rudel, K. M. Ryan, E. Sayan, L. Scorrano, F. Shao, Y. Shi, J. Silke, H. U. Simon, A. Sistigu, B. R. Stockwell, A. Strasser, G. Szabadkai, S. W. G. Tait, D. Tang, N. Tavernarakis, A. Thorburn, Y. Tsujimoto, B. Turk, T. Vanden Berghe, P. Vandenabeele, M. G. Vander Heiden, A. Villunger, H. W. Virgin, K. H. Vousden, D. Vucic, E. F. Wagner, H. Walczak, D. Wallach, Y. Wang, J. A. Wells, W. Wood, J. Yuan, Z. Zakeri, B. Zhivotovsky, L. Zitvogel, G. Melino and G. Kroemer (2018). "Molecular mechanisms of cell death: recommendations of the Nomenclature Committee on Cell Death 2018." Cell Death Differ **25**(3): 486-541.

Gamelin, E. and M. Boisdron-Celle (1999). "Dose monitoring of 5-fluorouracil in patients with colorectal or head and neck cancer--status of the art." Crit Rev Oncol Hematol **30**(1): 71-79.

Gao, D., I. Vela, A. Sboner, P. J. Iaquinta, W. R. Karthaus, A. Gopalan, C. Dowling, J. N. Wanjala, E. A. Undvall, V. K. Arora, J. Wongvipat, M. Kossai, S. Ramazanoglu, L. P. Barboza, W. Di, Z. Cao, Q. F. Zhang, I. Sirota, L. Ran, T. Y. MacDonald, H. Beltran, J. M. Mosquera, K. A. Touijer, P. T. Scardino, V. P. Laudone, K. R. Curtis, D. E. Rathkopf, M. J. Morris, D. C. Danila, S. F. Slovin, S. B. Solomon, J. A. Eastham, P. Chi, B. Carver, M. A. Rubin, H. I. Scher, H. Clevers, C. L. Sawyers and Y. Chen (2014). "Organoid cultures derived from patients with advanced prostate cancer." Cell **159**(1): 176-187.

Garcez, P. P., E. C. Loiola, R. Madeiro da Costa, L. M. Higa, P. Trindade, R. Delvecchio, J. M. Nascimento, R. Brindeiro, A. Tanuri and S. K. Rehen (2016). "Zika virus impairs growth in human neurospheres and brain organoids." Science **352**(6287): 816-818.

Gebert, A., H. J. Rothkotter and R. Pabst (1996). "M cells in Peyer's patches of the intestine." Int Rev Cytol **167**: 91-159.

Ghosh, S. and M. Karin (2002). "Missing pieces in the NF-kappaB puzzle." Cell **109 Suppl**: S81-96.

Gjorevski, N. and M. P. Lutolf (2017). "Synthesis and characterization of well-defined hydrogel matrices and their application to intestinal stem cell and organoid culture." Nat Protoc **12**(11): 2263-2274.

Gjorevski, N., N. Sachs, A. Manfrin, S. Giger, M. E. Bragina, P. Ordonez-Moran, H. Clevers and M. P. Lutolf (2016). "Designer matrices for intestinal stem cell and organoid culture." Nature **539**(7630): 560-564.

Gjorevski, N., N. Sachs, A. Manfrin, S. Giger, M. E. Bragina, P. Ordonez-Moran, H. Clevers and M. P. Lutolf (2016). "Designer matrices for intestinal stem cell and organoid culture." Nature.

Goldstein, J. C., N. J. Waterhouse, P. Juin, G. I. Evan and D. R. Green (2000). "The coordinate release of cytochrome c during apoptosis is rapid, complete and kinetically invariant." Nat Cell Biol **2**(3): 156-162.

Gonneaud, A., C. Asselin, F. Boudreau and F. M. Boisvert (2017). "Phenotypic Analysis of Organoids by Proteomics." Proteomics **17**(20).

Gonneaud, A., C. Jones, N. Turgeon, D. Levesque, C. Asselin, F. Boudreau and F. M. Boisvert (2016). "A SILAC-Based Method for Quantitative Proteomic Analysis of Intestinal Organoids." Sci Rep **6**: 38195.

Grabinger, T., K. J. Bode, J. Demgenski, C. Seitz, M. E. Delgado, F. Kostadinova, C. Reinhold, N. Etemadi, S. Wilhelm, M. Schweinlin, K. Hanggi, J. Knop, C. Hauck, H. Walles, J. Silke, H. Wajant, U. Nachbur, W. W.-L. W and T. Brunner (2017). "Inhibitor of Apoptosis Protein-1 Regulates Tumor Necrosis Factor-Mediated Destruction of Intestinal Epithelial Cells." Gastroenterology **152**(4): 867-879.

Grabinger, T., E. Delgado and T. Brunner (2016). "Analysis of Cell Death Induction in Intestinal Organoids In Vitro." Methods Mol Biol **1419**: 83-93.

Grabinger, T., L. Luks, F. Kostadinova, C. Zimberlin, J. P. Medema, M. Leist and T. Brunner (2014). "Ex vivo culture of intestinal crypt organoids as a model system for assessing cell death induction in intestinal epithelial cells and enteropathy." Cell Death Dis **5**: e1228.

Green, D. R., A. Oberst, C. P. Dillon, R. Weinlich and G. S. Salvesen (2011). "RIPK-dependent necrosis and its regulation by caspases: a mystery in five acts." Mol Cell **44**(1): 9-16.

Grell, M. (1995). "Tumor necrosis factor (TNF) receptors in cellular signaling of soluble and membrane-expressed TNF." J Inflamm **47**(1-2): 8-17.

Gunasekara, D. B., M. DiSalvo, Y. Wang, D. L. Nguyen, M. I. Reed, J. Speer, C. E. Sims, S. T. Magness and N. L. Allbritton (2018). "Development of Arrayed Colonic Organoids for Screening of Secretagogues Associated with Enterotoxins." Anal Chem **90**(3): 1941-1950.

Gyrd-Hansen, M. and P. Meier (2010). "IAPs: from caspase inhibitors to modulators of NF-kappaB, inflammation and cancer." Nat Rev Cancer **10**(8): 561-574.

Ha, J. H., D. Y. Hwang, J. Yu, D. H. Park and S. H. Ryu (2011). "Onset of Manic Episode during Chemotherapy with 5-Fluorouracil." Psychiatry Investig **8**(1): 71-73.

Hall, A. B., A. C. Tolonen and R. J. Xavier (2017). "Human genetic variation and the gut microbiome in disease." Nat Rev Genet **18**(11): 690-699.

Hannes, S., B. A. Abhari and S. Fulda (2016). "Smac mimetic triggers necroptosis in pancreatic carcinoma cells when caspase activation is blocked." Cancer Lett **380**(1): 31-38.

Hardie, M. E., H. W. Kava and V. Murray (2016). "Cisplatin Analogues with an Increased Interaction with DNA: Prospects for Therapy." Curr Pharm Des **22**(44): 6645-6664.

Hashmi, B., L. D. Zarzar, T. Mammoto, A. Mammoto, A. Jiang, J. Aizenberg and D. E. Ingber (2014). "Developmentally-inspired shrink-wrap polymers for mechanical induction of tissue differentiation." Adv Mater **26**(20): 3253-3257.

Hayden, M. S., A. P. West and S. Ghosh (2006). "NF-kappaB and the immune response." Oncogene **25**(51): 6758-6780.

He, S., S. Huang and Z. Shen (2016). "Biomarkers for the detection of necroptosis." Cell Mol Life Sci **73**(11-12): 2177-2181.

Heidelberger, C., N. K. Chaudhuri, P. Danneberg, D. Mooren, L. Griesbach, R. Duschinsky, R. J. Schnitzer, E. Pleven and J. Scheiner (1957). "Fluorinated pyrimidines, a new class of tumour-inhibitory compounds." Nature **179**(4561): 663-666.

Holze, C., C. Michaudel, C. Mackowiak, D. A. Haas, C. Benda, P. Hubel, F. L. Pennemann, D. Schnepf, J. Wettmarshausen, M. Braun, D. W. Leung, G. K. Amarasinghe, F. Perocchi, P. Staeheli, B. Ryffel and A. Pichlmair (2018). "Oxeiptosis, a ROS-induced caspase-independent apoptosis-like cell-death pathway." Nat Immunol **19**(2): 130-140.

Horvath, P., N. Aulner, M. Bickle, A. M. Davies, E. D. Nery, D. Ebner, M. C. Montoya, P. Ostling, V. Pietiainen, L. S. Price, S. L. Shorte, G. Turcatti, C. von Schantz and N. O. Carragher (2016). "Screening out irrelevant cell-based models of disease." Nat Rev Drug Discov **15**(11): 751-769.

Howell, K. J., J. Kraiczy, K. M. Nayak, M. Gasparetto, A. Ross, C. Lee, T. N. Mak, B. K. Koo, N. Kumar, T. Lawley, A. Sinha, P. Rosenstiel, R. Heuschkel, O. Stegle and M. Zilbauer (2017). "DNA Methylation and Transcription Patterns in Intestinal Epithelial Cells From Pediatric Patients With Inflammatory Bowel Diseases Differentiate Disease Subtypes and Associate With Outcome." Gastroenterology.

Huang, L., A. Holtzinger, I. Jagan, M. BeGora, I. Lohse, N. Ngai, C. Nostro, R. Wang, L. B. Muthuswamy, H. C. Crawford, C. Arrowsmith, S. E. Kalloger, D. J. Renouf, A. A. Connor, S. Cleary, D. F. Schaeffer, M. Roehrl, M. S. Tsao, S. Gallinger, G. Keller and S. K. Muthuswamy (2015). "Ductal pancreatic cancer modeling and drug screening using human pluripotent stem cell- and patient-derived tumor organoids." Nat Med **21**(11): 1364-1371.

Hubert, C. G., M. Rivera, L. C. Spangler, Q. Wu, S. C. Mack, B. C. Prager, M. Couce, R. E. McLendon, A. E. Sloan and J. N. Rich (2016). "A Three-Dimensional Organoid Culture System Derived from Human Glioblastomas Recapitulates the Hypoxic Gradients and Cancer Stem Cell Heterogeneity of Tumors Found In Vivo." Cancer Res **76**(8): 2465-2477.

Huch, M., C. Dorrell, S. F. Boj, J. H. van Es, V. S. Li, M. van de Wetering, T. Sato, K. Hamer, N. Sasaki, M. J. Finegold, A. Haft, R. G. Vries, M. Grompe and H. Clevers (2013). "In vitro expansion of single Lgr5+ liver stem cells induced by Wnt-driven regeneration." Nature **494**(7436): 247-250.

Hughes, C. S., L. M. Postovit and G. A. Lajoie (2010). "Matrigel: a complex protein mixture required for optimal growth of cell culture." Proteomics **10**(9): 1886-1890.

Igney, F. H. and P. H. Krammer (2002). "Death and anti-death: tumour resistance to apoptosis." Nat Rev Cancer **2**(4): 277-288.

In, J. G., J. Foulke-Abel, M. K. Estes, N. C. Zachos, O. Kovbasnjuk and M. Donowitz (2016). "Human mini-guts: new insights into intestinal physiology and host-pathogen interactions." Nat Rev Gastroenterol Hepatol.

Ingber, D. E. (2018). "Developmentally inspired human 'organs on chips'." Development **145**(16).

Jabs, J., F. M. Zickgraf, J. Park, S. Wagner, X. Jiang, K. Jechow, K. Kleinheinz, U. H. Toprak, M. A. Schneider, M. Meister, S. Spaich, M. Sutterlin, M. Schlesner, A. Trumpp, M. Sprick, R. Eils and C. Conrad (2017). "Screening drug effects in patient-derived cancer cells links organoid responses to genome alterations." Mol Syst Biol **13**(11): 955.

Jones, C. L., C. M. Gearheart, S. Fosmire, C. Delgado-Martin, N. A. Evensen, K. Bride, A. J. Waanders, F. Pais, J. Wang, T. Bhatla, D. S. Bitterman, S. R. de Rijk, W. Bourgeois, S. Dandekar, E. Park, T. M. Burleson, P. P. Madhusoodhan, D. T. Teachey, E. A. Raetz, M. L. Hermiston, M. Muschen, M. L. Loh, S. P. Hunger, J. Zhang, M. J. Garabedian, C. C. Porter and W. L. Carroll (2015). "MAPK signaling cascades mediate distinct glucocorticoid resistance mechanisms in pediatric leukemia." Blood **126**(19): 2202-2212.

Jost, P. J., S. Grabow, D. Gray, M. D. McKenzie, U. Nachbur, D. C. Huang, P. Bouillet, H. E. Thomas, C. Borner, J. Silke, A. Strasser and T. Kaufmann (2009). "XIAP discriminates between type I and type II FAS-induced apoptosis." Nature **460**(7258): 1035-1039.

Karin, M., Y. Cao, F. R. Greten and Z. W. Li (2002). "NF-kappaB in cancer: from innocent bystander to major culprit." Nat Rev Cancer **2**(4): 301-310.

Kaufmann, S. H., S. H. Lee, X. W. Meng, D. A. Loegering, T. J. Kottke, A. J. Henzing, S. Ruchaud, K. Samejima and W. C. Earnshaw (2008). "Apoptosis-associated caspase activation assays." Methods **44**(3): 262-272.

Kelliher, M. A., S. Grimm, Y. Ishida, F. Kuo, B. Z. Stanger and P. Leder (1998). "The death domain kinase RIP mediates the TNF-induced NF-kappaB signal." Immunity **8**(3): 297-303.

Kilgore, J. A., N. J. Dolman and M. W. Davidson (2013). "A review of reagents for fluorescence microscopy of cellular compartments and structures, Part II: reagents for non-vesicular organelles." Curr Protoc Cytom **66**: Unit 12 31.

Kim, K. A., M. Kakitani, J. Zhao, T. Oshima, T. Tang, M. Binnerts, Y. Liu, B. Boyle, E. Park, P. Emtage, W. D. Funk and K. Tomizuka (2005). "Mitogenic influence of human R-spondin1 on the intestinal epithelium." Science **309**(5738): 1256-1259.

Kim, S. J. and J. Li (2013). "Caspase blockade induces RIP3-mediated programmed necrosis in Toll-like receptor-activated microglia." Cell Death Dis **4**: e716.

Kim, S. W., J. Ehrman, M. R. Ahn, J. Kondo, A. A. M. Lopez, Y. S. Oh, X. H. Kim, S. W. Crawley, J. R. Goldenring, M. J. Tyska, E. C. Rericha and K. S. Lau (2017). "Shear stress induces

noncanonical autophagy in intestinal epithelial monolayers." Mol Biol Cell **28**(22): 3043-3056.

Kischkel, F. C., S. Hellbardt, I. Behrmann, M. Germer, M. Pawlita, P. H. Krammer and M. E. Peter (1995). "Cytotoxicity-dependent APO-1 (Fas/CD95)-associated proteins form a death-inducing signaling complex (DISC) with the receptor." EMBO J **14**(22): 5579-5588.

Kondo, J., T. Ekawa, H. Endo, K. Yamazaki, N. Tanaka, Y. Kukita, H. Okuyama, J. Okami, F. Imamura, M. Ohue, K. Kato, T. Nomura, A. Kohara, S. Mori, S. Dan and M. Inoue (2018). "High-Throughput Screening in Colorectal Cancer Tissue-Originated Spheroids." Cancer Sci.

Koo, B. K. and H. Clevers (2014). "Stem cells marked by the R-spondin receptor LGR5." Gastroenterology **147**(2): 289-302.

Kosinski, C., V. S. Li, A. S. Chan, J. Zhang, C. Ho, W. Y. Tsui, T. L. Chan, R. C. Mifflin, D. W. Powell, S. T. Yuen, S. Y. Leung and X. Chen (2007). "Gene expression patterns of human colon tops and basal crypts and BMP antagonists as intestinal stem cell niche factors." Proc Natl Acad Sci U S A **104**(39): 15418-15423.

Kostadinova, F., J. Schwaderer, V. Sebeo and T. Brunner (2014). "Why does the gut synthesize glucocorticoids?" Ann Med **46**(7): 490-497.

Kostic, A. D., R. J. Xavier and D. Gevers (2014). "The microbiome in inflammatory bowel disease: current status and the future ahead." Gastroenterology **146**(6): 1489-1499.

Kretzschmar, K. and H. Clevers (2016). "Organoids: Modeling Development and the Stem Cell Niche in a Dish." Dev Cell **38**(6): 590-600.

Krysko, D. V., T. Vanden Berghe, K. D'Herde and P. Vandenabeele (2008). "Apoptosis and necrosis: detection, discrimination and phagocytosis." Methods **44**(3): 205-221.

Laissue, P. P., R. A. Alghamdi, P. Tomancak, E. G. Reynaud and H. Shroff (2017). "Assessing phototoxicity in live fluorescence imaging." Nat Methods **14**(7): 657-661.

Lakhani, S. A., A. Masud, K. Kuida, G. A. Porter, Jr., C. J. Booth, W. Z. Mehal, I. Inayat and R. A. Flavell (2006). "Caspases 3 and 7: key mediators of mitochondrial events of apoptosis." Science **311**(5762): 847-851.

Lancaster, M. A. and J. A. Knoblich (2014). "Generation of cerebral organoids from human pluripotent stem cells." Nat Protoc **9**(10): 2329-2340.

Lancaster, M. A. and J. A. Knoblich (2014). "Organogenesis in a dish: modeling development and disease using organoid technologies." Science **345**(6194): 1247125.

Lander, A. D., J. Kimble, H. Clevers, E. Fuchs, D. Montarras, M. Buckingham, A. L. Calof, A. Trumpp and T. Oskarsson (2012). "What does the concept of the stem cell niche really mean today?" BMC Biol **10**: 19.

Lang, I., S. Fullsack, A. Wyzgol, A. Fick, J. Trebing, J. A. Arana, V. Schafer, D. Weisenberger and H. Wajant (2016). "Binding Studies of TNF Receptor Superfamily (TNFRSF) Receptors on Intact Cells." J Biol Chem **291**(10): 5022-5037.

Latt, S. A., G. Stetten, L. A. Juergens, H. F. Willard and C. D. Scher (1975). "Recent developments in the detection of deoxyribonucleic acid synthesis by 33258 Hoechst fluorescence." J Histochem Cytochem **23**(7): 493-505.

Lavrik, I. N., T. Mock, A. Golks, J. C. Hoffmann, S. Baumann and P. H. Krammer (2008). "CD95 stimulation results in the formation of a novel death effector domain protein-containing complex." J Biol Chem **283**(39): 26401-26408.

Lazebnik, Y. A., S. H. Kaufmann, S. Desnoyers, G. G. Poirier and W. C. Earnshaw (1994). "Cleavage of poly(ADP-ribose) polymerase by a proteinase with properties like ICE." Nature **371**(6495): 346-347.

Lee, S. H., W. Hu, J. T. Matulay, M. V. Silva, T. B. Owczarek, K. Kim, C. W. Chua, L. J. Barlow, C. Kandoth, A. B. Williams, S. K. Bergren, E. J. Pietzak, C. B. Anderson, M. C. Benson, J. A. Coleman, B. S. Taylor, C. Abate-Shen, J. M. McKiernan, H. Al-Ahmadie, D. B. Solit and M. M. Shen (2018). "Tumor Evolution and Drug Response in Patient-Derived Organoid Models of Bladder Cancer." Cell **173**(2): 515-528 e517.

Leist, M. and T. Hartung (2013). "Inflammatory findings on species extrapolations: humans are definitely no 70-kg mice." Arch Toxicol **87**(4): 563-567.

Leist, M. and J. G. Hengstler (2018). "Essential components of methods papers." ALTEX **35**(3): 429-432.

Lekshmi, A., S. N. Varadarajan, S. S. Lupitha, D. Indira, K. A. Mathew, A. Chandrasekharan Nair, M. Nair, T. Prasad, H. Sekar, A. K. Gopalakrishnan, A. Murali and T. R. Santhoshkumar (2017). "A quantitative real-time approach for discriminating apoptosis and necrosis." Cell Death Discov **3**: 16101.

Leushacke, M. and N. Barker (2014). "Ex vivo culture of the intestinal epithelium: strategies and applications." Gut **63**(8): 1345-1354.

Li, H., H. Zhu, C. J. Xu and J. Yuan (1998). "Cleavage of BID by caspase 8 mediates the mitochondrial damage in the Fas pathway of apoptosis." Cell **94**(4): 491-501.

Li, M. O., M. R. Sarkisian, W. Z. Mehal, P. Rakic and R. A. Flavell (2003). "Phosphatidylserine receptor is required for clearance of apoptotic cells." Science **302**(5650): 1560-1563.

Li, X., H. E. Francies, M. Secrier, J. Perner, A. Miremadi, N. Galeano-Dalmau, W. J. Barendt, L. Letchford, G. M. Leyden, E. K. Goffin, A. Barthorpe, H. Lightfoot, E. Chen, J. Gilbert, A. Noorani, G. Devonshire, L. Bower, A. Grantham, S. MacRae, N. Grehan, D. C. Wedge, R. C. Fitzgerald and M. J. Garnett (2018). "Organoid cultures recapitulate esophageal adenocarcinoma heterogeneity providing a model for clonality studies and precision therapeutics." Nat Commun **9**(1): 2983.

Lin, S. A. and N. Barker (2011). "Gastrointestinal stem cells in self-renewal and cancer." J Gastroenterol **46**(9): 1039-1055.

Lincoln, F. A., D. Imig, C. Boccellato, V. Juric, J. Noonan, R. E. Kontermann, F. Allgower, B. M. Murphy and M. Rehm (2018). "Sensitization of glioblastoma cells to TRAIL-induced apoptosis by IAP- and Bcl-2 antagonism." Cell Death Dis **9**(11): 1112.

Lindeboom, R. G., L. van Voorthuijsen, K. C. Oost, M. J. Rodriguez-Colman, M. V. Luna-Velez, C. Furlan, F. Baraille, P. W. Jansen, A. Ribeiro, B. M. Burgering, H. J. Snippert and M. Vermeulen (2018). "Integrative multi-omics analysis of intestinal organoid differentiation." Mol Syst Biol **14**(6): e8227.

Liu, W., H. Li, S. H. Hong, G. P. Piszczek, W. Chen and G. P. Rodgers (2016). "Olfactomedin 4 deletion induces colon adenocarcinoma in Apc(Min/+) mice." Oncogene **35**(40): 5237-5247.

Lobner, D. (2000). "Comparison of the LDH and MTT assays for quantifying cell death: validity for neuronal apoptosis?" J Neurosci Methods **96**(2): 147-152.

Loktionov, A. (2007). "Cell exfoliation in the human colon: myth, reality and implications for colorectal cancer screening." Int J Cancer **120**(11): 2281-2289.

Longley, D. B., D. P. Harkin and P. G. Johnston (2003). "5-fluorouracil: mechanisms of action and clinical strategies." Nat Rev Cancer **3**(5): 330-338.

Loo, D. T. (2011). "In situ detection of apoptosis by the TUNEL assay: an overview of techniques." Methods Mol Biol **682**: 3-13.

Lutolf, M. P. and J. A. Hubbell (2005). "Synthetic biomaterials as instructive extracellular microenvironments for morphogenesis in tissue engineering." Nat Biotechnol **23**(1): 47-55.

Mabbott, N. A., D. S. Donaldson, H. Ohno, I. R. Williams and A. Mahajan (2013). "Microfold (M) cells: important immunosurveillance posts in the intestinal epithelium." Mucosal Immunol **6**(4): 666-677.

Mahe, M. M., N. Sundaram, C. L. Watson, N. F. Shroyer and M. A. Helmrath (2015). "Establishment of human epithelial enteroids and colonoids from whole tissue and biopsy." J Vis Exp(97).

Mahoney, D. J., H. H. Cheung, R. L. Mrad, S. Plenchette, C. Simard, E. Enwere, V. Arora, T. W. Mak, E. C. Lacasse, J. Waring and R. G. Korneluk (2008). "Both cIAP1 and cIAP2 regulate TNFalpha-mediated NF-kappaB activation." Proc Natl Acad Sci U S A **105**(33): 11778-11783.

Makki, K., E. C. Deehan, J. Walter and F. Backhed (2018). "The Impact of Dietary Fiber on Gut Microbiota in Host Health and Disease." Cell Host Microbe **23**(6): 705-715.

Maloy, K. J. and F. Powrie (2011). "Intestinal homeostasis and its breakdown in inflammatory bowel disease." Nature **474**(7351): 298-306.

Mandal, D., A. Mazumder, P. Das, M. Kundu and J. Basu (2005). "Fas-, caspase 8-, and caspase 3-dependent signaling regulates the activity of the aminophospholipid translocase

and phosphatidylserine externalization in human erythrocytes." J Biol Chem **280**(47): 39460-39467.

Mannel, D. N. and B. Echtenacher (2000). "TNF in the inflammatory response." Chem Immunol **74**: 141-161.

Marx, V. (2015). "Tissue engineering: Organs from the lab." Nature **522**(7556): 373-377.

Matsui, T. K., M. Matsubayashi, Y. M. Sakaguchi, R. K. Hayashi, C. Zheng, K. Sugie, M. Hasegawa, T. Nakagawa and E. Mori (2018). "Six-month cultured cerebral organoids from human ES cells contain matured neural cells." Neurosci Lett **670**: 75-82.

Mayer, E. A., K. Tillisch and A. Gupta (2015). "Gut/brain axis and the microbiota." J Clin Invest **125**(3): 926-938.

Meneses, A. M. C., K. Schneeberger, H. S. Kruitwagen, L. C. Penning, F. G. van Steenbeek, I. A. Burgener and B. Spee (2016). "Intestinal Organoids-Current and Future Applications." Vet Sci **3**(4).

Micheau, O. and J. Tschopp (2003). "Induction of TNF receptor I-mediated apoptosis via two sequential signaling complexes." Cell **114**(2): 181-190.

Miguel, J. C., A. A. Maxwell, J. J. Hsieh, L. C. Harnisch, D. Al Alam, D. B. Polk, C. L. Lien, A. J. Watson and M. R. Frey (2017). "Epidermal growth factor suppresses intestinal epithelial cell shedding through a MAPK-dependent pathway." J Cell Sci **130**(1): 90-96.

Miyashita, T. and J. C. Reed (1995). "Tumor suppressor p53 is a direct transcriptional activator of the human bax gene." Cell **80**(2): 293-299.

Miyoshi, H. and T. S. Stappenbeck (2013). "In vitro expansion and genetic modification of gastrointestinal stem cells in spheroid culture." Nat Protoc **8**(12): 2471-2482.

Moe, H. (1953). "Mucus-producing goblet cells of the small intestine." Nature **172**(4372): 309.

Moor, K., M. Diard, M. E. Sellin, B. Felmy, S. Y. Wotzka, A. Toska, E. Bakkeren, M. Arnoldini, F. Bansept, A. D. Co, T. Voller, A. Minola, B. Fernandez-Rodriguez, G. Agatic, S. Barbieri, L. Piccoli, C. Casiraghi, D. Corti, A. Lanzavecchia, R. R. Regoes, C. Loverdo, R. Stocker, D. R. Brumley, W. D. Hardt and E. Slack (2017). "High-avidity IgA protects the intestine by enchaining growing bacteria." Nature **544**(7651): 498-502.

Moore, A. Y. (2009). "Clinical applications for topical 5-fluorouracil in the treatment of dermatological disorders." J Dermatolog Treat **20**(6): 328-335.

Morgan, R. G., E. Mortensson and A. C. Williams (2018). "Targeting LGR5 in Colorectal Cancer: therapeutic gold or too plastic?" Br J Cancer.

Morgan, R. G., E. Mortensson and A. C. Williams (2018). "Targeting LGR5 in Colorectal Cancer: therapeutic gold or too plastic?" Br J Cancer **118**(11): 1410-1418.

Mueller, M., I. Cima, M. Noti, A. Fuhrer, S. Jakob, L. Dubuquoy, K. Schoonjans and T. Brunner (2006). "The nuclear receptor LRH-1 critically regulates extra-adrenal glucocorticoid synthesis in the intestine." J Exp Med **203**(9): 2057-2062.

Muenzner, P., V. Bachmann, W. Zimmermann, J. Hentschel and C. R. Hauck (2010). "Human-restricted bacterial pathogens block shedding of epithelial cells by stimulating integrin activation." Science **329**(5996): 1197-1201.

Muppidi, J., M. Porter and R. M. Siegel (2004). "Measurement of apoptosis and other forms of cell death." Curr Protoc Immunol **Chapter 3**: Unit 3 17.

Murrow, L. M., R. J. Weber and Z. J. Gartner (2017). "Dissecting the stem cell niche with organoid models: an engineering-based approach." Development **144**(6): 998-1007.

Nishimura, R., T. Shirasaki, K. Tsuchiya, Y. Miyake, Y. Watanabe, S. Hibiya, S. Watanabe, T. Nakamura and M. Watanabe (2019). "Establishment of a system to evaluate the therapeutic effect and the dynamics of an investigational drug on ulcerative colitis using human colonic organoids." J Gastroenterol.

Noti, M., N. Corazza, C. Mueller, B. Berger and T. Brunner (2010). "TNF suppresses acute intestinal inflammation by inducing local glucocorticoid synthesis." J Exp Med **207**(5): 1057-1066.

Noti, M., N. Corazza, G. Tuffin, K. Schoonjans and T. Brunner (2010). "Lipopolysaccharide induces intestinal glucocorticoid synthesis in a TNFalpha-dependent manner." FASEB J **24**(5): 1340-1346.

Nozaki, K., W. Mochizuki, Y. Matsumoto, T. Matsumoto, M. Fukuda, T. Mizutani, M. Watanabe and T. Nakamura (2016). "Co-culture with intestinal epithelial organoids allows efficient expansion and motility analysis of intraepithelial lymphocytes." J Gastroenterol **51**(3): 206-213.

Ohlmacher, A. P. (1897). "Technical Note : I. A Modified Fixing Fluid for General Histological and Neuro-Histological Purposes. Ii. A Staining Combination of Gentian Violet and Picro-Acid Fuchsin." J Exp Med **2**(6): 671-676.

Oliver Metzig, M., D. Fuchs, K. E. Tagscherer, H. J. Grone, P. Schirmacher and W. Roth (2016). "Inhibition of caspases primes colon cancer cells for 5-fluorouracil-induced TNF-alpha-dependent necroptosis driven by RIP1 kinase and NF-kappaB." Oncogene **35**(26): 3399-3409.

Oun, R., Y. E. Moussa and N. J. Wheate (2018). "The side effects of platinum-based chemotherapy drugs: a review for chemists." Dalton Trans **47**(19): 6645-6653.

Owen, J. J. and E. J. Jenkinson (1992). "Apoptosis and T-cell repertoire selection in the thymus." Ann N Y Acad Sci **663**: 305-310.

Pan, G., J. Li, Y. Zhou, H. Zheng and D. Pei (2006). "A negative feedback loop of transcription factors that controls stem cell pluripotency and self-renewal." FASEB J **20**(10): 1730-1732.

Park, J. H., T. Kotani, T. Konno, J. Setiawan, Y. Kitamura, S. Imada, Y. Usui, N. Hatano, M. Shinohara, Y. Saito, Y. Murata and T. Matozaki (2016). "Promotion of Intestinal Epithelial Cell Turnover by Commensal Bacteria: Role of Short-Chain Fatty Acids." PLoS One **11**(5): e0156334.

Peden, E., D. J. Killian and D. Xue (2008). "Cell death specification in C. elegans." Cell Cycle **7**(16): 2479-2484.

Pedersen, J., E. C. LaCasse, J. B. Seidelin, M. Coskun and O. H. Nielsen (2014). "Inhibitors of apoptosis (IAPs) regulate intestinal immunity and inflammatory bowel disease (IBD) inflammation." Trends Mol Med **20**(11): 652-665.

Peeters, T. and G. Vantrappen (1975). "The Paneth cell: a source of intestinal lysozyme." Gut **16**(7): 553-558.

Peltzer, N., M. Darding and H. Walczak (2016). "Holding RIPK1 on the Ubiquitin Leash in TNFR1 Signaling." Trends Cell Biol **26**(6): 445-461.

Perkhofer, L., P. O. Frappart, M. Muller and A. Kleger (2018). "Importance of organoids for personalized medicine." Per Med.

Petersen, T. W., S. F. Ibrahim, A. H. Diercks and G. van den Engh (2004). "Chromatic shifts in the fluorescence emitted by murine thymocytes stained with Hoechst 33342." Cytometry A **60**(2): 173-181.

Pickard, J. M. and A. V. Chervonsky (2010). "Sampling of the intestinal microbiota by epithelial M cells." Curr Gastroenterol Rep **12**(5): 331-339.

Pietkiewicz, S., J. H. Schmidt and I. N. Lavrik (2015). "Quantification of apoptosis and necroptosis at the single cell level by a combination of Imaging Flow Cytometry with classical Annexin V/propidium iodide staining." J Immunol Methods **423**: 99-103.

Piguet, P. F., C. Vesin, Y. Donati and C. Barazzone (1999). "TNF-induced enterocyte apoptosis and detachment in mice: induction of caspases and prevention by a caspase inhibitor, ZVAD-fmk." Lab Invest **79**(4): 495-500.

Podolsky, D. K. (1997). "Healing the epithelium: solving the problem from two sides." J Gastroenterol **32**(1): 122-126.

Portugal, J. and M. J. Waring (1988). "Assignment of DNA binding sites for 4',6-diamidine-2-phenylindole and bisbenzimide (Hoechst 33258). A comparative footprinting study." Biochim Biophys Acta **949**(2): 158-168.

Proskuryakov, S. Y., A. G. Konoplyannikov and V. L. Gabai (2003). "Necrosis: a specific form of programmed cell death?" Exp Cell Res **283**(1): 1-16.

Purschke, M., N. Rubio, K. D. Held and R. W. Redmond (2010). "Phototoxicity of Hoechst 33342 in time-lapse fluorescence microscopy." Photochem Photobiol Sci **9**(12): 1634-1639.

Raja, W. K., A. E. Mungenast, Y. T. Lin, T. Ko, F. Abdurrob, J. Seo and L. H. Tsai (2016). "Self-Organizing 3D Human Neural Tissue Derived from Induced Pluripotent Stem Cells Recapitulate Alzheimer's Disease Phenotypes." PLoS One **11**(9): e0161969.

Rancoule, C., J. B. Guy, A. Vallard, M. Ben Mrad, A. Rehailia and N. Magne (2017). "[50th anniversary of cisplatin]." Bull Cancer **104**(2): 167-176.

Rashtbar, M., J. Hadjati, J. Ai, I. Jahanzad, M. Azami, S. Shirian, S. Ebrahimi-Barough and E. Sadroddiny (2017). "Characterization of decellularized ovine small intestine submucosal layer as extracellular matrix-based scaffold for tissue engineering." J Biomed Mater Res B Appl Biomater.

Rauert, H., A. Wicovsky, N. Muller, D. Siegmund, V. Spindler, J. Waschke, C. Kneitz and H. Wajant (2010). "Membrane tumor necrosis factor (TNF) induces p100 processing via TNF receptor-2 (TNFR2)." J Biol Chem **285**(10): 7394-7404.

Ravichandran, K. S. (2011). "Beginnings of a good apoptotic meal: the find-me and eat-me signaling pathways." Immunity **35**(4): 445-455.

Raymond, E., A. Hanauske, S. Faivre, E. Izbicka, G. Clark, E. K. Rowinsky and D. D. Von Hoff (1997). "Effects of prolonged versus short-term exposure paclitaxel (Taxol) on human tumor colony-forming units." Anticancer Drugs **8**(4): 379-385.

Reboldi, A. and J. G. Cyster (2016). "Peyer's patches: organizing B-cell responses at the intestinal frontier." Immunol Rev **271**(1): 230-245.

Riccardi, C. and I. Nicoletti (2006). "Analysis of apoptosis by propidium iodide staining and flow cytometry." Nat Protoc **1**(3): 1458-1461.

Rickard, J. A., J. A. O'Donnell, J. M. Evans, N. Lalaoui, A. R. Poh, T. Rogers, J. E. Vince, K. E. Lawlor, R. L. Ninnis, H. Anderton, C. Hall, S. K. Spall, T. J. Phesse, H. E. Abud, L. H. Cengia, J. Corbin, S. Mifsud, L. Di Rago, D. Metcalf, M. Ernst, G. Dewson, A. W. Roberts, W. S. Alexander, J. M. Murphy, P. G. Ekert, S. L. Masters, D. L. Vaux, B. A. Croker, M. Gerlic and J. Silke (2014). "RIPK1 regulates RIPK3-MLKL-driven systemic inflammation and emergency hematopoiesis." Cell **157**(5): 1175-1188.

Riedl, S. J. and Y. Shi (2004). "Molecular mechanisms of caspase regulation during apoptosis." Nat Rev Mol Cell Biol **5**(11): 897-907.

Rieger, A. M., K. L. Nelson, J. D. Konowalchuk and D. R. Barreda (2011). "Modified annexin V/propidium iodide apoptosis assay for accurate assessment of cell death." J Vis Exp(50).

Ritsma, L., S. I. Ellenbroek, A. Zomer, H. J. Snippert, F. J. de Sauvage, B. D. Simons, H. Clevers and J. van Rheenen (2014). "Intestinal crypt homeostasis revealed at single-stem-cell level by in vivo live imaging." Nature **507**(7492): 362-365.

Rock, K. L. and H. Kono (2008). "The inflammatory response to cell death." Annu Rev Pathol **3**: 99-126.

Roerink, S. F., N. Sasaki, H. Lee-Six, M. D. Young, L. B. Alexandrov, S. Behjati, T. J. Mitchell, S. Grossmann, H. Lightfoot, D. A. Egan, A. Pronk, N. Smakman, J. van Gorp, E. Anderson, S. J. Gamble, C. Alder, M. van de Wetering, P. J. Campbell, M. R. Stratton and H. Clevers (2018). "Intra-tumour diversification in colorectal cancer at the single-cell level." Nature **556**(7702): 457-462.

Rossi, G., A. Manfrin and M. P. Lutolf (2018). "Progress and potential in organoid research." Nat Rev Genet.

Ruchaud, S., N. Korfali, P. Villa, T. J. Kottke, C. Dingwall, S. H. Kaufmann and W. C. Earnshaw (2002). "Caspase-6 gene disruption reveals a requirement for lamin A cleavage in apoptotic chromatin condensation." EMBO J **21**(8): 1967-1977.

Russell, D. G. (1914). "The Effect of Gentian Violet on Protozoa and on Tissues Growing in Vitro, with Especial Reference to the Nucleus." J Exp Med **20**(6): 545-553.

Saam, J., G. C. Critchfield, S. A. Hamilton, B. B. Roa, R. J. Wenstrup and R. R. Kaldate (2011). "Body surface area-based dosing of 5-fluoruracil results in extensive interindividual variability in 5-fluorouracil exposure in colorectal cancer patients on FOLFOX regimens." Clin Colorectal Cancer **10**(3): 203-206.

Sachs, N. and H. Clevers (2014). "Organoid cultures for the analysis of cancer phenotypes." Curr Opin Genet Dev **24**: 68-73.

Sachs, N., Y. Tsukamoto, P. Kujala, P. J. Peters and H. Clevers (2017). "Intestinal epithelial organoids fuse to form self-organizing tubes in floating collagen gels." Development **144**(6): 1107-1112.

Saeed, K., V. Rahkama, S. Eldfors, D. Bychkov, J. P. Mpindi, B. Yadav, L. Paavolainen, T. Aittokallio, C. Heckman, K. Wennerberg, D. M. Peehl, P. Horvath, T. Mirtti, A. Rannikko, O. Kallioniemi, P. Ostling and T. M. Af Hallstrom (2017). "Comprehensive Drug Testing of Patient-derived Conditionally Reprogrammed Cells from Castration-resistant Prostate Cancer." Eur Urol **71**(3): 319-327.

Sato, T. and H. Clevers (2013). "Primary mouse small intestinal epithelial cell cultures." Methods Mol Biol **945**: 319-328.

Sato, T., D. E. Stange, M. Ferrante, R. G. Vries, J. H. Van Es, S. Van den Brink, W. J. Van Houdt, A. Pronk, J. Van Gorp, P. D. Siersema and H. Clevers (2011). "Long-term expansion of epithelial organoids from human colon, adenoma, adenocarcinoma, and Barrett's epithelium." Gastroenterology **141**(5): 1762-1772.

Sato, T., J. H. van Es, H. J. Snippert, D. E. Stange, R. G. Vries, M. van den Born, N. Barker, N. F. Shroyer, M. van de Wetering and H. Clevers (2011). "Paneth cells constitute the niche for Lgr5 stem cells in intestinal crypts." Nature **469**(7330): 415-418.

Sato, T., R. G. Vries, H. J. Snippert, M. van de Wetering, N. Barker, D. E. Stange, J. H. van Es, A. Abo, P. Kujala, P. J. Peters and H. Clevers (2009). "Single Lgr5 stem cells build crypt-villus structures in vitro without a mesenchymal niche." Nature **459**(7244): 262-265.

Scaffidi, C., I. Schmitz, J. Zha, S. J. Korsmeyer, P. H. Krammer and M. E. Peter (1999). "Differential modulation of apoptosis sensitivity in CD95 type I and type II cells." J Biol Chem **274**(32): 22532-22538.

Schmidt, N., L. Kowald, S. J. L. van Wijk and S. Fulda (2019). "Differential involvement of TAK1, RIPK1 and NF-kappaB signaling in Smac mimetic-induced cell death in breast cancer cells." Biol Chem **400**(2): 171-180.

Schutze, S., K. Wiegmann, T. Machleidt and M. Kronke (1995). "TNF-induced activation of NF-kappa B." Immunobiology **193**(2-4): 193-203.

Schwaderer, J., A. K. Gaiser, T. S. Phan, M. E. Delgado and T. Brunner (2017). "Liver receptor homolog-1 (NR5a2) regulates CD95/Fas ligand transcription and associated T-cell effector functions." Cell Death Dis **8**(4): e2745.

Schwank, G. and H. Clevers (2016). "CRISPR/Cas9-Mediated Genome Editing of Mouse Small Intestinal Organoids." Methods Mol Biol **1422**: 3-11.

Schwartz, D. M., M. O. Pehlivaner Kara, A. Goldstein, H. C. Ott and A. Ekenseair (2017). "Spray Delivery of Intestinal Organoids to Reconstitute Epithelium on Decellularized Native Extracellular Matrix." Tissue Eng Part C Methods.

Schweinlin, M., S. Wilhelm, I. Schwedhelm, J. Hansmann, R. Rietscher, C. Jurowich, H. Walles and M. Metzger (2016). "Development of an Advanced Primary Human In Vitro Model of the Small Intestine." Tissue Eng Part C Methods **22**(9): 873-883.

Scott, F. L., B. Stec, C. Pop, M. K. Dobaczewska, J. J. Lee, E. Monosov, H. Robinson, G. S. Salvesen, R. Schwarzenbacher and S. J. Riedl (2009). "The Fas-FADD death domain complex structure unravels signalling by receptor clustering." Nature **457**(7232): 1019-1022.

Sei, Y., J. Feng, L. Samsel, A. O. White, X. Zhao, S. Yun, D. Citrin, J. P. McCoy, S. Sundaresan, M. M. Hayes, J. L. Merchant, A. B. Leiter and S. A. Wank (2018). "Mature Enteroendocrine Cells Contributes to Basal and Pathological Stem Cell Dynamics in the Small Intestine." Am J Physiol Gastrointest Liver Physiol.

Sekirov, I., S. L. Russell, L. C. Antunes and B. B. Finlay (2010). "Gut microbiota in health and disease." Physiol Rev **90**(3): 859-904.

Serban, M. A. and G. D. Prestwich (2008). "Modular extracellular matrices: solutions for the puzzle." Methods **45**(1): 93-98.

Shan, B., H. Pan, A. Najafov and J. Yuan (2018). "Necroptosis in development and diseases." Genes Dev **32**(5-6): 327-340.

Shoshkes-Carmel, M., Y. J. Wang, K. J. Wangensteen, B. Toth, A. Kondo, E. E. Massassa, S. Itzkovitz and K. H. Kaestner (2018). "Subepithelial telocytes are an important source of Wnts that supports intestinal crypts." Nature **557**(7704): 242-246.

Sidler, D., P. Renzulli, C. Schnoz, B. Berger, S. Schneider-Jakob, C. Fluck, D. Inderbitzin, N. Corazza, D. Candinas and T. Brunner (2011). "Colon cancer cells produce immunoregulatory glucocorticoids." Oncogene **30**(21): 2411-2419.

Silke, J. and P. Meier (2013). "Inhibitor of apoptosis (IAP) proteins-modulators of cell death and inflammation." Cold Spring Harb Perspect Biol **5**(2).

Silke, J. and D. Vucic (2014). "IAP family of cell death and signaling regulators." Methods Enzymol **545**: 35-65.

Simeonov, A. and M. I. Davis (2004). Interference with Fluorescence and Absorbance. Assay Guidance Manual. G. S. Sittampalam, N. P. Coussens, K. Brimacombe et al. Bethesda (MD).

Snippert, H. J., L. G. van der Flier, T. Sato, J. H. van Es, M. van den Born, C. Kroon-Veenboer, N. Barker, A. M. Klein, J. van Rheenen, B. D. Simons and H. Clevers (2010). "Intestinal crypt homeostasis results from neutral competition between symmetrically dividing Lgr5 stem cells." Cell **143**(1): 134-144.

Sode, J., U. Vogel, S. Bank, P. S. Andersen, M. K. Thomsen, M. L. Hetland, H. Locht, N. H. Heegaard and V. Andersen (2014). "Anti-TNF treatment response in rheumatoid arthritis patients is associated with genetic variation in the NLRP3-inflammasome." PLoS One **9**(6): e100361.

Spit, M., B. K. Koo and M. M. Maurice (2018). "Tales from the crypt: intestinal niche signals in tissue renewal, plasticity and cancer." Open Biol **8**(9).

Sprossmann, F., P. Pankert, U. Sausbier, A. Wirth, X. B. Zhou, J. Madlung, H. Zhao, I. Bucurenciu, A. Jakob, T. Lamkemeyer, W. Neuhuber, S. Offermanns, M. J. Shipston, M. Korth, A. Nordheim, P. Ruth and M. Sausbier (2009). "Inducible knockout mutagenesis reveals compensatory mechanisms elicited by constitutive BK channel deficiency in overactive murine bladder." FEBS J **276**(6): 1680-1697.

Steele, N. G., J. Chakrabarti, J. Wang, J. Biesiada, L. Holokai, J. Chang, L. M. Nowacki, J. Hawkins, M. Mahe, N. Sundaram, N. Shroyer, M. Medvedovic, M. Helmrath, S. Ahmad and Y. Zavros (2018). "An Organoid-Based Preclinical Model of Human Gastric Cancer." Cell Mol Gastroenterol Hepatol **7**(1): 161-184.

Sterzel, W., P. Bedford and G. Eisenbrand (1985). "Automated determination of DNA using the fluorochrome Hoechst 33258." Anal Biochem **147**(2): 462-467.

Stewart, A. S., J. M. Freund and L. M. Gonzalez (2018). "Advanced three-dimensional culture of equine intestinal epithelial stem cells." Equine Vet J **50**(2): 241-248.

Sugimoto, S., Y. Ohta, M. Fujii, M. Matano, M. Shimokawa, K. Nanki, S. Date, S. Nishikori, Y. Nakazato, T. Nakamura, T. Kanai and T. Sato (2017). "Reconstruction of the Human Colon Epithelium In Vivo." Cell Stem Cell.

Sun, H., J. Lu, L. Liu, C. Y. Yang and S. Wang (2014). "Potent and selective small-molecule inhibitors of cIAP1/2 proteins reveal that the binding of Smac mimetics to XIAP BIR3 is not

required for their effective induction of cell death in tumor cells." ACS Chem Biol **9**(4): 994-1002.

Sun, W., Z. Luo, J. Lee, H. J. Kim, K. Lee, P. Tebon, Y. Feng, M. R. Dokmeci, S. Sengupta and A. Khademhosseini (2019). "Organ-on-a-Chip for Cancer and Immune Organs Modeling." Adv Healthc Mater: e1801363.

Suzuki, A., S. Sekiya, E. Gunshima, S. Fujii and H. Taniguchi (2010). "EGF signaling activates proliferation and blocks apoptosis of mouse and human intestinal stem/progenitor cells in long-term monolayer cell culture." Lab Invest **90**(10): 1425-1436.

Suzuki, T., K. Fujikura, T. Higashiyama and K. Takata (1997). "DNA staining for fluorescence and laser confocal microscopy." J Histochem Cytochem **45**(1): 49-53.

Swaminathan, S., Q. Hamid, W. Sun and A. M. Clyne (2019). "Bioprinting of 3D breast epithelial spheroids for human cancer models." Biofabrication.

Takahashi, N., L. Vereecke, M. J. Bertrand, L. Duprez, S. B. Berger, T. Divert, A. Goncalves, M. Sze, B. Gilbert, S. Kourula, V. Goossens, S. Lefebvre, C. Gunther, C. Becker, J. Bertin, P. J. Gough, W. Declercq, G. van Loo and P. Vandenabeele (2014). "RIPK1 ensures intestinal homeostasis by protecting the epithelium against apoptosis." Nature **513**(7516): 95-99.

Thalheim, T., M. Quaas, M. Herberg, U. D. Braumann, C. Kerner, M. Loeffler, G. Aust and J. Galle (2017). "Linking stem cell function and growth pattern of intestinal organoids." Dev Biol.

Thalheim, T., M. Quaas, M. Herberg, U. D. Braumann, C. Kerner, M. Loeffler, G. Aust and J. Galle (2018). "Linking stem cell function and growth pattern of intestinal organoids." Dev Biol **433**(2): 254-261.

Thorne, C. A., I. W. Chen, L. E. Sanman, M. H. Cobb, L. F. Wu and S. J. Altschuler (2018). "Enteroid Monolayers Reveal an Autonomous WNT and BMP Circuit Controlling Intestinal Epithelial Growth and Organization." Dev Cell **44**(5): 624-633 e624.

Tibbitt, M. W. and K. S. Anseth (2009). "Hydrogels as extracellular matrix mimics for 3D cell culture." Biotechnol Bioeng **103**(4): 655-663.

Ting, A. T. and M. J. M. Bertrand (2016). "More to Life than NF-kappaB in TNFR1 Signaling." Trends Immunol **37**(8): 535-545.

Tong, Z., K. Martyn, A. Yang, X. Yin, B. E. Mead, N. Joshi, N. E. Sherman, R. S. Langer and J. M. Karp (2017). "Towards a defined ECM and small molecule based monolayer culture system for the expansion of mouse and human intestinal stem cells." Biomaterials **154**: 60-73.

Tournier, C., P. Hess, D. D. Yang, J. Xu, T. K. Turner, A. Nimnual, D. Bar-Sagi, S. N. Jones, R. A. Flavell and R. J. Davis (2000). "Requirement of JNK for stress-induced activation of the cytochrome c-mediated death pathway." Science **288**(5467): 870-874.

Treindl, F., B. Ruprecht, Y. Beiter, S. Schultz, A. Dottinger, A. Staebler, T. O. Joos, S. Kling, O. Poetz, T. Fehm, H. Neubauer, B. Kuster and M. F. Templin (2016). "A bead-based western for high-throughput cellular signal transduction analyses." Nat Commun **7**: 12852.

Troger, V., J. L. Fischel, P. Formento, J. Gioanni and G. Milano (1992). "Effects of prolonged exposure to cisplatin on cytotoxicity and intracellular drug concentration." Eur J Cancer **28**(1): 82-86.

Van Antwerp, D. J., S. J. Martin, T. Kafri, D. R. Green and I. M. Verma (1996). "Suppression of TNF-alpha-induced apoptosis by NF-kappaB." Science **274**(5288): 787-789.

Van Antwerp, D. J. and I. M. Verma (1996). "Signal-induced degradation of I(kappa)B(alpha): association with NF-kappaB and the PEST sequence in I(kappa)B(alpha) are not required." Mol Cell Biol **16**(11): 6037-6045.

Van der Flier, L. G., J. Sabates-Bellver, I. Oving, A. Haegebarth, M. De Palo, M. Anti, M. E. Van Gijn, S. Suijkerbuijk, M. Van de Wetering, G. Marra and H. Clevers (2007). "The Intestinal Wnt/TCF Signature." Gastroenterology **132**(2): 628-632.

van der Hee, B., L. M. P. Loonen, N. Taverne, J. J. Taverne-Thiele, H. Smidt and J. M. Wells (2018). "Optimized procedures for generating an enhanced, near physiological 2D culture system from porcine intestinal organoids." Stem Cell Res **28**: 165-171.

van Engeland, M., L. J. Nieland, F. C. Ramaekers, B. Schutte and C. P. Reutelingsperger (1998). "Annexin V-affinity assay: a review on an apoptosis detection system based on phosphatidylserine exposure." Cytometry **31**(1): 1-9.

Vanden Berghe, T., A. Linkermann, S. Jouan-Lanhouet, H. Walczak and P. Vandenabeele (2014). "Regulated necrosis: the expanding network of non-apoptotic cell death pathways." Nat Rev Mol Cell Biol **15**(2): 135-147.

Vandenabeele, P., W. Declercq, F. Van Herreweghe and T. Vanden Berghe (2010). "The role of the kinases RIP1 and RIP3 in TNF-induced necrosis." Sci Signal **3**(115): re4.

Varfolomeev, E., J. W. Blankenship, S. M. Wayson, A. V. Fedorova, N. Kayagaki, P. Garg, K. Zobel, J. N. Dynek, L. O. Elliott, H. J. Wallweber, J. A. Flygare, W. J. Fairbrother, K. Deshayes, V. M. Dixit and D. Vucic (2007). "IAP antagonists induce autoubiquitination of c-IAPs, NF-kappaB activation, and TNFalpha-dependent apoptosis." Cell **131**(4): 669-681.

Vince, J. E., W. W. Wong, N. Khan, R. Feltham, D. Chau, A. U. Ahmed, C. A. Benetatos, S. K. Chunduru, S. M. Condon, M. McKinlay, R. Brink, M. Leverkus, V. Tergaonkar, P. Schneider, B. A. Callus, F. Koentgen, D. L. Vaux and J. Silke (2007). "IAP antagonists target cIAP1 to induce TNFalpha-dependent apoptosis." Cell **131**(4): 682-693.

Vita, M. F., N. Nagachar, D. Avramidis, Z. M. Delwar, M. H. Cruz, A. Siden, K. M. Paulsson and J. S. Yakisich (2011). "Pankiller effect of prolonged exposure to menadione on glioma cells: potentiation by vitamin C." Invest New Drugs **29**(6): 1314-1320.

Vlachogiannis, G., S. Hedayat, A. Vatsiou, Y. Jamin, J. Fernandez-Mateos, K. Khan, A. Lampis, K. Eason, I. Huntingford, R. Burke, M. Rata, D. M. Koh, N. Tunariu, D. Collins, S. Hulkki-Wilson, C. Ragulan, I. Spiteri, S. Y. Moorcraft, I. Chau, S. Rao, D. Watkins, N. Fotiadis, M. Bali, M. Darvish-Damavandi, H. Lote, Z. Eltahir, E. C. Smyth, R. Begum, P. A. Clarke, J. C. Hahne, M. Dowsett, J. de Bono, P. Workman, A. Sadanandam, M. Fassan, O. J. Sansom, S. Eccles, N. Starling, C. Braconi, A. Sottoriva, S. P. Robinson, D. Cunningham and N. Valeri (2018). "Patient-derived organoids model treatment response of metastatic gastrointestinal cancers." Science **359**(6378): 920-926.

Volkmann, N., F. M. Marassi, D. D. Newmeyer and D. Hanein (2014). "The rheostat in the membrane: BCL-2 family proteins and apoptosis." Cell Death Differ **21**(2): 206-215.

von Moltke, J., M. Ji, H. E. Liang and R. M. Locksley (2016). "Tuft-cell-derived IL-25 regulates an intestinal ILC2-epithelial response circuit." Nature **529**(7585): 221-225.

Wajant, H., K. Pfizenmaier and P. Scheurich (2003). "Tumor necrosis factor signaling." Cell Death Differ **10**(1): 45-65.

Walsh, A. J., R. S. Cook, M. E. Sanders, C. L. Arteaga and M. C. Skala (2016). "Drug response in organoids generated from frozen primary tumor tissues." Sci Rep **6**: 18889.

Wang, F., D. Scoville, X. C. He, M. M. Mahe, A. Box, J. M. Perry, N. R. Smith, N. Y. Lei, P. S. Davies, M. K. Fuller, J. S. Haug, M. McClain, A. D. Gracz, S. Ding, M. Stelzner, J. C. Dunn, S. T. Magness, M. H. Wong, M. G. Martin, M. Helmrath and L. Li (2013). "Isolation and characterization of intestinal stem cells based on surface marker combinations and colony-formation assay." Gastroenterology **145**(2): 383-395 e381-321.

Wang, L., F. Du and X. Wang (2008). "TNF-alpha induces two distinct caspase-8 activation pathways." Cell **133**(4): 693-703.

Wang, Q., E. Hummler, M. Maillard, J. Nussberger, B. C. Rossier, H. R. Brunner and M. Burnier (2001). "Compensatory up-regulation of angiotensin II subtype 1 receptors in alpha ENaC knockout heterozygous mice." Kidney Int **59**(6): 2216-2221.

Wang, S. (2011). "Design of small-molecule Smac mimetics as IAP antagonists." Curr Top Microbiol Immunol **348**: 89-113.

Weisberg, E., A. Ray, R. Barrett, E. Nelson, A. L. Christie, D. Porter, C. Straub, L. Zawel, J. F. Daley, S. Lazo-Kallanian, R. Stone, I. Galinsky, D. Frank, A. L. Kung and J. D. Griffin (2010). "Smac mimetics: implications for enhancement of targeted therapies in leukemia." Leukemia **24**(12): 2100-2109.

Welz, P. S., A. Wullaert, K. Vlantis, V. Kondylis, V. Fernandez-Majada, M. Ermolaeva, P. Kirsch, A. Sterner-Kock, G. van Loo and M. Pasparakis (2011). "FADD prevents RIP3-mediated epithelial cell necrosis and chronic intestinal inflammation." Nature **477**(7364): 330-334.

Whitehead, R. H., P. E. VanEeden, M. D. Noble, P. Ataliotis and P. S. Jat (1993). "Establishment of conditionally immortalized epithelial cell lines from both colon and small intestine of adult H-2Kb-tsA58 transgenic mice." Proc Natl Acad Sci U S A **90**(2): 587-591.

Willemse, J., R. Lieshout, L. J. W. van der Laan and M. M. A. Verstegen (2017). "From organoids to organs: Bioengineering liver grafts from hepatic stem cells and matrix." Best Pract Res Clin Gastroenterol **31**(2): 151-159.

Wills, E. S. and J. P. Drenth (2017). "Building pancreatic organoids to aid drug development." Gut **66**(3): 393-394.

Win, S., T. A. Than, J. Zhang, C. Oo, R. W. M. Min and N. Kaplowitz (2018). "New insights into the role and mechanism of c-Jun-N-terminal kinase signaling in the pathobiology of liver diseases." Hepatology **67**(5): 2013-2024.

Wu, C. and B. A. Alman (2008). "Side population cells in human cancers." Cancer Lett **268**(1): 1-9.

Wu, Y. T., H. L. Tan, Q. Huang, X. J. Sun, X. Zhu and H. M. Shen (2011). "zVAD-induced necroptosis in L929 cells depends on autocrine production of TNFalpha mediated by the PKC-MAPKs-AP-1 pathway." Cell Death Differ **18**(1): 26-37.

Xia, Z., M. Dickens, J. Raingeaud, R. J. Davis and M. E. Greenberg (1995). "Opposing effects of ERK and JNK-p38 MAP kinases on apoptosis." Science **270**(5240): 1326-1331.

Xue, X. and Y. M. Shah (2013). "In vitro organoid culture of primary mouse colon tumors." J Vis Exp(75): e50210.

Ye, P., Y. J. Chiang, Z. Qi, Y. Li, S. Wang, Y. Liu, X. Li and Y. G. Chen (2018). "Tankyrases maintain homeostasis of intestinal epithelium by preventing cell death." PLoS Genet **14**(9): e1007697.

Yen, T. H. and N. A. Wright (2006). "The gastrointestinal tract stem cell niche." Stem Cell Rev **2**(3): 203-212.

Yin, X., B. E. Mead, H. Safaee, R. Langer, J. M. Karp and O. Levy (2016). "Engineering Stem Cell Organoids." Cell Stem Cell **18**(1): 25-38.

Yu, H., N. M. Hasan, J. G. In, M. K. Estes, O. Kovbasnjuk, N. C. Zachos and M. Donowitz (2017). "The Contributions of Human Mini-Intestines to the Study of Intestinal Physiology and Pathophysiology." Annu Rev Physiol **79**: 291-312.

Yuan, J., A. Najafov and B. F. Py (2016). "Roles of Caspases in Necrotic Cell Death." Cell **167**(7): 1693-1704.

Yui, S., T. Nakamura, T. Sato, Y. Nemoto, T. Mizutani, X. Zheng, S. Ichinose, T. Nagaishi, R. Okamoto, K. Tsuchiya, H. Clevers and M. Watanabe (2012). "Functional engraftment of colon epithelium expanded in vitro from a single adult Lgr5(+) stem cell." Nat Med **18**(4): 618-623.

Yumoto, F., P. Nguyen, E. P. Sablin, J. D. Baxter, P. Webb and R. J. Fletterick (2012). "Structural basis of coactivation of liver receptor homolog-1 by beta-catenin." Proc Natl Acad Sci U S A **109**(1): 143-148.

Zhang, H., X. Zhou, T. McQuade, J. Li, F. K. Chan and J. Zhang (2011). "Functional complementation between FADD and RIP1 in embryos and lymphocytes." Nature **471**(7338): 373-376.

Zhang, L., J. M. Valdez, B. Zhang, L. Wei, J. Chang and L. Xin (2011). "ROCK inhibitor Y-27632 suppresses dissociation-induced apoptosis of murine prostate stem/progenitor cells and increases their cloning efficiency." PLoS One **6**(3): e18271.

Zhang, W. and H. T. Liu (2002). "MAPK signal pathways in the regulation of cell proliferation in mammalian cells." Cell Res **12**(1): 9-18.

8.1 Chemical structures taken from pubchem

Hoechst 33342:
https://pubchem.ncbi.nlm.nih.gov/image/imagefly.cgi?cid=197366&width=500&height=500

Propidium Iodide:
https://pubchem.ncbi.nlm.nih.gov/image/imagefly.cgi?cid=104981&width=500&height=500

8.2 Further Online References

- https://www.corning.com/media/worldwide/cls/documents/CLS-DL-CC-026%20DL.pdf

→ Matrigel: frequently asked questions

9. Appendix

9.1 Abbreviations

x g	times gravity
°C	degree Celsius
A	Ampere
aa	amino acid
Ab	antibody
Amp	ampicillin
Apaf1	apoptotic protease activating factor 1
APS	ammonium persulfate
ATP	adenosine triphosphate
BF	brightfield
BIR	Baculoviral repeat
BMP	bone morphogenetic protein
BSA	bovine serum albumin
Caspase	Cysteine-dependent aspartate-directed proteases
CAD	Caspase-activated DNAse
CRISPR/Cas9	Clustered Regularly Interspaced Short Palindromic Repeats/ CRISPR-associated
C-terminus	carboxy-terminus of a peptide
Da	Dalton
DD	Death domain
DED	Death effector domain
DISC	Death inducing signaling complex
DMEM	Dulbecco's modified eagle medium
DMSO	dimethyl sulfoxide
DNA	deoxyribonucleic acid
ECL	electrochemiluminescence
EDTA	ethylenediaminetetraacetic acid
EtOH	ethanol
FADD	Fas-associated protein with death domain

FBS	fetal bovine serum
FCS	fetal calf serum
FUT2	Fucosyltransferase 2
GFP	green fluorescent protein
h	hours
HBSS	Hank's balanced salt solution
HEK	human embryonic kidney
HRP	horse radish peroxidase
IAP	Inhibitor of Apoptosis Protein
ICAD	Inhibitor of Caspase-activated DNAse
mIFNγ	murine Interferon gamma
IMDM	Iscove's modified Dulbecco's medium
iPSCs	induced pluripotent stem cells
ISCs	intestinal stem cells
k	kilo
l	liter
LB	Lysogeny Broth
LDH	Lactate Dehydrogenase
Lgr	Leucine-rich repeat-containing G-protein coupled receptor
LRH-1	Liver receptor homologue-1
mM	milli-molar
M	molar
MAPK	Mitogen Activated Protein Kinase
MeOH	methanol
min	minute
MOMP	mitochondrial outer membrane permeabilization
MTT	3-(4,5-Dimethylthiazol-2-yl)-2,5-diphenyltetrazoliumbromid
NADH	Nicotinamide adenine dinucleotide
nm	nanometer
nM	nanomolar
NOD2	Nucleotide binding oligomerization domain-containing protein 2
N-terminus	amino-terminus of a peptide

NFκB	nuclear factor “kappa light chain enhancer” of activated B cells
Nr5a2	Nuclear receptor 5a2
OD_{562}	optical density at a wavelength of 562 nm
PARP	Poly (ADP-ribose) polymerase
PBS	phosphate-buffered saline
PI	Propidium Iodide
PP	peyer’s patch
qPCR	quantitative polymerase chain reaction
RFU	relative fluorescence units
RLU	relative luminescence units
rpm	rounds per minute
RT	room temperature
SDS	sodium dodecyl sulfate
SDS-PAGE	SDS polyacrylamide gelelectrophoresis
STAR2	Selective TNF-based agonist of receptor 2
TBS-T	Tris buffered saline-Tween
TEMED	N, N, N’, N’-tetramethylethylendiamine
hTNF-α	human tumor necrosis factor -α
mTNF-α	murine tumor necrosis factor -α
TNFR	TNF Receptor
TRAIL	TNF-related apoptosis-inducing ligand
TRADD	TNF-receptor type 1-associated death domain protein
TWEAK	TNF-related weak inducer of apoptosis
V	Volt
v/v	volume/volume
WB	Western Blot
Wnt	wingless-type
WT	wildtype
w/v	weight/volume
YAMC	Young Adult Mouse Colon
µm	micrometer
µM	mikromolar

9.2 Human RSpondin-1 conditioned media

Human RSpondin-1 (hRSpondin1/RSpondin) conditioned (cond.) medium was generated as described in 7.2.13 and 7.2.14. Subsequently, the functionality of conditioned medium was tested in comparison to commercially available rec. RSpondin. Therefore, murine small intestinal organoids were cultured for several days in indicated media. Overall development and growth were determined visually by brightfield microscopy (Figure 33). Since organoids cultured in different conditioned media (1-3) showed similar growth and morphology compared to the rec. RSpondin control, these media were used to culture organoids. Cultivation in medium of the transfection control (empty vector) did not result in any organoid development (Figure 33, w/o RSpondin).

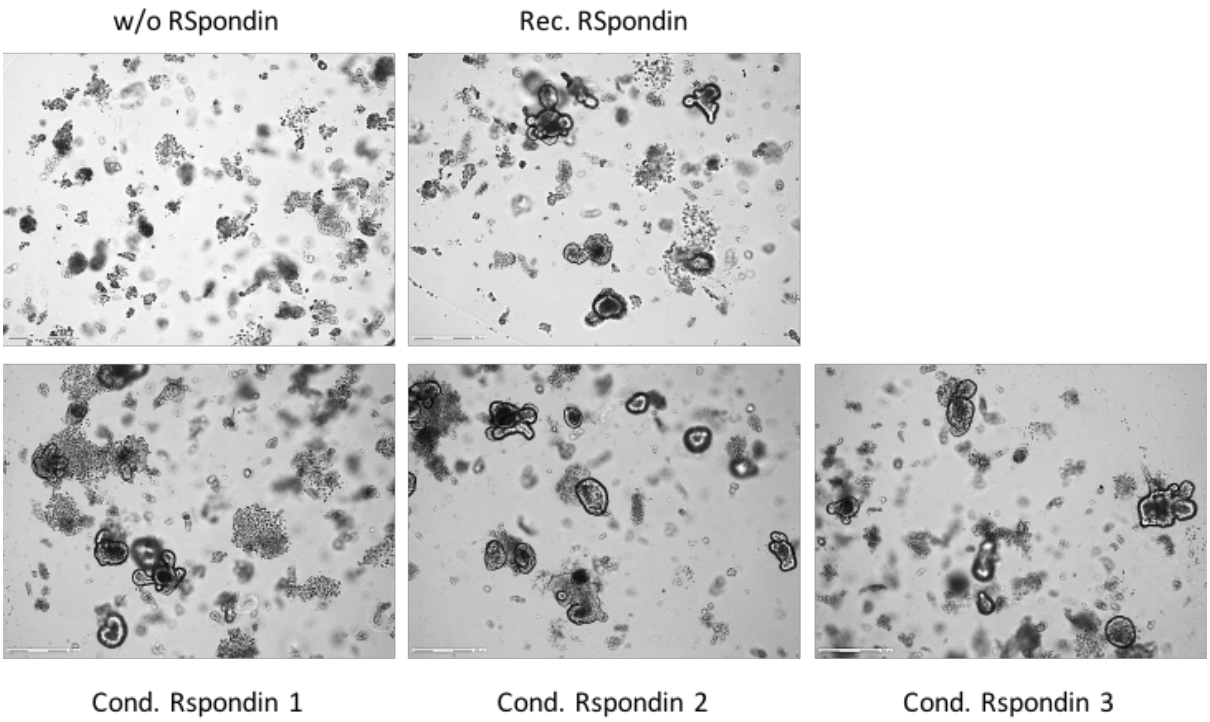

Figure 33: Comparison of RSpondin-1-conditioned media

Small intestinal crypts were cultured in indicated media and growth as well as morphology were assessed for several days after isolation.

10. Table of figures